COASTAL ENGINEERING
IN JAPAN

VOL. IV

PUBLICATIONS OF THE COMMITTEE ON COASTAL ENGINEERING, Japan

English edition

Coastal Engineering in Japan, vol. 1, 1958 (U.S. $1.50)
Coastal Engineering in Japan, vol. 2, 1959 (U.S. $1.50)
Coastal Engineering in Japan, vol. 3, 1960 (U.S. $2.50)
Coastal Engineering in Japan, vol. 4, 1961 (U.S. $3.00)

Japanese edition

Proceedings, 1st Conf. on Coastal Engineering, 1954 (out of print)
Proceedings, 2nd Conf. on Coastal Engineering, 1955 (out of print)
Proceedings, 3rd Conf. on Coastal Engineering, 1956 (out of print)
Proceedings, 4th Conf. on Coastal Engineering, 1957
Proceedings, 5th Conf. on Coastal Engineering, 1958
Proceedings, 6th Conf. on Coastal Engineering, 1959
Proceedings, 7th Conf. on Coastal Engineering, 1960
Proceedings, 8th Conf. on Coastal Engineering, 1961
Design Manual of Coastal Protection Works, 1957 (out of print)

PREFACE

The history of the engineering science on coastal problems is not long in any countries, to fulfil the demands of engineers engaging in coastal works. Even lately we had to come across so many examples of walls, dikes or groins in Japanese coast which were badly destroyed by storm waves or lie invalid for the purpose of their construction. These examples must be said to some from the defect of knowledge in coastal engineering.

In the present stage, the most important thing to be promoted seems to be the accumulation of data of our experiences in coastal works, successful or unsuccessful, acompanying the research of coastal hydraulics and the field observations of phenomena concerning coastal process. This publication "Coastal Engineering in Japan", shall be edited to contribute such aims.

The Committee on Coastal Engineering of J.S.C.E. takes this opportunity to thank the authors of the papers for their co-operation and the Ministry of Education for his financial helf for the printing.

September, 1961

Masashi Hom-ma
Chairman
Committee on Coastal Engineering
Japan Society of Civil Engineers
1-chome, Yotsuya, Shinjuku-ku,
Tokyo, Japan

Digitized by the Internet Archive
in 2023 with funding from
Kahle/Austin Foundation

https://archive.org/details/coastal-engineering-journal_1961-12_4

CONTENTS

page

Preface ··M. Hom-ma

A Note on the Storm Tide of the Japanese Coast ············S. Unoki············ 1

On Storm Surges caused by the Ise Bay Typhoon and their Theoretical Computations ············M. Miyazaki, S. Unoki, T. Ueno ······ 11

Stability of the Breakwater against Sliding due to Pressure of Breaking Waves ························T. Hayashi, S. Hattori ········· 23

Hydraulic Model Experiment on the Oscillation of Water Level in Sakai Channel ···············H. Higuchi ········· 35

Stable Configuration of Coast Line ·································Y. Mashima ······ 47

Some Experiments on Bamboo Samplers ························ H. Fukushima, M. Kashiwamura 61

Behavior of Sand-Spit-Bar at a River Mouth —A Model Experiment of Tonda Fishery Port— ·····················M. Yoshitaka ······ 65

Recent Coastal Processes in Niigata Prefecture ················T. Haruta ········· 73

A Study on Submerged Breakwaters ·····························M. Hom-ma, K. Horikawa ······ 85

Beach Erosion and Protection Works in Imazu-Sakano Beach ·························M. Kubo, N. Iwasa ············ 103

Improvement of the Mouth of the Musa River ···············T. Kishi, M. Taniguchi ······ 115

A NOTE ON THE STORM TIDE OF THE JAPANESE COAST

*Sanae Unoki**

I. INTRODUCTION

The purpose of this report is to describe briefly the storm tides on the Japanese coast and to give a preliminary knowledge indispensable to the prevention of disaster due to them. In our country, we have often suffered great damages by storm tides, for example, sixty times with a heavy loss for this half a century from 1900 to 1953 [Wadati and Hirono, 1954].

Particularly, in 1959, Nagoya and neighbouring district in the central Japan were seriously damaged by a destructive storm tide accompanied with "Ise Bay typhoon" (No. 5915). Total damages sustained from this typhoon were 4,697 dead, 38,921 injured, 153,890 houses destroyed or swept away, 363,611 homes flooded, embankments at 5,760 places broken, 4,160

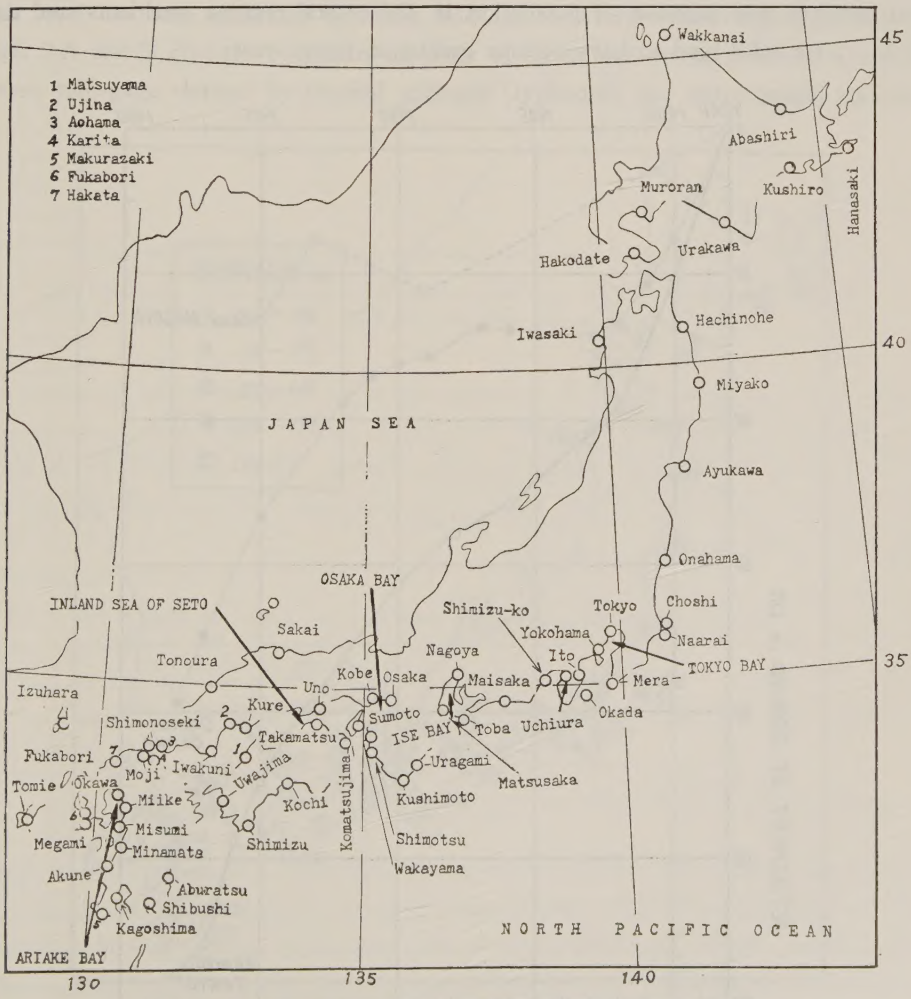

Fig. 1 Localities of tidal stations.

---

* Dr. Sc., Meteorological Research Institute

bridges swept away and 2,431 ships lost.

Reasons why we have suffered such serious damages so frequently are considered chiefly as follows: First, meteorologically speaking, the islands of Japan are liable to be attacked by typhoons or remarkably developed tropical cyclones in the western Pacific, at least a few times every year. Second, geographically speaking, our important industrial or commercial regions are located in close immediately to the head of bay such as Tokyo Bay, Ise Bay and Osaka Bay etc. (Fig. 1). Because either of them is comparatively large and fairly shallow it is very favourable for the development of storm tide. Third, ways and means to prevent damages due to dangerous storm tide have not been considered sufficiently for many reasons combined.

To make matter worse, recently, the grounds near the above-mentioned industrial regions are settling considerably rapidly. An example is shown in Fig. 2, representing that the speed of settlement at Tokyo and Osaka reaches several centimeters per year. Such conspicuous settlement is said to be caused by heavy pumping of underground water. Moreover, reclaimed grounds from the sea are abundant around the bays, but the prevention from abnormal waves and storm tides is not necessarily complete. From these reasons, in proportion to the development of industry and increase of population in the coastal regions, accidents and damages caused by storm tides tend to have become greater in recent years.

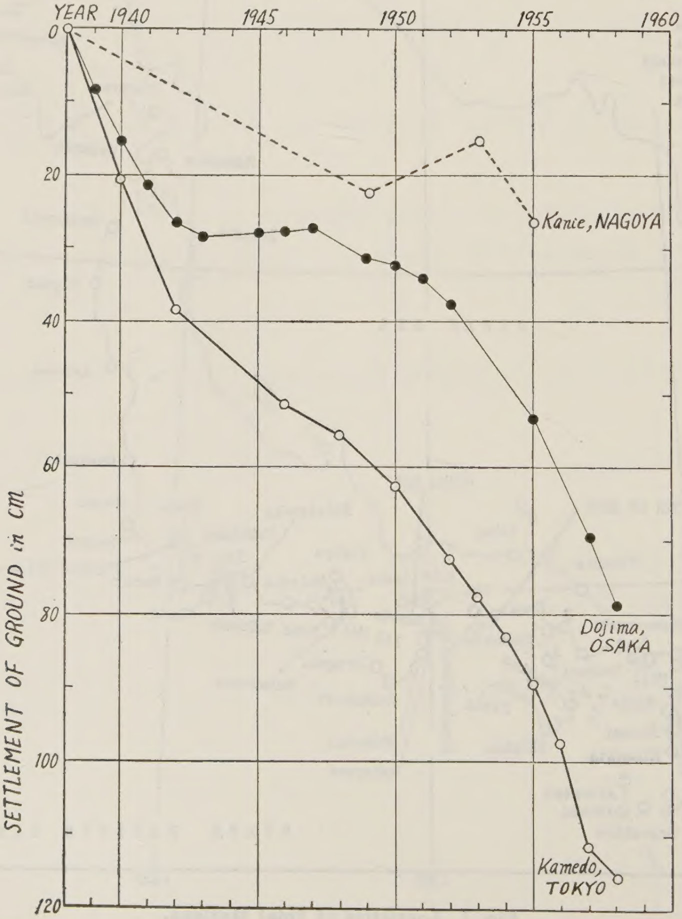

Fig. 2 Settlement of ground at three cities, Tokyo, Osaka and Nagoya (based upon the materials of the Geographic Survey Institute, Japan)

Similarly to the case of hurricanes, the disturbed water levels associated with the passage of typhoons are also classified into three stages : forerunners, the typhoon surge (hurricane surge in the former case), and resurgences, whose definition is indicated in the paper of Redfield and Miller [1957]. In this report, however, we shall notice only the peak of storm tide, and forerunners and resurgences due to typhoons will be discussed in future.

Synthetic reports on storm tides in Japan have already been done by Wadati and Hirono [1954] and Miyazaki [1957]. This report implies some of their results in addition to what was arranged by the present author in order to understand quantitatively the magnitude, distribution and some other problems of storm tides. The localities of bays and tidal stations which will be taken into account are represented in Fig. 1.

II. METEOROLOGICAL DISTURBANCES BY WHICH THE STORM TIDE OCCURS

The highest water level, in our country, has been brought about by a tsunami due to a submarine earthquake. In the case of Sanriku-tsunami of 1896 the water level rised to a height more than 20 meters above the usual sea surface. Except tsunamis, an abnormal rising of water level has been generated by storm tide due to severe meteorological disturbances.

Figs. 3 A and B give the maximum anomaly of water level above predicted one produced at various tide gage stations by tropical cyclones (typhoons) and extratropical cyclones, re-

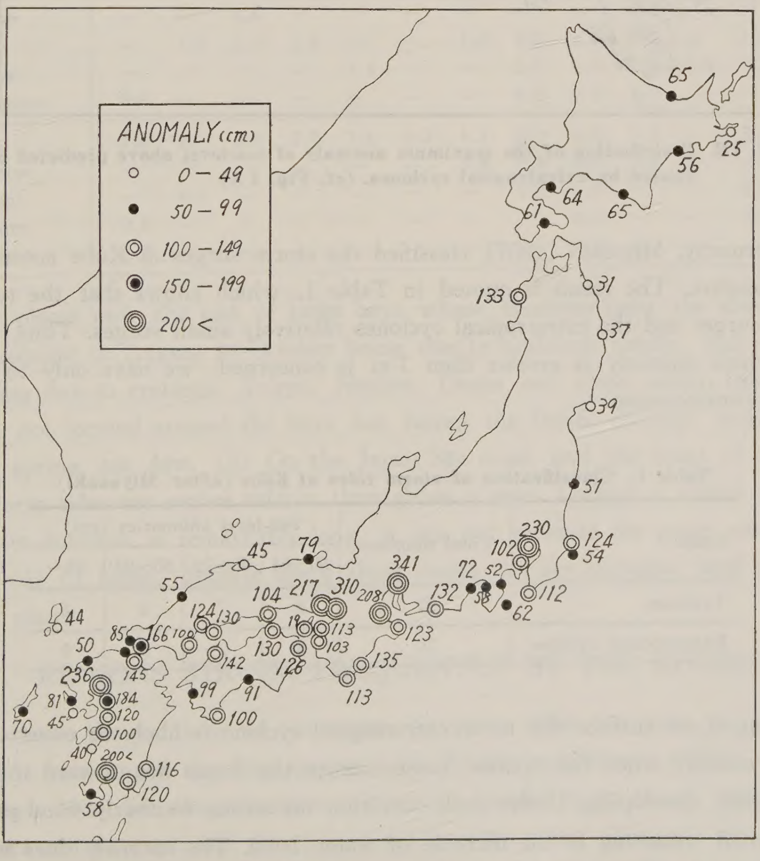

Fig. 3 A Distribution of the maximum anomaly of sea-level above predicted one, caused by typhoons. The data are based upon tide gages, but the period of observation is various.

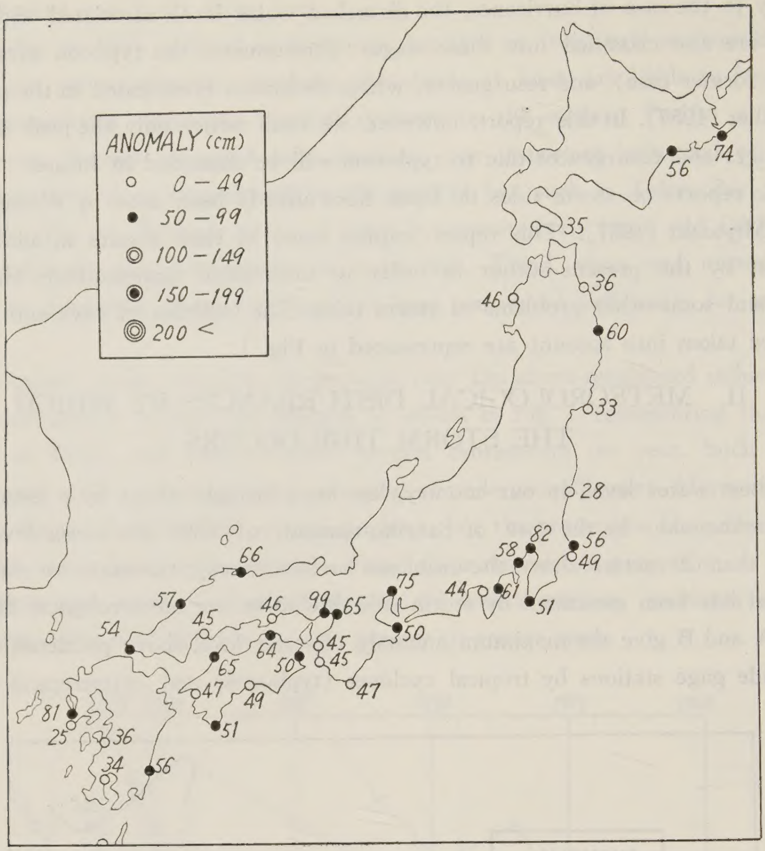

Fig. 3 B Distribution of the maximum anomaly of sea-level above predicted one, caused by extratropical cyclones. (cf. Fig. 3 A)

spectively. Formerly, Miyazaki [1957] classified the storm surges at Kobe according as their causes and heights. The result is quoted in Table 1, which shows that the typhoon often causes great surges and the extratropical cyclones relatively small surges. Thus, so far as the storm tide whose anomaly is greater than 1 m is concerned, we have only to take tropical cyclones into consideration.

Table 1. Classification of storm tides at Kōbe (after Miyazaki)

Cause	Total numbers	Sea-level anomaries (cm)			
		50~64	65~79	80~94	95~
Typhoon	21	6	7	2	6
Extratropical cyclone	10	8	2	0	0

The rising of sea surface due to an extratropical cyclone is likely to occur on the Pacific coast of our country when the cyclone passes across the Japan Sea toward the east or the northeast, rapidly developing. Under such condition the strong southerly wind prevails in the region concerned, resulting in the increase of water level. The anomaly does not reach one meter as recognized in Fig. 3 B, but the water is sometimes elevated above the dangerous level and some damages are caused on the high water of the spring tide. [Miyazaki, 1957]

III. SEASON WHEN THE STORM TIDE IS LIABLE TO OCCUR

In order to understand the season of occurrence of storm tide, in Table 2 is represented the maximum anomaly in each month at selected several stations, and in Table 3 the frequency of the anomaly exceeding 50 cm above predicted water level during 10 years. From them the following facts are recognized:

Table 2. The greatest anomaly above predicted sea-level in each month at tidal stations.

Station	Jan.	Feb.	Mar.	Apr.	May	June	July	Aug.	Sept.	Oct.	Nov.	Dec.	Period
Kushiro	49	50	35	26	**56**	22	46	49	**56**	30	30	31	1952—59
Miyako	31	33	**60**	35	34	24	21	25	37	37	33	46	1942—59
Tokyo	41	62	35	58	41	33	114	**140**	109	84	36	82	1949—59
Nagoya	45	44	41	43	61	47	34	67	**341**	124	75	59	1951—59
Kushimoto	61	47	44	29	41	44	39	65	**113**	63	39	37	1936—59
Osaka	59	64	64	55	64	74	65	58	**237**	108	40	60	1950—59
Aburatsu	37	30	26	28	27	27	**116**	56	69	69	27	30	1946—59
Megami	48	77	38	41	32	33	39	**81**	**81**	47	36	61	1936—59
Tonoura	54	31	40	38	28	45	41	39	**57**	56	31	**57**	1936—59
Iwasaki	79	46	31	45	38	27	29	39	**133**	34	40	41	1951—59

Table 3. Frequency when the anomaly above predicted sea-level exceeds+50 cm for ten years.

Station	Jan.	Feb.	Mar.	Apr.	May	June	July	Aug.	Sept.	Oct.	Nov.	Dec.	Sum
Kushiro	—	1.7	—	—	1.7	—	—	—	1.4	—	—	—	4.8
Miyako	—	—	0.6	—	—	—	—	—	—	—	—	—	0.6
Tokyo	—	1.3	1.3	1.3	—	—	1.3	3.0	3.3	2.2	—	1.3	15.0
Nagoya	—	—	—	—	1.4	—	—	2.5	3.3	2.5	1.3	1.3	12.3
Kushimoto	0.6	—	—	—	—	—	—	0.6	1.7	1.7	—	—	4.6
Osaka	1.1	1.1	3.3	2.2	1.1	3.3	1.1	3.3	3.3	1.1	—	2.2	23.1
Aburatsu	—	—	—	—	—	—	0.8	0.9	0.8	0.8	—	—	3.3
Megami	—	0.7	—	—	—	—	—	1.2	1.3	—	—	0.6	3.8
Tonoura	0.5	—	—	—	—	—	—	—	0.4	—	—	1.4	2.3
Iwasaki	1.4	—	—	—	—	—	—	—	1.3	—	—	—	2.7

(1) At places near the end of large bays whose entrance faces the south, storm tides are most frequent in August to October being due to typhoons chiefly, and next, in March to May being due to cyclones. Tokyo, Nagoya, Osaka etc. come within this category. (2) At stations not located around the bays but facing the Pacific directly, storm tides due to cyclones in spring are few. (3) On the Japan Sea coast and the coast of Hokkaido, conspicuous storm tides are rather seldom throughout a year. Though a winter monsoon is not weak and its duration is remarkably long, it can not generate the great storm tide on the Japan Sea side of Japan, because along these coasts the sea becomes deep rapidly offshore except few places.

IV. REGIONS STRUCK FREQUENTLY BY THE STORM TIDE

Fig. 4 shows the numbers of occurrence of storm tides for sixty years from 1900 to 1959. This is based upon the data arranged by Wadati and Hirono [1954] and recent new materials since 1954, but the estimation can not be avoided to be rough, because the data in old times are not so exact and also it is probable that a few abnormal rises of sea surface due to other phenomena are included in the numbers. Comparing Fig. 4 with Fig. 3, it will be seen, at places where the storm surge occurs frequently, that the anomaly is also large

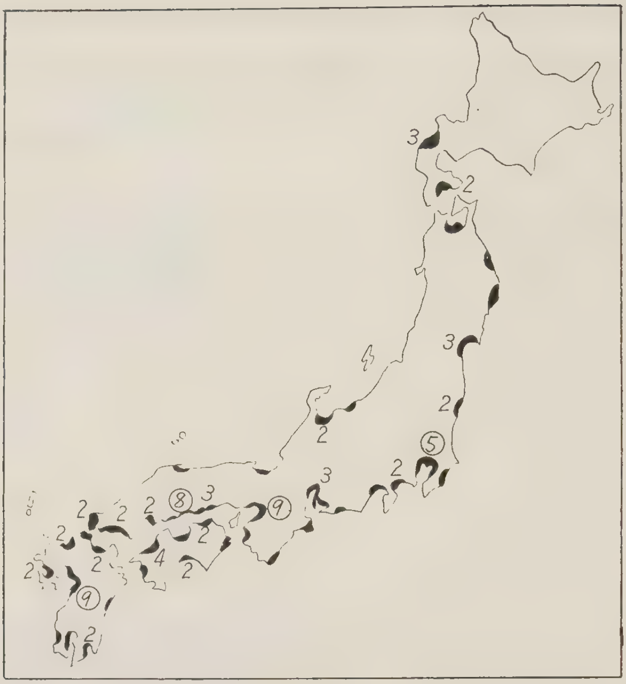

Fig. 4 Storm tides in Japan occurring since 1900 to 1959. Numerals show numbers of occurrences. The places without numerals are once in each.

Table 4. Storm tides whose anomaly exceeded 2 m during 60 years from 1900 to 1959.

Date	Generating area	Maximum anomaly (cm)	Cause
Aug. 25, 1914	Ariake Bay	2∼2.5	typhoon
Oct. 1, 1917	Tokyo Bay	2.3	typhoon
Sept. 13, 1927	Ariake Bay	about 3	typhoon
Sept. 21, 1934	Osaka Bay	3.1	Muroto-typhoon
Sept. 17, 1945	Kagoshima Bay	>2	Makurazaki-typhoon
Sept. 3, 1950	Osaka Bay	2.4	Jane-typhoon
Sept. 26, 1959	Ise Bay	3.1	Ise-Bay-typhoon

though it is a matter of course.

Storm tides whose anomaly exceeds 2 m are seven in number since 1900 as summarized in Table 4. The effect of storm tides is destructive when the anomaly is more than 2 m, but it is never neglected even in the case when the anomaly does not reach 2 m if its occurrence time happens to coincide with that of the high water and the disaster prevention is not sufficient.

Hence we may say that regions where the remarkable storm tide occurs frequently are Osaka Bay, Ariake Sea, Island Sea of Seto and Tokyo Bay. In Ise Bay and Kagoshima Bay it sometimes occurs with an extreme anomaly. The greatest anomaly is 3.14 m at Nagoya in Ise Bay. The next is 3.1 m at Osaka. On the coasts facing the Pacific directly, the maximum anomaly is 1 m or so, and the area of abnomal rise is also limited. On the Japan Sea side, the rising of sea level is not conspicuous and the anomaly has scarcely attained to 1 m, except a special case.

An example of disturbed water level in an island is indicated in Fig. 5, observed at Okada in Oshima. The rise in level with the approach of the typhoon coincided roughly with the effect of fall of barometric pressure as expected. The anomaly was 36 cm and the pres-

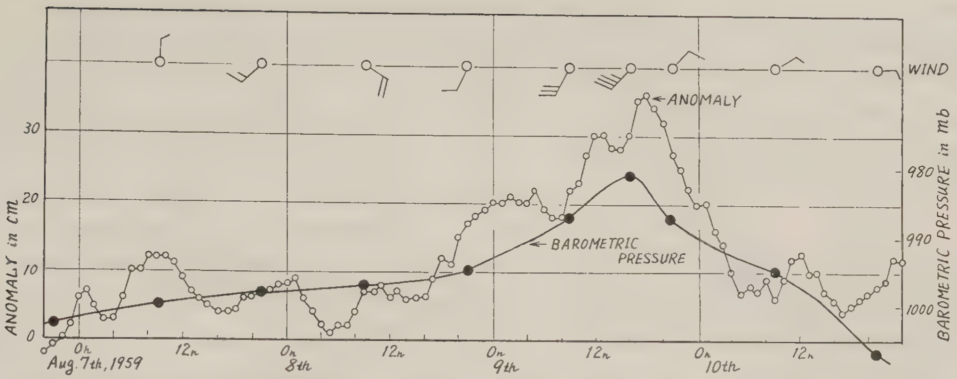

Fig. 5 The anomaly of sea-level at Okada in Oshima (island) due to the typhoon No. 5906. The wind and pressure were observed at the Oshima Weather Station.

Table 5. Number of typhoons which landed at respective regions (1927–1955)

Region at which the typhoon landed	Kyushu	Shikoku to Kii	Kii to Kanto	not landed	total
Number of the typhoon	21	14	8	5	48

sure fall in the island 24 mb. On the coast of island, it is usual that the rise of water level due to storm is very small, and the effect of wind is less important than that of atmospheric pressure contrary to the shallow waters.

Table 5 represents the number of typhoon, which landed at respective district and caused the rise of sea level, since 1927 to 1955. Generally storm tides tend to occur more frequently in the western Japan than in the eastern Japan, and it is partly attributed to that the number of typhoon which lands at the former is more than at the latter.

In the whole country, the number of storm tide with an anomaly more than 2 m is seven for the past sixty years as shown in Table 4, and that with an anomaly more than 1 m is fourteen for fourteen years. Thus in our country, on the average, we can roughly expect the storm tide with an anomaly more than 2 m once per about nine years, and that with an anomaly more than 1 m once per year.

The probability of anomaly in water level with which storm tide occurs was computed by Miyazaki at four important harbours. According to him, for example, at Osaka where the violent storm tide is most frequent in our country, the yearly maximum anomalies which exceed 0.5, 1.0 and 2.0 meters are expected once per 0.7 years, 3 years and 34 years, respectively.

V. TRACKS OF TYPHOON, OCCURRENCE TIME AND EXTENT OF STORM TIDE

Tracks of five typhoons which caused significant storm tides at Tokyo Bay, Ise Bay, Osaka Bay and Ariake Sea are indicated in Figs. 6 A, B, C, and D, respectively. We clearly find that the strong storm tide always occurs when a typhoon passes to the left of the bay. When the typhoon takes other pathes, the storm tide does not develop. This fact, pointed out by many investigators, is very noticeable. The circumstances are recognized more quantitatively in Table 6 obtained by Miyazaki, representing the relations among the typhoon track and surge characteristics at Kobe. Consider the case when a typhoon progresses through the left of bay toward the north or the northeast. According as the approach of the storm the

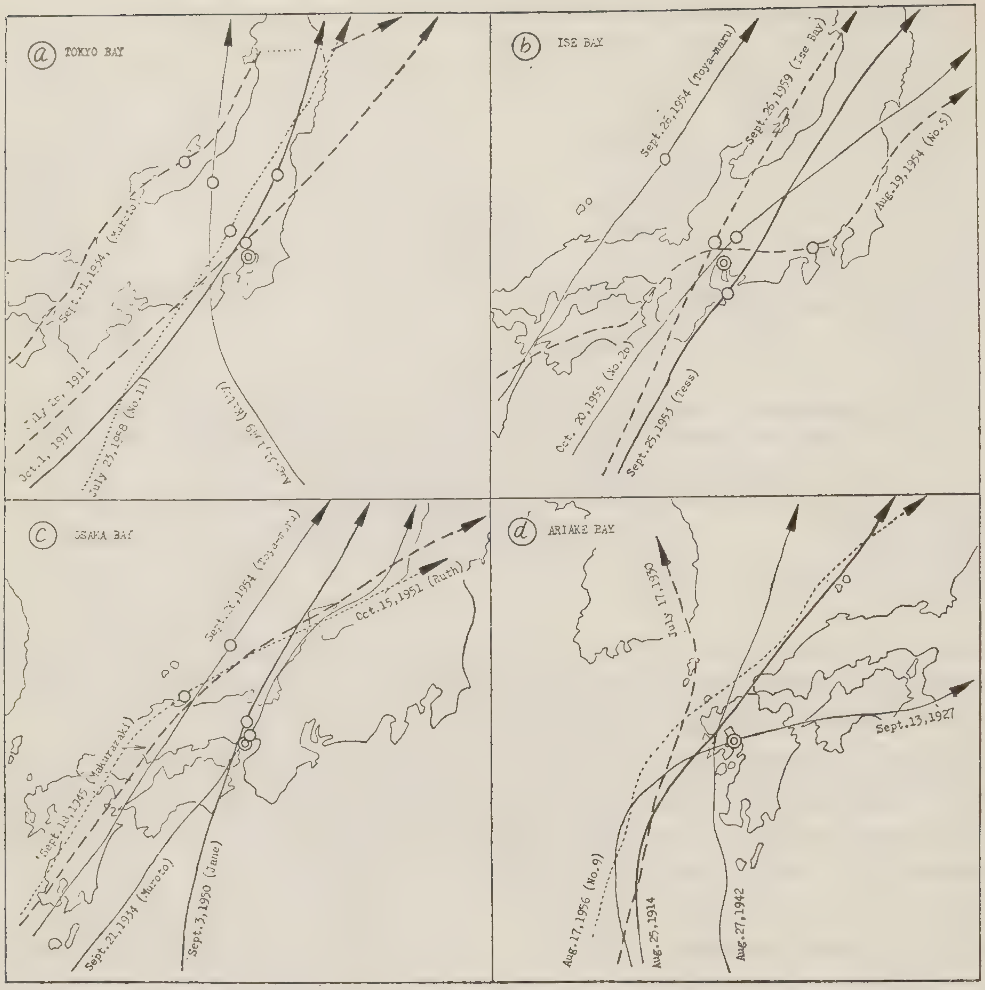

Fig. 6 Tracks of typhoons which caused conspicuous storm tides at respective places; Tokyo, Nagoya, Osaka and Ariake Bay. Small circles on the tracks indicate the position of typhoon when the maximum anomaly appeared at the place concerned.

Table 6. Storm tides caused by typhoons with various tracks. (observed at Kōbe during 1940-54) (after Miyazaki)

Track	Explanation	Number of Surges	Average		Number of typhoons	Probablity of occurrence
			Anomaly	Depth		
I	Left of Kōbe, within 500 km	2	72 cm	955 mb	12	0.17
II	〃 within 300 km	7	93 cm	968 mb	27	0.30
III	Close to Kōbe, Within 30 km	4	113 cm	973 mb	8	0.50
IV	Right of Kōbe, within 300 km	0	—	—	22	0.00

wind turns from east to south, increasing its velocity rapidly. Then, the wind reaches maximum with the speed more than 30 m/s or sometimes 40 m/s. This extremely strong southerly wind blowing over the bay derives sea water within the bay towards the northern coast. At the same time, the deep fall of barometric pressure causes the suction of sea water dynamically. In addition to them, the inflow of sea water from the open sea into the bay is considerably important, though details have remained unknown. In the case of Ise Bay typhoon, Kunishi and Yoshida [1960] suggested that the ratio of the effect of wind, barometric pressure and inflow on the storm surge at Nagoya is 2 : 1 : 1.

Occurrence time of peak in water level depends upon the track and speed of storm, the height of astronomical tide and geographical features. Based upon the data for seven developed typhoons, we may say statistically as follows: Tidal stations at which the peak in water level occurred before the arrival of storm center occupied 28% of all stations, stations at which the peak did near the arrival of storm center 16%, and stations at which the peak did after the arrival of storm center 56%.

In the case of remarkable storm tide, it is usual that the southerly wind reaches maximum immediately after the arrival of center, but the maximum anomaly of sea level occurs a little after the arrival of center. The retardation of the maximum anomaly after the occurrence of the strongest wind is an hour or so in Tokyo Bay and Osaka Bay, though its value varies depending upon the circumstances.

Table 7 shows the relation between the central pressure of typhoon and the farthest distance to which the damages due to the storm tide extend.

Table 7. Relation between the central pressure of typhoon and the farthest distance to which the damages due to storm tide extend.

Central pressure of typhoon (mb)	980>	970>	960>	950>	945>
Farthest distance (km)	100	200	300	400	500

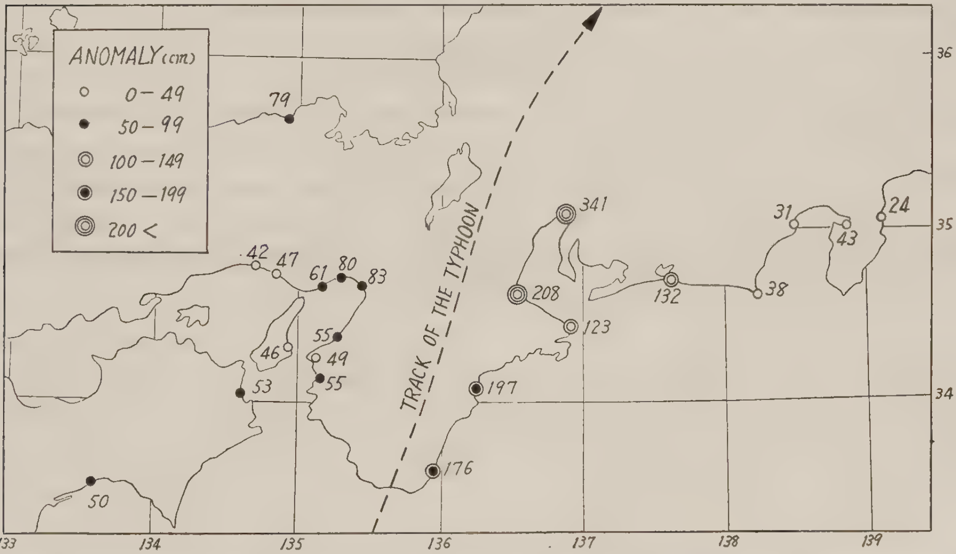

Fig. 7 Distribution of storm tides due to Ise Bay typhoon (Sept. 26, 1959). The date are due to "Report of the typhoon Ise-wan", Bull. Kobe Marine Obs. No. 165, 1960.

The area of damages becomes wide as the typhoon does strong. Fig 7 gives the distribution of storm tide when a remarkably developed typhoon attacked the central Japan. The asymmetry of the distribution is clearly recognized.

Now, let us consider distances from the storm center to tidal stations located within a region where the anomaly of storm tide is over 1 m. Frequency of such distances for fourteen typhoons since 1945 to 1958 is summarized in Fig 8, in which a positive sign means that the storm traveled to the left of the station and a negative sign shows the opposite course. Therefore, it is said that the storm tide whose anomaly exceeds one meter appears

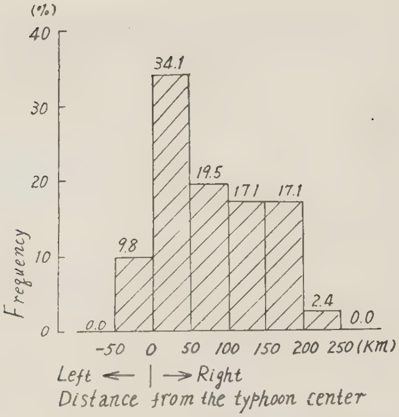

Fig. 8 **Extent of storm tide whose anomaly exceeds 1 m. Ordinate shows the number of tidal stations located within this extent.**

almost always within 200 km in the right region of the typhoon center and within 50 km in the left region.

Moreover, the anomaly of storm tide increases generally from the entrance toward the head of bay (Fig 7). But, when the typhoon takes an abnormal track the distribution is considerably complicated. Effect of shear-line in a typhoon and hurricane seems also to be important, as Wadati and Hirono [1954] and Redfield and Miller [1957] emphasized. But the sufficient analysis has not been done yet in the case of typhoon.

REFERENCES

Miyazaki, M. [1957] : On storm surges which recently struck the Japanese coast. Oceanogr. Mag. Vol. 9, pp. 209–225.

Redfield, A.C. and A.R. Miller [1957] : Water levels accompanying Atlantic coast hurricanes. Meteor. Monogr. Vol. 2, pp. 1–23.

Wadati, K. and T. Hirono [1954] : Storm tides caused by typhoons. Proc. UNESCO Symp. on Typhoons, Jap. Nat. Comm. for UNESCO, Tokyo, pp. 31–48.

ON STORM SURGES CAUSED BY THE ISE BAY TYPHOON AND THEIR THEORETICAL COMPUTATIONS

*Masamori Miyazaki**
*Sanae Unoki***
*Takeo Ueno****

I. STORM SURGES CAUSED BY THE ISE BAY TYPHOON

A severe typhoon "5915" struck the coast of Ise Bay and its neighbourhood on September 26, 1959. Enormous surges were generated in this bay, and more than 5,000 lives were lost at that time. This typhoon was thus called by the name "Ise Bay Typhoon".

The highest sea level was 3.89 m above T.P. (Standard mean sea level of Tokyo Bay) at Nagoya; the corresponding departure or the storm-surge height is 3.41 m, which exceeds the prior record of 3.1 m. The last value was observed at Osaka during the pass of the Muroto Typhoon in 1934.

Fig. 1 shows the tide-gauge record of Nagaya in this period. The full line is the observed curve, and the dotted lines are the predicted curve and the estimated tidal curve after the break of the record, respectively. The departure was already remarkable from about noon, when the wind speed was 10 m/sec or more. At about 19 h, the wind speed exceeded 20 m/sec, and the departure increased rapidly. The highest sea level was recorded at 21 h 35 m, which was slightly after the instant of lowest pressure 21 h 27 m. The highest level was 3.89 m above T.P. as already expressed, and was 5.31 m above the standard level of the Nagoya Harbour. The designed height of coastal embankments was then 4.80 m above this level, and most of them were flooded at that time.

Fig. 1 also shows a sharp peak of the storm surge, which suddenly rise and fall with the typhoon approach. The record breaks at about 22 h 30 m by the obstacles, and the tidal curve after it is estimated from the record of the neighbouring river-side station, Otōbashi, and actual measurements in the tidal well.

Table 1 indicates the distribution of highest sea levels along the coast of Ise Bay, which were observed by tide gauges. It shows that the maximum heights are generally increasing from mouth to depth of bays, and that they exceed 2 m above T.P. in the most part of this area.

Table 1 Highest sea levels recorded by tide gauges (above T.P.)

Station	Time	Sea level	Highest level in the case of Typhoon 5313
	h m	(cm)	(cm)
Toba	20 26	188	204
Matsuzaka	20 05	222	263
Nagoya	21 35	389	233
Morozaki	21 30	190	—
Maeshiba	22 40	204	282
Fukue	21 58	212	250
Konakayama	21 55	217	—

---

* Japan Meteorological Agency
** Meteorological Research Inst.
*** Japan Meteorological Agency

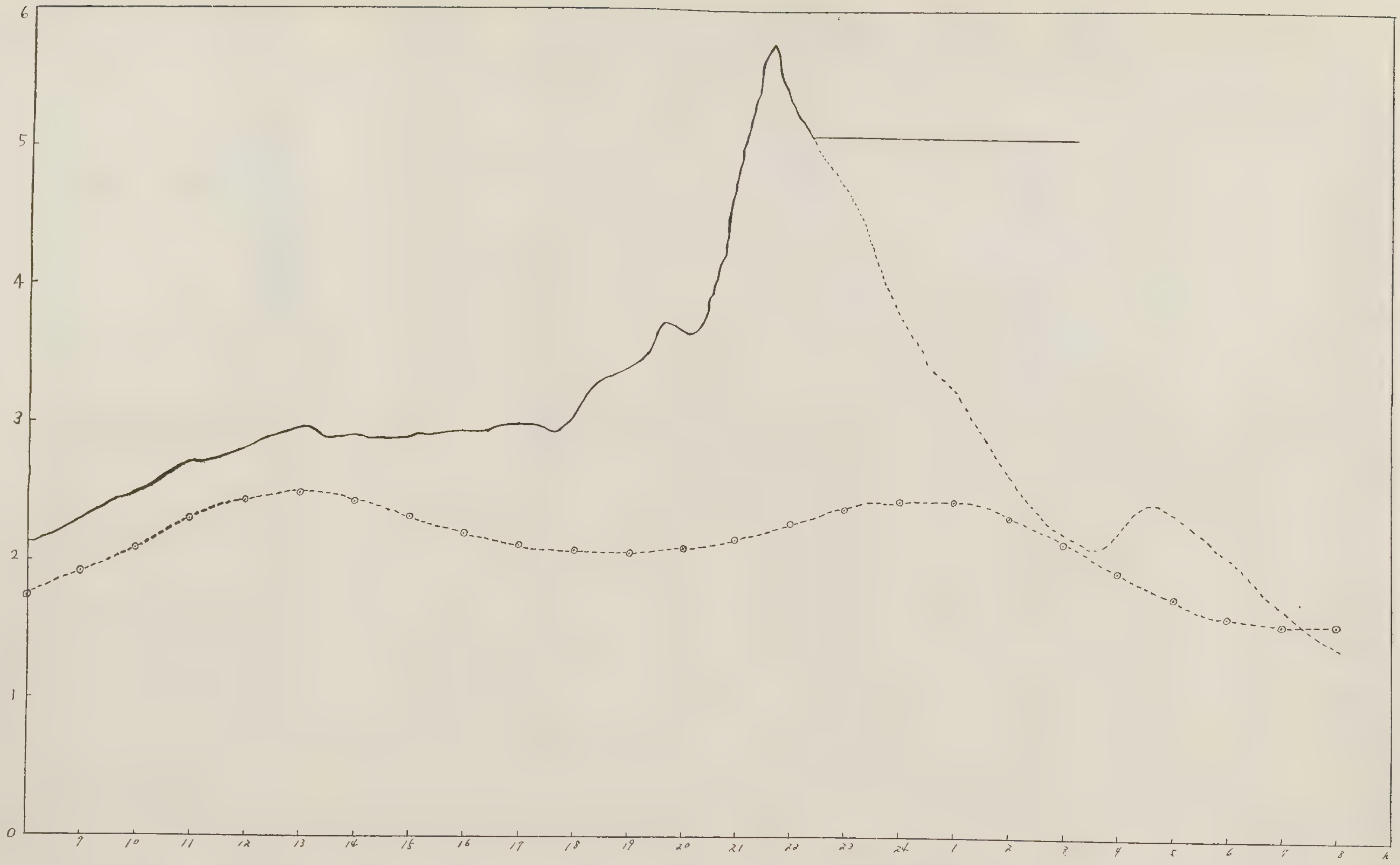

Fig. 1 Tidal curve at Nagoya during the passing of Ise Bay Typhoon.

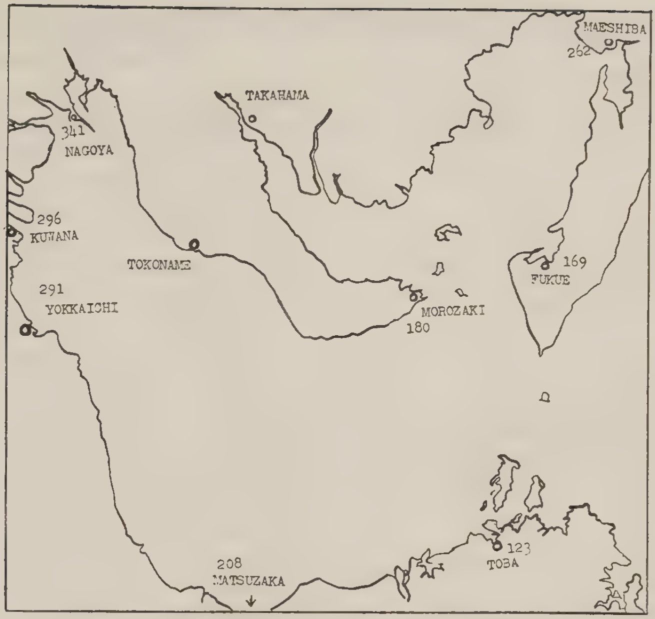

Fig. 2 Distribution of storm-surge heights (cm).

II. DISTRIBUTION OF STORM SURGES

Fig. 2 shows the distribution of storm-surge heights computed from these data. The pattern fairly resembles to that of highest levels. Storm surges are also large in the depth of bays. For instance, they are 3.41 m at Nagoya and 2.61 m at Maeshiba, while it is only 1.23 m at Toba located near the mouth.

It is now to be noted that all of these stations are located to the right side of the typhoon track. Therefore, variations of the wind direction are all clockwise east to south in this area, and they drift the sea water inward to the depth of bays.

The track of the Typhoon was nearly parallel to the main axis of Ise Bay, and about 60–100 km westward from it. Unfortunately, for the case of the Ise Bay Typhoon, the wind maximum zone was 60–100 km shifted eastward from the center, and the circumstances were very serious to enlarge storm surges in this area.

In Table 1, we also show the highest levels in the case of the Typhoon 5313, which passed through the east part of Bay on September 25, 1953. The sea levels were rather higher in this case than in ours near the mouth. It is chiefly because the Typhoon 5313 struck this area nearly with the high water of springs.

III. NUMERICAL COMPUTATIONS

Undoubtfully, it will be one of the most important problems for us to investigate the numerical relations among storm surges and meteorological conditions.

In these hundred years, the empirical formulas have been used for this purpose. These formulas are fairly useful in order to estimate the maximum surge. For instance, MIYAZAKI (1956) obtained the following formula for the maximum surge of Nagoya.

$$h=1.6743(P_0-P)+0.16534\,V^2\cos\theta \cdots\cdots(3.1)$$

where h is the maximum surge in cm, P is the lowest pressure in mb, P_0 is the monthly mean pressure in mb, V is the maximum wind speed in m/sec, and θ is the angle between

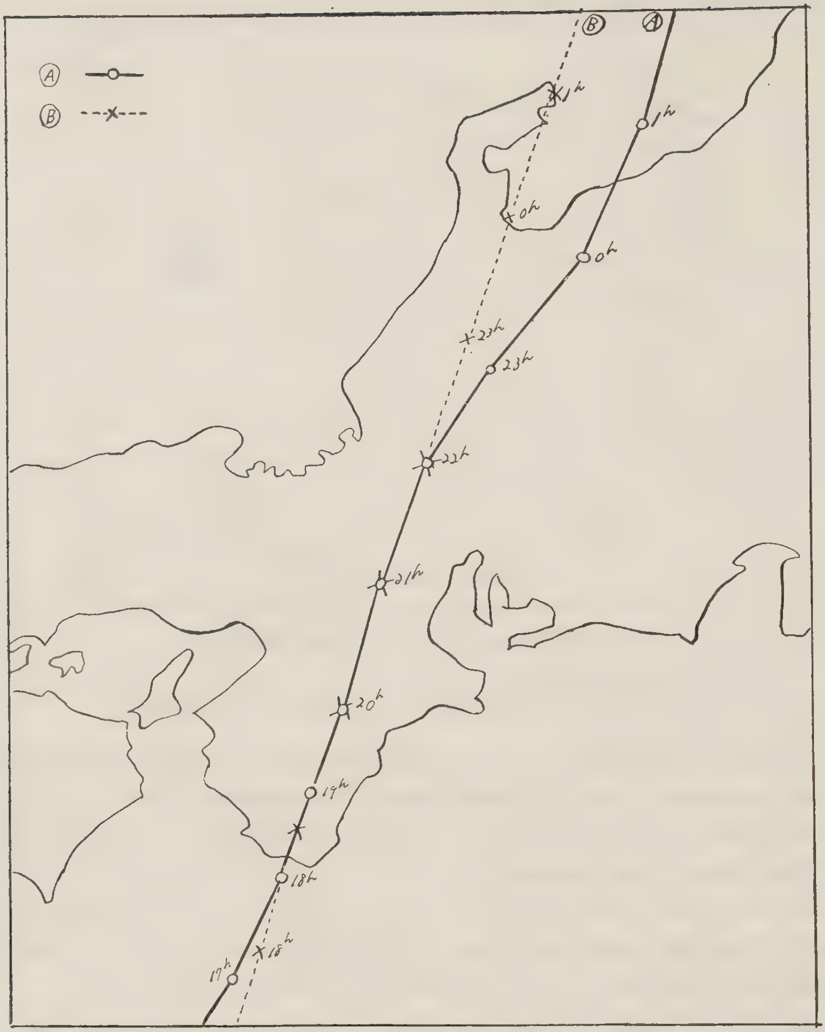

Fig. 3 Observed and computed tracks of the Ise Bay Typhoon.

wind and the main axis of Ise Bay (SSE), respectively. This formula was given from 11 surge records, and its probable error is 16 cm. For the case of Ise Bay Typhoon, we have $h=320$ (cm), which is in fair agreement with the observation.

However, the empirical formulas are only useful to estimate the maximum surges at selected points. We can obtain no knowledge on the distribution of surges in time or space from them. The solution of dynamic equations will be necessary for this purpose.

Such theoretical investigations have been also made in these fifty years. Great developments were made in Japan after the Muroto Typhoon in 1934, which struck the coast of Osaka Bay and generated heavy surges in this bay. However, the theoretical computations always require some simple assumptions, and they are not always in good agreement with the actual conditions. These discrepancies will be greatly improved by the modern development of electronic computers. These computers have been also used in Europe and U.S.A. for the computation of storm surges in these few years (HANSEN (1956), PLATZMAN (1958)).

We have here tried to compute the storm-surge distributions for our case by the computer IBM 704, and to estimate the variations of surges by embankments which will be buit outside of the Nagoya Harbour.

IV. BASIC EQUATIONS AND BOUNDARY CONDITIONS

The basic equations are as follows :

$$\left.\begin{aligned}\frac{\partial u}{\partial t}&=-g\frac{\partial}{\partial x}(\zeta-\zeta_0)+\nu\frac{\partial^2 u}{\partial z^2},\\ \frac{\partial v}{\partial t}&=-g\frac{\partial}{\partial y}(\zeta-\zeta_0)+\nu\frac{\partial^2 v}{\partial z^2},\\ \frac{\partial \zeta}{\partial t}&=-\int_{-\zeta}^{h}\left(\frac{\partial u}{\partial x}+\frac{\partial v}{\partial y}\right)dz\end{aligned}\right\}\cdots\cdots(4.1)$$

where x, y, z are the rectangular coordinates, and z axis is taken downwards from the mean surface. t is the time, u, v are the velocity components, ζ is the surface elevation from the mean surface, ζ_0 is the static elevation produced by the pressure fall, h is the water depth, and ν is the vertical eddy viscosity, respectively.

Now, integrating (4.1) with respect to z from surface to bottom, we obtain

$$\left.\begin{aligned}\frac{\partial S_x}{\partial t}&=-gh\frac{\partial}{\partial x}(\zeta-\zeta_0)+\tau_s^{(x)}-\tau_b^{(x)},\\ \frac{\partial S_y}{\partial t}&=-gh\frac{\partial}{\partial y}(\zeta-\zeta_0)+\tau_s^{(y)}-\tau_b^{(y)},\\ \frac{\partial \zeta}{\partial t}&=-\frac{\partial S_x}{\partial x}-\frac{\partial S_y}{\partial y},\end{aligned}\right\}\cdots\cdots(4.2)$$

where S_x, S_y are components of the volume transport, and τ_s, τ_b are the surface and bottom stresses, respectively. The suffices (x), (y) denote the x and y components of stresses. The Coriolis term, and inertia terms are here disregarded.

In (4.2), ζ_0 is given from the surface pressure, τ_s is given from the surface wind, and τ_b is given from the current profile near the bottom, respectively. The functional forms of τ_s and τ_b are now necessary for the computations.

For the surface stress, we have a famous formula

$$\tau_s=3.2\times10^{-6}W^2 \cdots\cdots(4.3)$$

where W is the wind speed in cm at the anemometer height. This formula is ascertained by several authorities, and is believed to be agreeable for the wind speed from about 6 m/sec to about 20 m/sec. According to the recent measurements, the coefficient 3.2×10^{-6} is likely to be too large for smaller wind speeds in this region. However, we have now no knowledge how to estimate this coefficient when the wind speed is more than 20 m/sec. We have thus assumed that (4.3) holds in our case.

The bottom stress τ_b is more difficult to estimate. When the flow is nearly independent of the depth except near the bottom, we shall have

$$\tau_b=\gamma\,\rho_w|\boldsymbol{V}|\boldsymbol{V}\cdots\cdots(4.4)$$

where $\boldsymbol{V}$ is the mean flow vector, ρ_w is the water density, and γ is a constant. HANSEN (1956) used this formula for the case of storm surges by taking $\gamma=2.6\times10^{-3}$. However, for the case of storm surges, we have the vertical profile of flow, and this formula will be not always agreeable. YAMADA (1950) assumed that the vertical profile is the quadratic function with respect to the depth, and derived the following formula

$$\tau_b=-\frac{\tau_s}{2}+\frac{3\nu \boldsymbol{V}}{h}\cdots\cdots(4.5)$$

This formula is given under the assumption of constant eddy viscosity, and discrepancy may occur from this assumption. However, in the case of shallow water surges, we shall often find remarkable vertical profiles of flow, and (4.5) will be more agreeable than (4.4). We adopted the formula (4.5) for the bottom stress as long as it is not neglected.

The boundary condition at the coast is taken as

$$S_x = S_y = 0 \cdots\cdots\cdots\cdots\cdots\cdots\cdots\cdots\cdots\cdots\cdots\cdots \quad (4.6)$$

for the natural boundaries. The parallel flow will be present at the vertical wall provided that the slip exists along it.

Lastly, the mouth condition is one of the most important problems. The anomalies from statical elevations will be not negligible even at the mouth. The edge waves, shelf seiches, and the direct transport from the typhoon area will be the causes of these anomalies. However, we have no sufficient knowledge on these problems. We now extend the region of computation as offwards as possible, and assume the statical elevation at the off-side edge.

V. METEOROLOGICAL CONDITIONS

Our next problem is to compute the external forces, which are given from the pressure and wind distributions. One of the most important factors in our case will be the winds

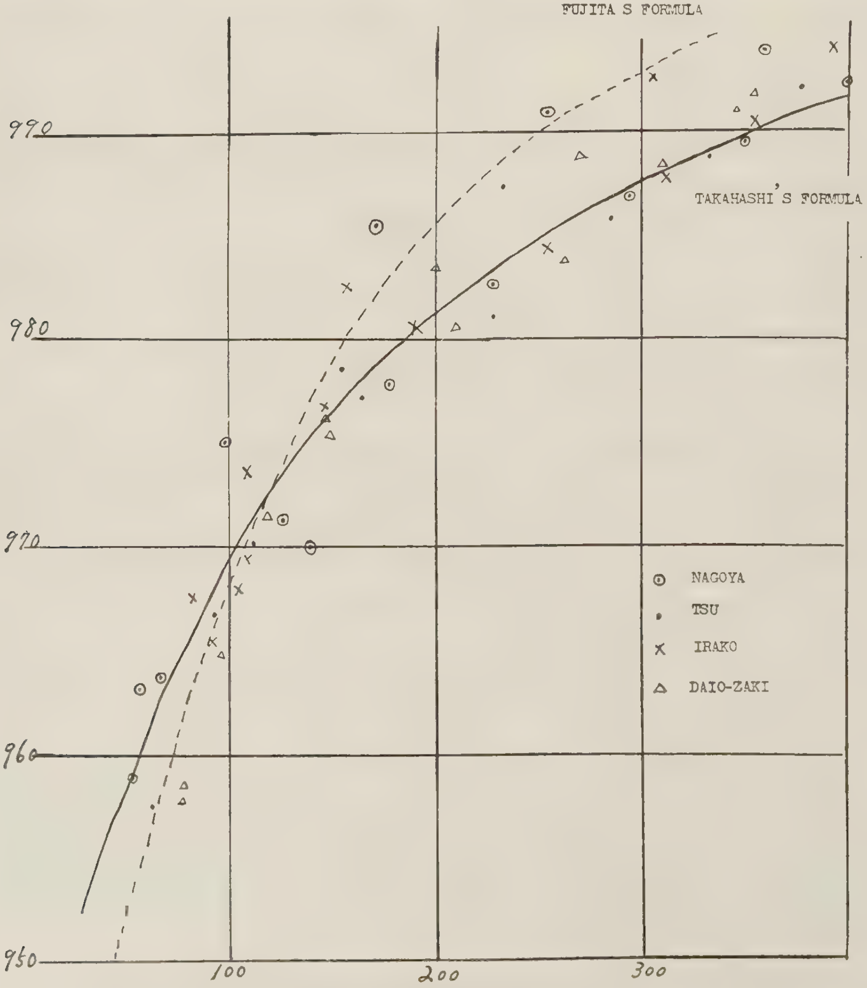

Fig. 4 Pressure distribution as the function of the central distance.

blowing over the sea. However, they are not obtained in our case. We only have the data at four coastal stations in this area. Therefore, we have no way to estimate the winds on the sea except for computing them theoretically from coastal data. The wind speed in the typhoon area will be theoretically approximated by the formula of gradient winds, which are the function of the pressure distribution. Then, the pressure distribution is of important for our purpose.

The pressure pattern in the typhoon area is usually given as the function of the distance from its center. Many formulas are obtained. Among them, Takahashi's formula (TAKAHASHI 1939) seems to be most suitable for our purpose, since this formula is in good agreement with the observation with the exception of the central area. The Ise Bay Typhoon passed fairly westward of the computing area, and the discrepancy in the central area will be not important.

Provided that P_∞ is the outside pressure, r_0 is a constant distance, and a is the maximum pressure fall at the center, we have

$$P = P_\infty - \frac{a}{1 + r/r_0} \qquad \cdots\cdots(5.1)$$

according to him. We have $P_\infty = 1010$ (mb), $a = 80$ (mb), and $r_0 = 105$ (km), for the case of the Ise Bay Typhoon. Fig. 4 shows the variations of the observed and computed pressure with the central distance.

The Fujita's formula (FUJITA 1952)

$$P = P_\infty - \frac{a}{\sqrt{1 + (r/r_0)^2}} \qquad \cdots\cdots(5.2)$$

is believed to hold approximately in the whole area, and this formula will be better than Takahashi's when the typhoon center passes through the computing area. The constants are $P_\infty = 1010$ (mb), $a = 70$ (mb), and $r_0 = 75$ (km) for our case.

The decay of the typhoon will be also not negligible in our case. The decay of the typhoon depth was nearly 10 mb per 3 hours. We assumed here that the depth decreased exponentially with this rate.

The wind distribution is, in general cases, not the function of the central distance only. The wind speed is stronger in the right side of the typhoon than in the left side of it. However, for our case, the typhoon passed to the left of Ise Bay; all regions are in her dangerous side, and the wind directions are nearly similar at the same instant.

From this view-point, we first suppose that the wind speed is approximated by the gradient-wind law, and that the wind direction is the function of time only. We now assume that

$$W = \frac{rf}{2}\left\{-1 + \sqrt{1 + \frac{4}{\rho a r f^2}\frac{\partial p}{\partial r}}\right\}, \qquad \cdots\cdots(5.3)$$

where $\frac{\partial p}{\partial r}$ is given from (5.1) (or (5.2)). Fig. 5 shows the variations of the observed and computed wind speeds with the central distance.

According to this figure, the wind speed can be approximated by (5.1) and (5.3) before the approach of the typhoon center, but the formulas fail to explain the observations fairly after her passing away. It is shown from these results that our method of the wind estimation will be agreeable as long as problems are concerned with the forerunners and typhoon surges excepting their tails.

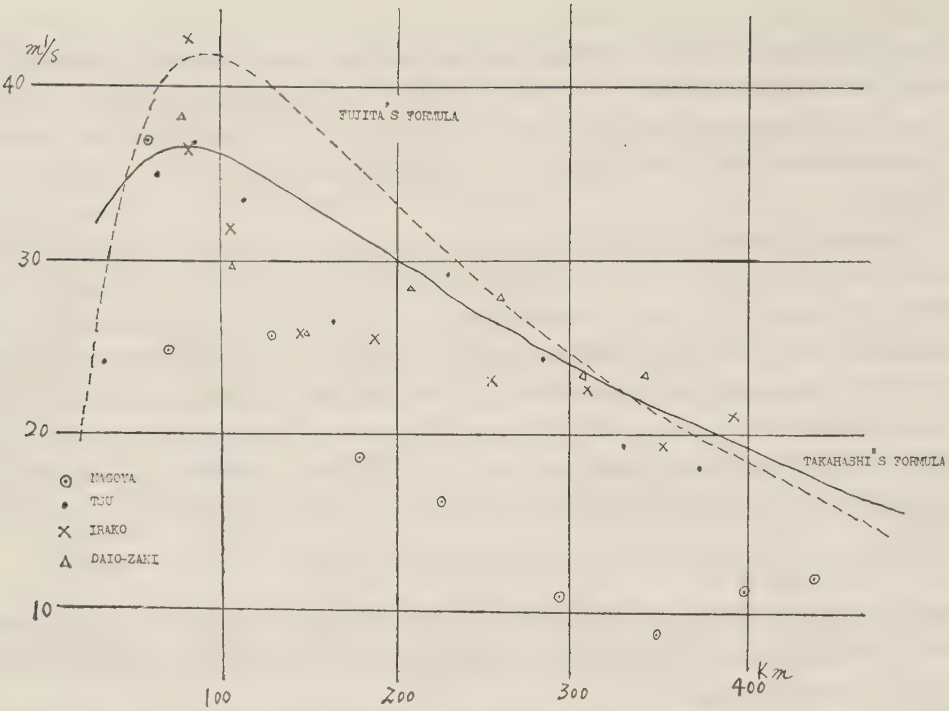

Fig. 5 Wind-speed distribution as the function of the central distance.

However, the above method is not for the general use. We next suppose that the wind in the typhoon area consists of two parts. One is the symmetric wind, which blows in against the pressure contour with the angle 30°. Its speed is assumed to be proportional to the gradient wind. Another is the field wind, which is proportional to the typhoon movement. The field wind is also assumed to decrease exponentially with the central distance, since it will be absent fairly outside of the typhoon.

VI. RESULTS OF COMPUTATIONS

The numerical computations have been made by rewriting the formulas (4.2) as the form of the difference equations, the computing area being also given by the net of grid points of 2 km interval. From these difference equations, we obtain the value $\Delta S/\Delta t$, say, by computing the space differences and external forces in the right hand terms. We here adopt the central differences, and the transport components are given at time steps t_0, $t_0+2\Delta t$, $t_0+4\Delta t$,…… at the grid points of 4 km interval, and elevations are given at time steps $t_0+\Delta t$, $t_0+3\Delta t$, $t_0+5\Delta t$,…… at the intermediate grid points, respectively. It is well known that the stability condition of computation

$$\frac{\Delta S}{\Delta t} > \sqrt{2gh_{\max}} \cdots\cdots\cdots\cdots\cdots\cdots (6.1)$$

must hold in our case. Since $h_{\max}=60$(m), we have $\Delta t<58$(sec). We take $\Delta t=54.5$(sec) in our computations.

The results of computations are shown in Figs. 6–10. Figs. 6 and 7 are the distributions of the computed surges and transports at the time 21 h 30 m, where we disregard the bottom stress. The wind direction is here assumed to be the function of time only. The computed surge height is in good agreement with the observation at the depth of bays. We also find from Fig. 7 strong southward transport in the middle of Ise Bay. This transport con-

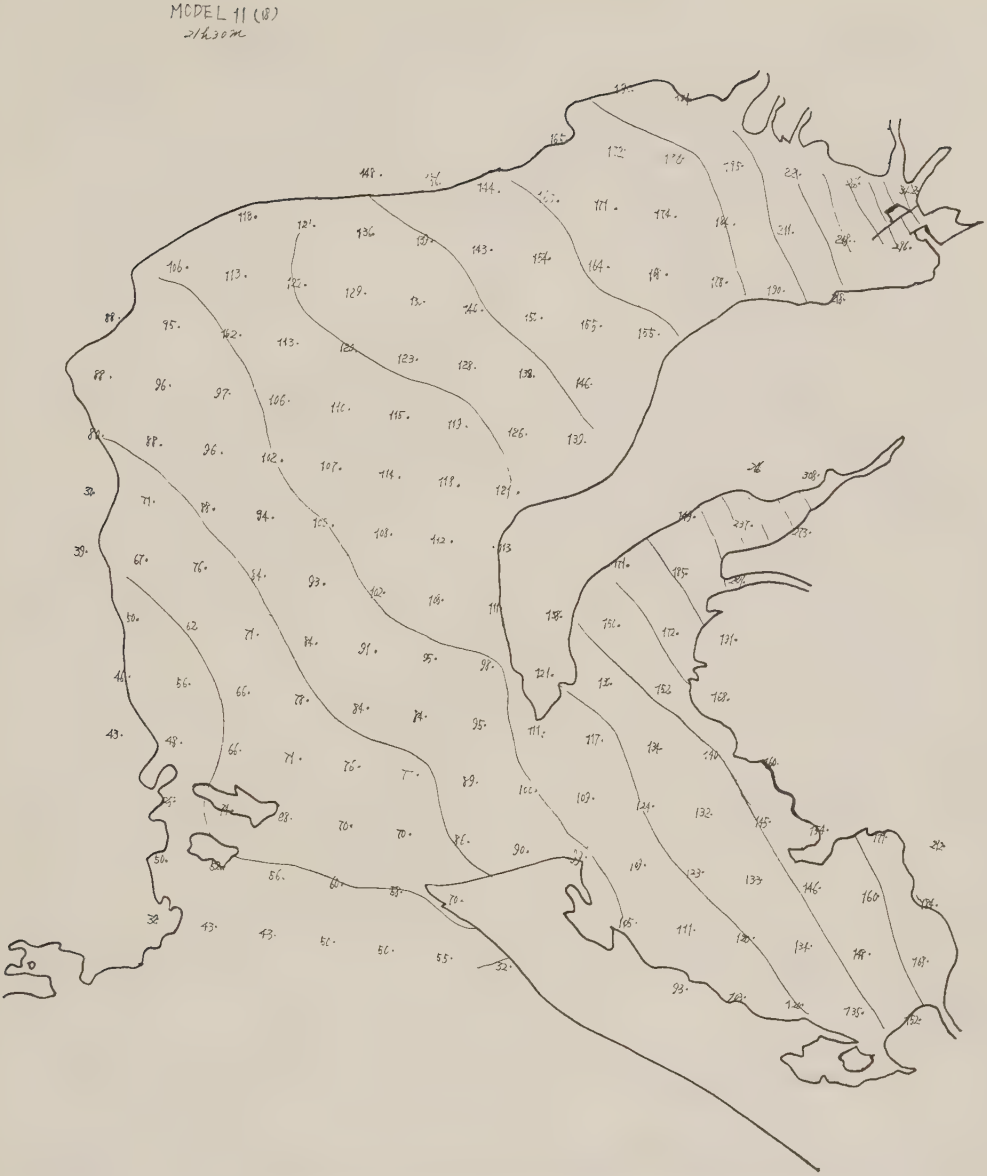

Fig. 6 Horizontal distribution of the computed surge.

tinues almost throughout the computed period.

Fig. 8 shows the computed variations of surges at Nagoya for three models. In Model 11 we neglected the bottom stress, and in Model 1 we assumed Yamada's law for the bottom stress. In both cases, the wind direction was assumed to be the function of time only. In Model 13, the Yamada's law was assumed, and the wind was supposed to consist of two parts. The observed curve is also plotted in this figure. Fig. 9 shows the corresponding variations at Maeshiba. Figs. 8 and 9 show that the agreement between computations and observations is fair. When we disregard the bottom stress, the phase of maximum is in good agreement with the observation, but seiches are fairly larger than that. In contrast with it, when we count in the bottom stress, the phase of maximum rather lags, but the patterns seem to be more consistent with observations.

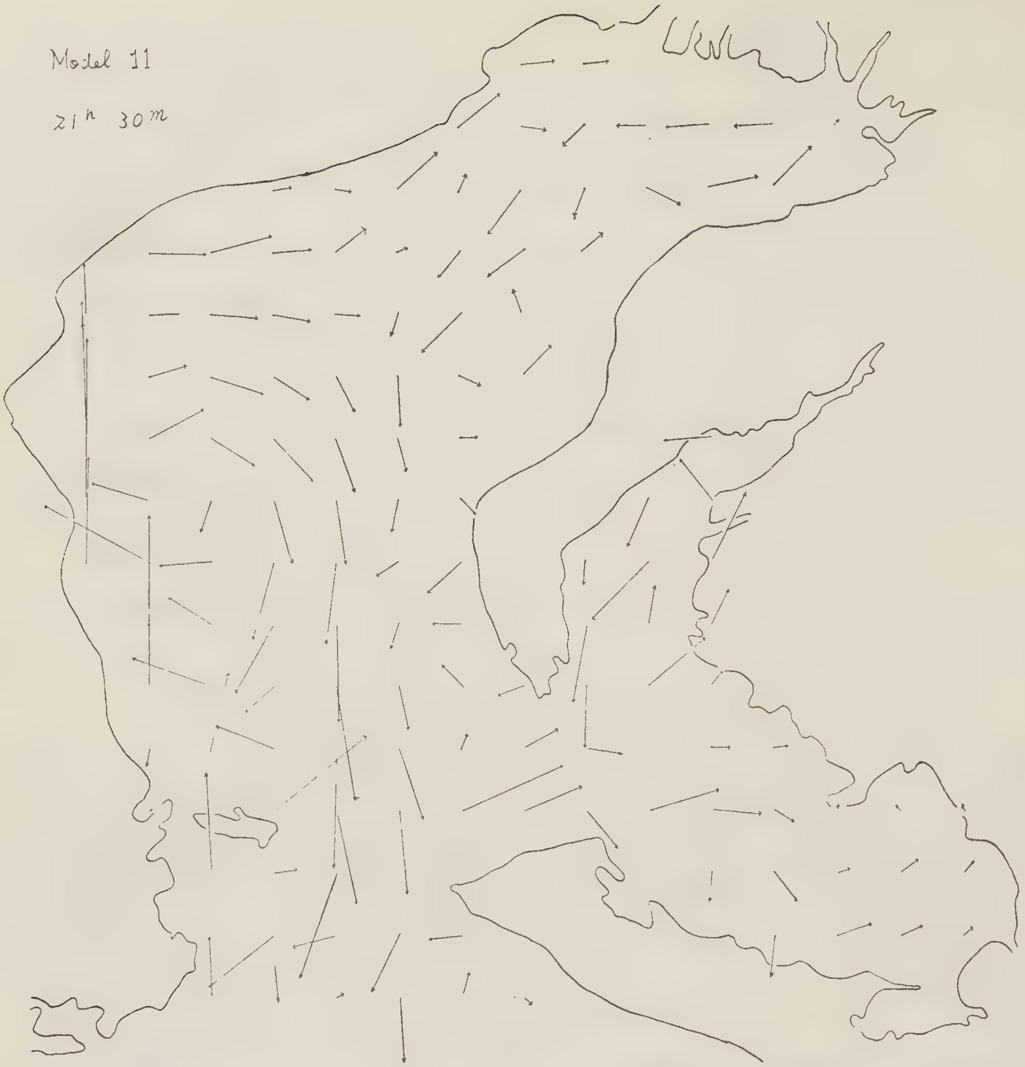

Fig. 7 Horizontal distribution of the volume transport accompanied with the surge.

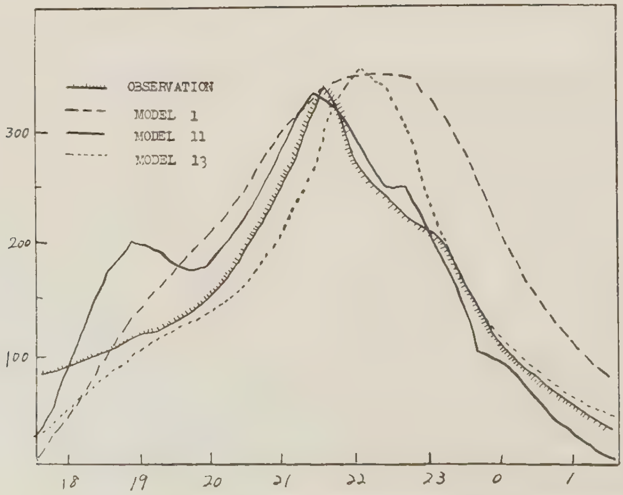

Fig. 8 Variations of the computed surges for several models (Nagoya).

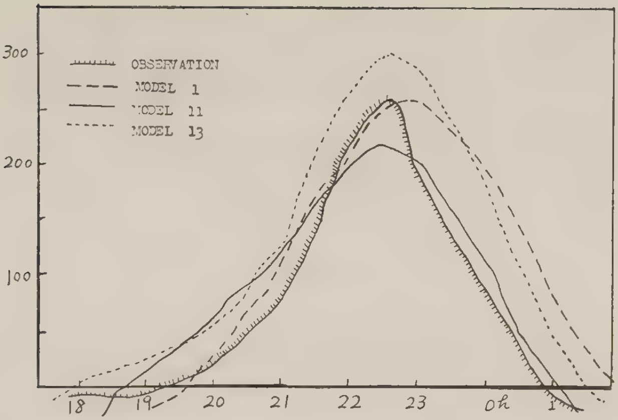

Fig. 9 Variations of the computed surge for several models (Maeshiba).

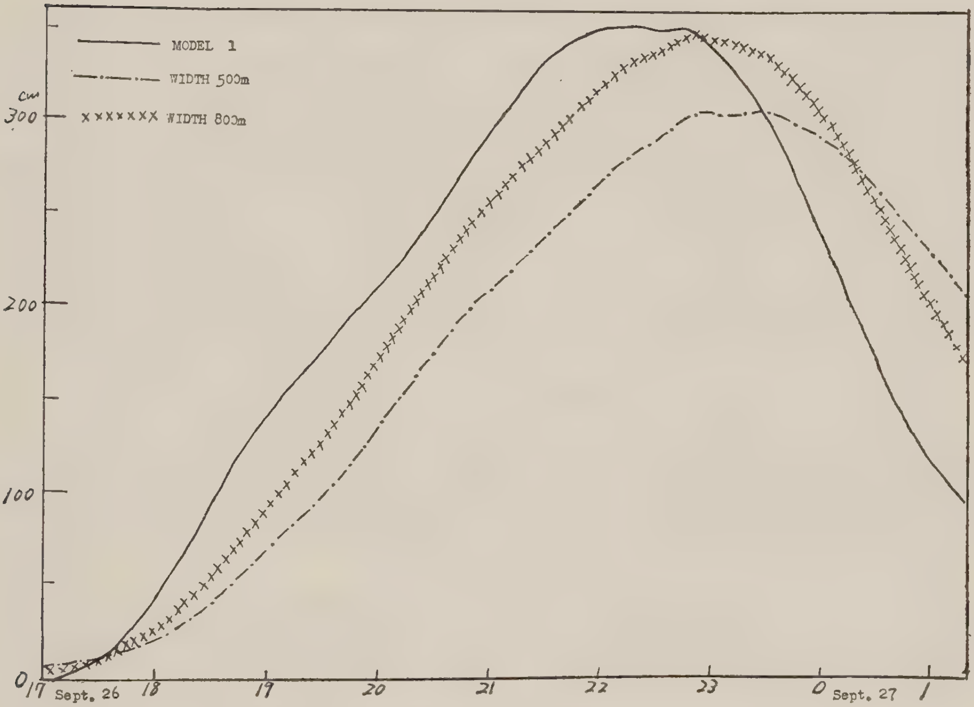

Fig. 10 Effects of embankments for surge heights at Nagoya.

Lastly, we have estimated the effects of the embankment, which will be built outside of the Nagoya Harbour. Fig. 10 is the computed surge variations at Nagoya for three cases. The width of the gate is taken to be (i) very large, (ii) 800 m, and (iii) 500 m in these cases. Case i corresponds to Model 1. The assumptions in Model 1 are commonly used in these computations. Fig. 10 shows that the elevation decrease will be about 50 cm when the gate width is 500 m, but merely 10 cm or so when the gate width is 800 m.

REFERENCES

1) Fujita, T. [1952] : Pressure distribution in typhoon. Geophys. Mag. **23**.

2) Hansen, W. [1956] : Theorie zur Errechnung des Wasserstandes und der Stroemungen in Randmeeren nebst Anwendungen. Tellus. **8** (3).

3) Miyazaki, M. 〔1956〕: On storm surges which recently struck the Japanese coasts. Proc. of 3rd Conf. on Coastal Engineering in Japan (In Japanese)

4) Platzman, G.W. 〔1958〕: Numerical computation of the surge of 26 June, 1954, on Lake Michigan. Geophysica **6** (3/4).

5) Takahashi, K. 〔1939〕: Pressure and wind-speed distributions in the typhoon area. Journ. Met. Soc. Japan. **17**. (In Japanese)

STABILITY OF THE BREAKWATER AGAINST SLIDING DUE TO PRESSURE OF BREAKING WAVES

*Taizo Hayashi**
*Masataro Hattori***

SYNOPSIS

Theoretical study on the shearing force which should act between horizontal joint surfaces due to the impact of the breaking wave. Suitable dimensionless parameters are used throughout.

I. INTRODUCTION

Stability of the breakwater against sliding due to waves has been examined by the statical condition $\mu W > P$, where μ is the coefficient of friction of the wall, W the weight of the wall, P the maximum horizontal force of the waves exerted upon the wall. In the case of breaking waves the same condition has been applied. Although the shock pressure of the breaking wave is sometimes much larger than the pressure of the clapotis, duration of the shock pressure is very short or rather instantaneous. Thus application of this statical condition is questionable.

In view of this the authors work out the theory on the shearing force which should act between horizontal joint surfaces due to dynamic horizontal force, thus examining the conventional condition of the stability.

II. ROCKING OF THE BREAKWATER

Breakwater is a massive structure loaded on a rubble mound ; due to its rigidity the deformation by either bending moment or shearing force is in fact quite negligible. Due to the considerable elasticity however, which the rubble mound has, rocking of the breakwater may exist.

Existence of such phenomenon of rocking is described in Minikin's book [1] ; the breakwater oscillates with the amplitude of 1° even under the action of non-shock type wave. The same phenomenon was observed at Haboro Harbour [2], where the period of oscillation was 0.2–0.3 sec.

The acceleration which the wall thus may subject to may "absorb" a portion of the instantaneous shock pressure and, as the consequence of that, the shearing force which does act on the plane under the action of the breaking wave is reduced by this amount.

III. SHEARING FORCE WHICH DOES ACT ON A SLIDING PLANE UNDER THE ACTION OF AN ARBITRARY WAVE

Let us consider firstly the case of the monolithic wall (Fig. 1). Let the x-axis be taken horizontally inward along the sliding plane to be considered, the origin of the axis at the middle point of the plane.

We make the following notations :

---

* Dr. Eng., Professor, Department of Civil Engineering, Faculty of Engineering, Chuo University, Tokyo
** Instructor, Depertment of Civil Engineering, Faculty of Engineering, Chuo University, Tokyo.

θ : angle of rocking
V : horizontal velocity of the center of gravity of the wall
t : time
P : instantaneous resultant pressure exerted upon the wall
F : instantaneous shearing resistance which does act on the sliding plane
m : mass of the wall
H : height of the point of application of the resultant pressure
L : height of the center of gravity of the wall
B : width of the base of the wall
E : coefficient of resistance of the foundation

The equation of horizonal motion of the center of gravity of the wall is :

$$m\dot{V}=P-F \quad \cdots\cdots (1)$$

where the dot represents differentiation with respect to time.

On the other hand the equation of rotation of the wall around Point O is

$$I\ddot{\theta}=P\cdot H-M \quad \cdots\cdots (2)$$

where

I : moment of inertia of the wall around Point O
M : resisting moment of the foundation

Assuming the perfect elasticity of the foundation, the bearing reaction of the foundation becomes as shown in Fig. 1. Then, the resisting moment of the bearing force is given by :

$$M=-\int_{-\frac{B}{2}}^{\frac{B}{2}}(E\,6\,x)\cdot x\,dx$$

$$=\frac{1}{12}EB^3\,\theta \quad \cdots\cdots (3)$$

or $$M=K\theta \quad \cdots\cdots (4)$$

where

$$K=\frac{1}{12}EB^3 \quad \cdots\cdots (5)$$

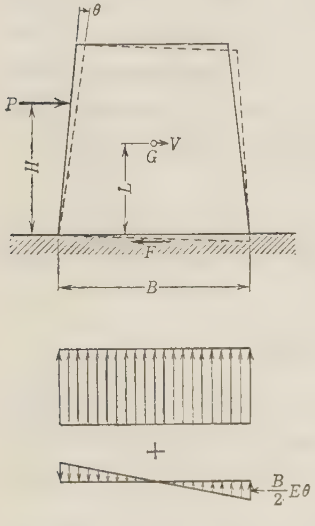

Fig. 1 Symbols

Substituting (4) in (2) and divinding through by I, we obtain

$$\ddot{\theta}+\frac{K}{I}\theta=\frac{P\cdot H}{I} \quad \cdots\cdots (6)$$

The general solution of the homogeneous equation associated with (6) is given by

$$\theta=C_1\sin\sqrt{\frac{K}{I}}t+C_2\cos\sqrt{\frac{K}{I}}t$$

where

$$\omega=\sqrt{K/I} \quad \cdots\cdots (7)$$

This constant is easily seen to be the angular velocity of the free oscillation (rocking) of the wall.

Substituting (7) into (6), we obtain

$$\ddot{\theta}+\omega^2\theta=\frac{P\cdot H}{I} \quad \cdots\cdots (8)$$

Meantime the kinematical relation between θ and V is :

$$V=L\cdot\dot{\theta} \quad \cdots\cdots (9)$$

Three unknown quantities V, θ and F are to be determined by the three equations (1), (8) and (9) thus developed.

Let us eliminate two variables, say V and θ, from these three equations :

Substituting (9) in (1) and dividing through by mL,

$$\ddot{\theta}=\frac{1}{mL}(P-F) \cdots\cdots (10)$$

Substituting (10) in (8), we obtain

$$\omega^2\,\theta=\frac{P\cdot H}{I}-\frac{1}{mL}(P-F)$$

$$=F\cdot\frac{1}{mL}+P\cdot\left(\frac{H}{I}-\frac{1}{mL}\right) \cdots\cdots (11)$$

Taking the notation

R : radius of moment of inertia around point O

$(I=mR^2)$

and putting

$$k=HL/R^2 \cdots\cdots (12)$$

we can rewrite (11) as :

$$\theta=\frac{1}{\omega^2\,mL}[F-(1-k)P] \cdots\cdots (13)$$

Assuming that the height of the point of application of the resultant pressure and, therefore, that the value of k remains constant with respect to time, we have from (13)

$$\ddot{\theta}=\frac{1}{\omega^2\,mL}[\ddot{F}-(1-k)\ddot{P}] \cdots\cdots (14)$$

Substituting (14) in (10), we obtain

$$\ddot{F}+\omega^2 F=(1-k)P+\omega^2\,\ddot{P} \cdots\cdots (15)$$

which is the fundamental equation for F ; integration of this ordinary linear differential equation of the second order (so-called oscillation equation) will give the solution of F.

Let us take the initial conditions as follows :

$$(\theta)_{t=0}=\theta_0 \cdots\cdots (16)$$

and $$(\dot{\theta})_{t=0}=\omega_0 \cdots\cdots (17)$$

By substituting (13) in (16) and (17), these equations are respectively rewritten as follows :

$$(F)_{t=0}=\omega^2\,mL\,\theta_0+(1-k)(P)_{t=0} \cdots\cdots (18)$$

and $$(\dot{F})_{t=0}=\omega^2\,mL\,\omega_0+(1-k)(\dot{P})_{t=0} \cdots\cdots (19)$$

These equations are the initial conditions to be imposed on the variable F.

IV. THE CASE OF SHOCK PRFSSURE

In order to examine the resisting behaviour against sliding of the wall under the action of an impulsive force, let us assume a function for P as follows :

$$P=P_m\frac{1}{K}e^{-2a(t/t_m)}\sin\left(a\frac{t}{t_m}\right) \cdots\cdots (20)$$

where

$a=\tan^{-1}(1/2)=0.4637$

$k=e^{-2}\sin a=0.17692$

P_m : maximum value of the impulsive force

t_m : instant when P_m occurs.

This function, which is essentially the same with that utilized by Muto for the problem of the bomb-shell blast [3,4] is drawn to scale in Fig. 2.

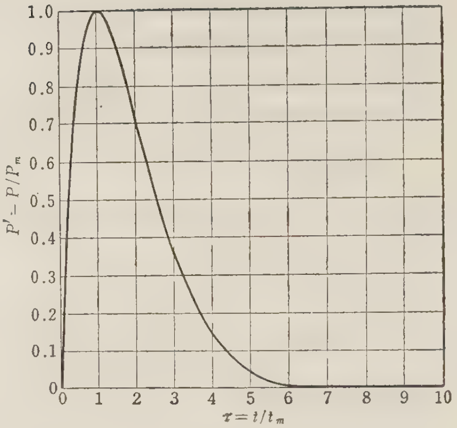

Fig. 2 Shock function.

In order to reduce the number of parameters in this problem we take the dimensionless quantities defined as follows :

$$\left.\begin{aligned} P' &= P/P_m \\ F' &= F/F_m \\ \tau &= t/t_m \end{aligned}\right\} \qquad \cdots\cdots (21)$$

Then (15) and (20) are expressed respectively as follows :

$$\frac{d^2F'}{d\tau^2} + (\omega\tau_m)^2F' = (1-k)\frac{d^2P'}{d\tau^2} + (\omega\tau_m)^2P' \qquad \cdots\cdots (22)$$

and $$P' = \frac{1}{K}e^{-2a\tau}\sin a\tau \qquad \cdots\cdots (23)$$

Let us furthur introduce a dimensionless quantity defined by

$$\frac{t_m}{\pi/\omega} = \lambda \qquad \cdots\cdots (24)$$

This quantity, the ratio of t_m to half a period of rocking, should be an important parameter. By the use of this parameter (22) is rewritten as :

$$\frac{d^2F'}{d\tau^2} + (\pi\lambda)^2F' = (1-k)\frac{d^2P'}{d\tau^2} + (\pi\lambda)^2P' \qquad \cdots\cdots (25)$$

Substituting (24) in (26) thus developed, we obtain

$$\frac{d^2F'}{d\tau^2} + (\pi\lambda)^2F' = \frac{\Gamma}{K}e^{-2a\tau}\sin(a\tau - \delta_1) \qquad \cdots\cdots (26)$$

where

$$\Gamma = \sqrt{\{3a^2(1-k) + (\pi\lambda)^2\}^2 + \{4a^2(1-k)\}^2} \qquad \cdots\cdots (27)$$

$$\left.\begin{aligned} \sin\delta_1 &= [4a^2(1-k)]/\Gamma \\ \cos\delta_1 &= [3a^2(1-k) - (\pi\lambda)^2]/\Gamma \end{aligned}\right\} \qquad \cdots\cdots (28)$$

The solution of (26) is :

$$F' = A\sin\pi\lambda\tau + B\cos\pi\lambda\tau - \frac{\mu}{K}e^{-2a\tau}\sin(a\tau + \delta) \qquad \cdots\cdots (29)$$

where

A, B : integration constants

$$\mu = \sqrt{\frac{\{3a^2(1-k) + (\pi\lambda)^2\}^2 + \{4a^2(1-k)\}^2}{\{(2a)^2 + (a+\pi\lambda)\}\{(2a)^2 + (a-\pi\lambda)^2\}}} \qquad \cdots\cdots (30)$$

$$\delta = -\delta_1 - \delta_4 \qquad \cdots\cdots (31)$$

$$\left.\begin{aligned} \sin\delta_4 &= -\frac{4a^2}{\sqrt{25a^4 - 6a^2(\pi\lambda)^2 + (\pi\lambda)^4}} \\ \cos\delta_4 &= -\frac{3a^2 + (\pi\lambda)^2}{\sqrt{25a^4 + 6a^2(\pi\lambda)^2 + (\pi\lambda)^4}} \end{aligned}\right\} \qquad \cdots\cdots (32)$$

The two integration constants are determined by the two initial conditions (18) and (19) as follows :

$$\left.\begin{aligned} B &= \omega^2 mL\,\theta_0 + \frac{\mu}{K}\sin\delta \\ A &= \frac{1}{\pi\lambda}\left[\omega^2 mL\,\omega_0 + (1-k)\frac{a}{K} + \frac{\mu}{K}a(-2\sin\delta) + \cos\delta\right] \end{aligned}\right\} \qquad \cdots\cdots (33)$$

Substituting (33) in (29), we obtain the solution in this case as follows :

$$F' = \Gamma' \cdot \sin(\pi\lambda\tau + \delta') - \frac{\mu}{K} e^{-2a\tau} \sin(a\tau + \delta) \quad \cdots\cdots (34)$$

where

$$\Gamma' = \sqrt{\left[\frac{1}{\pi\lambda}\left\{\omega^2 mL\, \omega_0 (1-k)\frac{a}{K} + \frac{\mu}{K} a(-2\sin\delta + \cos\delta)\right\}\right]^2 + \left[\frac{\mu}{K}\sin\delta\right]^2} \quad \cdots\cdots (35)$$

$$\left.\begin{aligned} \sin\delta' &= \frac{\mu}{K}\sin\delta / \Gamma' \\ \cos\delta' &= \left[\frac{1}{\pi\lambda}\left\{\omega^2 mL\, \omega_0 + (1-k)\frac{a}{K} + \frac{\mu}{K} a(-2\sin\delta + \cos\delta)\right\}\right] \Big/ \Gamma' \end{aligned}\right\} \quad \cdots\cdots (36)$$

In the case of negligible sway of the wall before the shock pressure acts upon the wall,

$$\theta_0 = 0 \qquad \omega_0 = 0 \quad \cdots\cdots (37)$$

Then eqs. (35), (36), (37) reduce respectively to :

$$F' = \Gamma' \sin(\pi\lambda\tau + \delta') - \frac{\mu}{K} e^{-2a\tau} \sin(a\tau + \delta) \quad \cdots\cdots (38)$$

where

$$\Gamma' = \sqrt{\left[\frac{1}{\pi\lambda}\frac{a}{K}\{(1-k) + \mu(-2\sin\delta + \cos\delta)\}\right]^2 + \left[\frac{\mu}{K}\sin\delta\right]^2} \quad \cdots\cdots (39)$$

$$\left.\begin{aligned} \sin\delta' &= \frac{\mu}{K}\sin\delta / \Gamma' \\ \cos\delta' &= \left[\frac{1}{\pi\lambda}\frac{a}{K}\{(1-k) + \mu(-2\sin\delta + \cos\delta)\}\right] \Big/ \Gamma' \end{aligned}\right\} \quad \cdots\cdots (40)$$

V. SPECIAL CASES

When $k=0$, that is, when the instantaneous resultant wave pressure should act on the base of the wall, μ and δ reduce to :

$$\mu = 1, \qquad \delta = \pi \quad \cdots\cdots (41)$$

Thus F' reduces to :

$$F' = \frac{1}{K} e^{-2a\tau} \sin(a\tau + \delta)$$

Therefore, we obtain

$$F' = P' \quad \cdots\cdots (42)$$

which relation shows that F becomes the same to P when P acts on the base of the wall.

When $\lambda = \infty$, that is, when the shock pressure acts "statically", we likewise obtain the relations $\mu = 1$ and $\delta = \pi$, and thus the relation :

$$F' = P' \quad \cdots\cdots (43)$$

When $\lambda = 0$, that is, when the duration of the shock is infinitely instantaneous, we obtain :

$$F' = (1-k)P' \quad \cdots\cdots (44)$$

This relation shows that F' is proportional to and $(1-k)$ times smaller than P' ; it is to be noted that when $k > 1$, the direction of F' beomes reverse.

VI. VARIATION OF F' WITH RESPECT TO TWO PARAMETERS λ AND k

Inspection of Equations (34), (35) and (36) shows that these three equations contain eventualy only two independent parameters, λ and k ; through these two parameters effect of any factor on F' may systematically be examined. Typical example is shown in Fig. 3 for

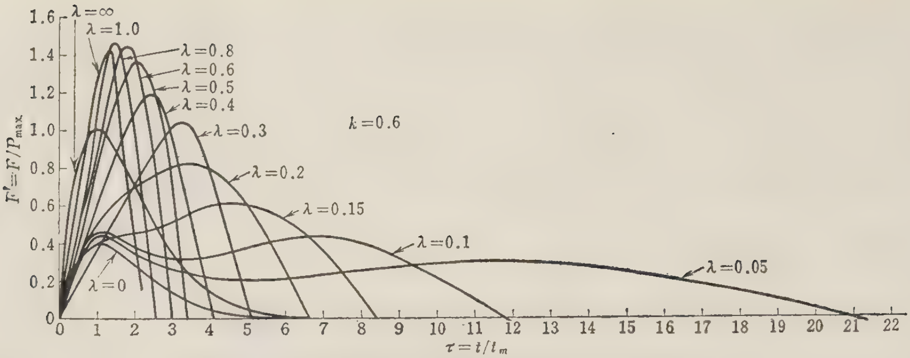

Fig. 3 Variation of F' with respect to λ. ($k=0.6$).

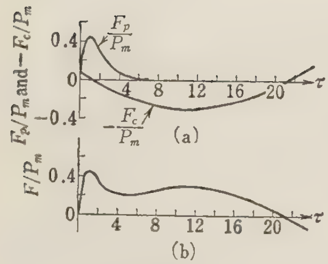

Fig. 4

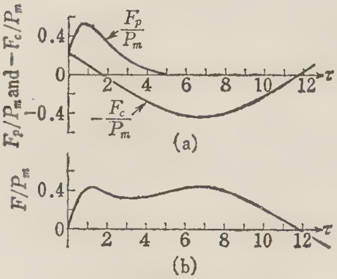

Fig. 5

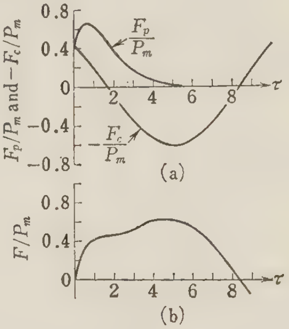

Fig. 6

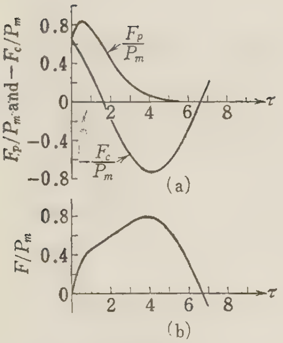

Fig. 7

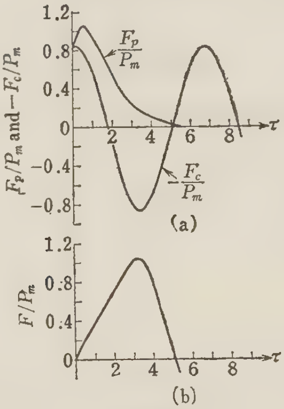

Fig. 8

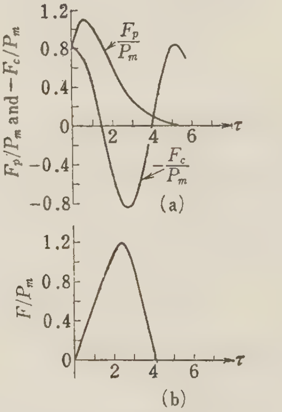

Fig. 9

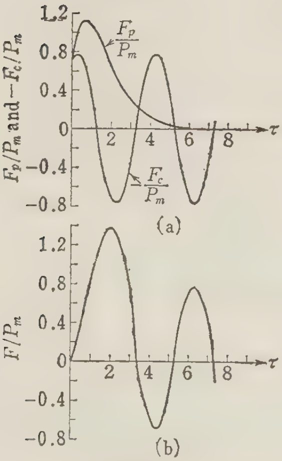

Fig. 10

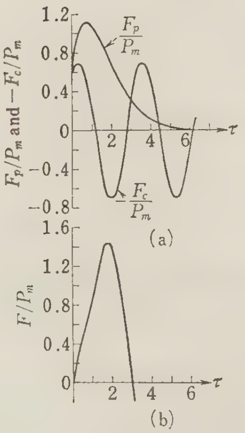

Fig. 11

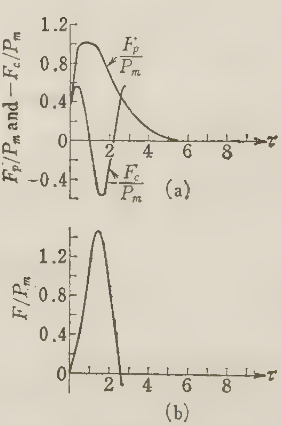

Fig. 12

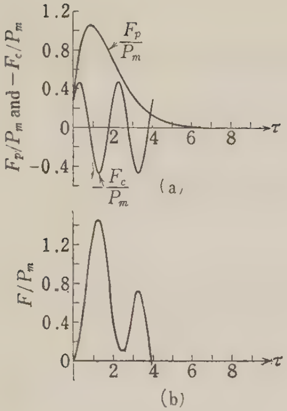

Fig. 13

showing the variation of curves of F' for various values of λ. Figs. 4~13 show how the curves in Fig. 3 have come out ; in each of these figures both the particular solution and the complementary solution are shown, hence the vertical distance showing the value F'. For $\lambda=0$, F' is given by (44) ; $F'=(1-k)P'$. For $\lambda=0.15$ the curve of F' has two maxima in the figure ; the first maximum is due to the shock pressure and the second is due to the oscillation of the wall. With the decrease of the value of λ the first maximum decreases, but the second increases. That shows that although the inertia of the wall reduces the immediate reaction to the shock, the subsequent oscillation comes to augment the second maximum value of F'. It is to be noticed that F' becomes larger than unity for a certain range of λ.

It is to be noted, however, that, for $\lambda=\infty$ F' becomes identical to P' and thus the maximum value of F' becomes unity.

Fig. 14 shows the maximum values of F' versus λ for various values of k, and Fig. 15 the maximum values versus k for various values of λ (λ and k are interchanged).

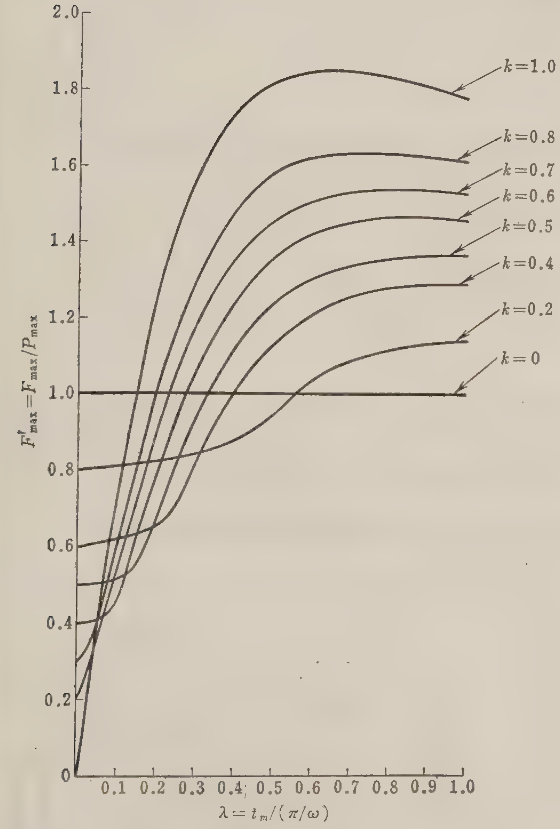

Fig. 14 The maximum values of F' versus k for various values of λ.

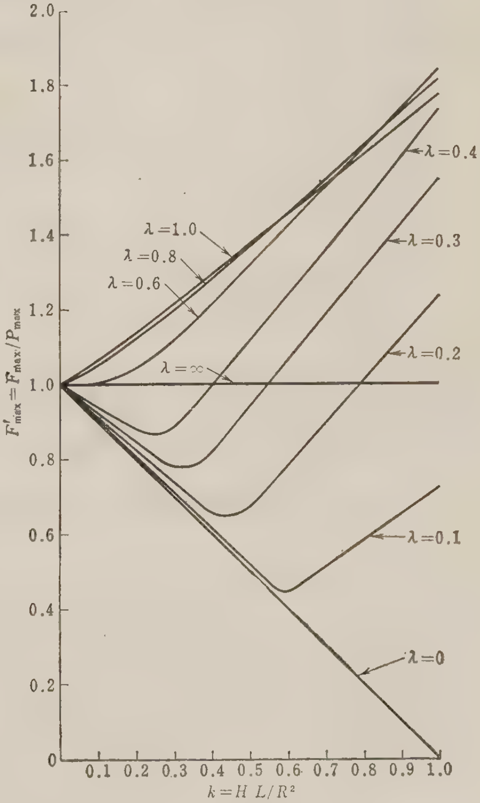

Fig. 15 The maximum values of F' versus λ for various values of k.

VII. VALUES OF λ

The duration of the shock pressure recorded either in field observations or at laboratory experiments are summarized in Table 1.

Table 1 Duration of shock pressure.

Field observations and laboratory experiments		Duration (sec)	Wave ht. (m)
Field observations	Port Dieppe [5]	0.05	
	Port Haboro [2]	0.07	
Laboratory experiments	Larras [6]	0.01 ~0.02	0.095~0.14
	Denny [7]	0.002	0.18 ~0.36
	The authors [8]	0.007~0.02	0.15 ~0.20
	Rundgren [9]	0.002~0.007	0.05 ~0.10
	Nagai [10]	0.015~0.03	0.10 ~0.25
	Mitsuyasu [11]	0.02	0.10

Wave height to be used for design of the break water is $H=2\sim6$ m. If the Froude similarity is still valid in the problem under consideration, duration in prototype dimensions taken back from these laboratory experiments may be estimated as $t_s=0.05\sim0.09$ sec, which range of t_s agrees with the data of field observation cited in Table 1. Thus we estimate as

$t_s=0.05\sim0.09$ sec

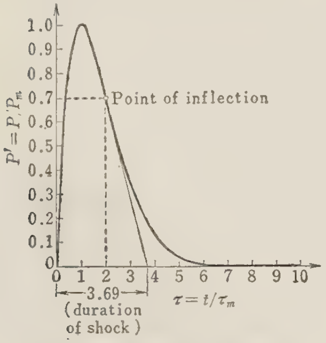

Fig. 16 Duration time of shock function.

On the other hand, the period of rocking of the wall is considered to be

$$T=0.15\sim0.35 \text{ sec}$$

Therefore,

$$t_s/T=0.2\sim0.5 \qquad (45)$$

With regard to the shock function P' defined by (23) we take t_s as shown in Fig. 16. Then,

$$t_s=3.69\,t_m$$

hence

$$\lambda=t_m\Big/\frac{T}{2}=\frac{t_s}{3.69}\Big/\frac{T}{2}=\frac{1}{1.85}\frac{t_s}{T}$$

Accordingly, for (45) we have

$$\lambda=0.11\sim0.27 \qquad (46)$$

Inspection of Fig. 11 shows that, within this range of λ, $F'_{\max}$ is smaller than unity for $k\leqq 0.6$ approximately, but for $k>0.6$, $F'_{\max}$ becomes larger even than unity.

VIII. THE CASE OF BREAKWATER OF HORIZONTAL BLOCK CONSTRUCTION

In a similar way as in the case of the monolithic wall let us consider the shearing resistance which does act on any sliding plane, say plane A B of Fig. 17 : The basic equations regarding the upper portion of the wall above plane AB are as follows:

$$m_1\dot{V}_1=P_1-F_1 \qquad (47)$$

$$I_1\ddot{\theta}=P_1H_1-F_1L-M_1 \qquad (48)$$

$$V_1=L_1\dot{\theta} \qquad (49)$$

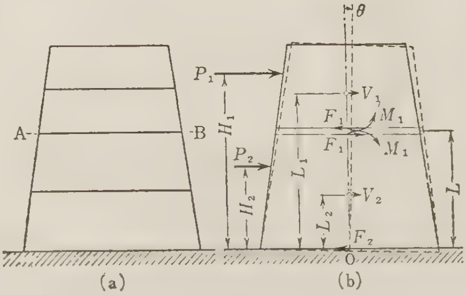

Fig. 17 Wall of block construction.

where

m_1 : mass of the upper portion of the wall,

P_1 : resultant instantaneous pressure acting on the portion of the wall above plane AB,

F_1 : shearing resistance which acts on plane AB,

I_1 : moment of inertia of the upper portion under consideration of the wall around point 0,

M_1 : bending moment acting on plane AB,

H_1 : height of P_1,

L_1 : height of center of gravity of the upper portion of the wall,

L : height of the plane AB.

Similarly for the portion of the wall below plane AB, the basic equations are given by

$$m_2\dot{V}_2 = P_2 + F_1 - F_2 \tag{50}$$

$$I_2\ddot{\theta} = M_1 + P_2H_2 + F_1L - K\theta \tag{51}$$

$$V_2 = L_2\dot{\theta} \tag{52}$$

where

I_2 : moment of inertia of the portion of the wall below plane AB around point 0,

P_2 : resultant instantaneous pressure acting on the portion of the wall below plane AB,

m_2 : mass of the lower portion of the wall.

From these six equations six unknown quantities V_1, F_1, M_1, θ, V_2, F_2 may be solved.

Let us obtain the equation for F_1 by eliminating the other five quantities:

Substituting (49) into (47), (52) into (50), we obtain the equations respectively as follows:

$$\ddot{\theta} = \frac{1}{m_1L_1}(P_1 - F_1) \tag{53}$$

$$\ddot{\theta} = \frac{1}{m_2L_2}(P_2 + F_1 - F_2) \tag{54}$$

On the other hand, eliminating M_1 between (48) and (51), we obtain

$$\ddot{\theta} = \frac{1}{I}(P_1H_1 + P_2H_2 + K\theta) \tag{55}$$

where

I : moment of inertia of the wall as a whole around point 0 ($I = I_1 + I_2$).

As is easily seen K/I in the above equation represents square of the angular velocity of sway of the wall. Accordingly we put as:

$$\omega^2 = \frac{K}{I} \tag{56}$$

With this notation (55) is rewritten as:

$$\ddot{\theta} + \omega^2\theta = \frac{1}{I}(P_1H_1 + P_2H_2) \tag{57}$$

As is obvious,

$$I = (m_1 + m_2)R^2 \tag{58}$$

where

R : moment of inertia of the wall as a whole around point 0,

Let us introduce dimensionless quantities defined as follows:

$$\left.\begin{aligned} l_1 &= L_1/R \\ h_1 &= H_1/R \\ h_2 &= H_2/R \end{aligned}\right\} \tag{59}$$

Then, eliminating $\ddot{\theta}$ between (54) and (57), we obtain

$$\theta=\frac{1}{\omega^2 m_1 L_1}\left[F_1-P_1\left(1-\frac{m_1}{m_1+m_2}l_1h_1\right)+\frac{m_1l_1h_2}{m_1+m_2}P_2\right]$$

Differentiating the above equation twice with respect to t, we have

$$\ddot{\theta}=\frac{1}{\omega^2 m_1 L_1}\left[\ddot{F}_1-\ddot{P}_1\left(1-\frac{m_1}{m_1+m_2}l_1h_1\right)+\frac{m_1l_1h_2}{m_1+m_1}\ddot{P}_2\right] \quad\cdots\cdots(60)$$

Eliminating $\ddot{\theta}$ finally between (60) and (54), we obtain

$$\ddot{F}_1+\omega^2F_1=\left(1-\frac{m_1}{m_1+m_2}l_1h_1\right)\ddot{P}_1-\frac{m_1}{m_1+m_2}l_1h_2\ddot{P}_2+\omega^2P_1 \quad\cdots\cdots(61)$$

Let us further introduce the following dimensionless quantities:

$$\left.\begin{aligned}\frac{m_1}{m_1+m_2}l_1h_1&=k_1\\ \frac{m_1}{m_1+m_2}l_1h_2&=k_2\end{aligned}\right\} \quad\cdots\cdots(62)$$

With these dimensionless parameters (61) is rewritten as:

$$\ddot{F}_1+\omega^2F_1=(1-k_1)\ddot{P}_1-k_2\ddot{P}_2-\omega^2P_1 \quad\cdots\cdots(63)$$

which is the basic equation for F_1.

The right member of the above equation may be expressed as a known function of t, and the above equation is, as before, an ordinary linear differential equation of the second order; this equation may be solved in similar way as was done in the case of the monolithic wall.

When the shock pressure acts only near the still water level and above plane AB, we may assume

$$P_2=0 \quad\cdots\cdots(64)$$

Then the solution of F_1 is same to (34), except that k_1 appears in place of k.

Detailed examination of this case will be made in the subsequent paper.

IX. CONCLUSION

This research leads to the following conclusions:

1) The usual criterion of stability against sliding $P>\mu W$ is not theoretically correct, where P is the resultant instantaneous pressure, μ coefficient of static friction, W submerged weight of the wall.

Theoretically, the criterion of stability of the wall against sliding should be $F>\mu W$, F being the "actual" shearing resistance which is equal to P minus (or plus) the inertia resistance of the wall.

2) The actual shearing resistance, F, in the case of the monolithic wall is given by the basic equation (15). This equation has been derived almost rigorously except for neglect of damping of oscillation of the wall due to water; this equation may hold not only in the case of shock pressures but also in the case of either the periodic wave or mere static pressure.

3) When the time variation of the shock pressure may be approximated by the equation (20), the actual shearing resistance, F, is given by (34), where only two parameters, λ and k, are present. The theoretical values of $F_{\max}/P_{\max}$ obtained by numerical calculation are drawn to scale with respect to those two dimensionless quantities in Figs. 12 and 13.

It is to be noted that the value of $F_{\max}/P_{\max}$ is larger than unity for a certain range of those dimensionless quantities. This theoretical value beyond unity is due to superposition of the inertia resistance of the wall to the shock pressure of the breaking wave at the stage of the counter-sway of the wall (sway to the offing side). However, the effect of damping of oscillation of the wall would modify considerably the theoretical values of $F_{\max}/P_{\max}$ obtained in this paper. The modification will be made in the subsequent paper.

4) According to field observations and laboratory experiments the value of λ is considered to be $\lambda = 0.11 \sim 0.27$.

5) In the case of the wall of horizontal block construction the resisting shearing force F_1 which should act on any horizontal construction plane is given by (63).

6) When the shock acts only upon the upper part above the construction plane under consideration and when the shock pressure may be approximated by shock equation (20), the solution of F_1 is the same with (34), except that k_1 appears in place of k.

ACKNOWLEDGEMENTS

The authors are grateful to Mr. Kenkichi Hayashi, Postgraduate student at Chuo University, and to Messrs. Keiji Kurita and Sigeaki Hisajima, both of whom have been the students at the same university, for their cooperation in doing numerical calculation.

REFERENCES

1) Minikin, R.R. : Winds, waves and maritime structures, (Charles Griffin), 1950.
2) Kuribayashi, T., Y. Muraki and G. Udai : Field investigation of wave forces on breakwater, Coastal Engineering in Japan, Vol. 2, (Japan Society of Civil Engrs.), 1959, pp. 17-27.
3) Muto, K. : On the elastic oscillation of structures due to explosion, Proceeding of Japan Society of Structural Engineering, April, 1940, pp. 347-355 (in Japanese)
4) Muto, K. : World of impulse fracture, Proc. of the Japan Soc. of Structural Eng., Apr., 1941, pp. 246-251 (in Japanese)
5) de Rouville, A. P. Besson et P. Pétry : Etat actuel des études internationales sur les efforts dus aux lames, Annales des Ponts et Chausées, 1938, pp. 5-113.
6) Larras, J. : Le déferlement des lames sur les jetées verticales, Annales des Ponts et Chausées, 1937, pp. 643-680.
7) Denny, D.F. : Further experiments on wave pressures, Journ. Inst. Civ. Eng., 1951, pp. 330-345.
8) Hayashi, T. and M. Hattori : Pressure of the breaker against a vertical wall, Coastal Engineering in Japan, Vol. 1, (Japan Society of Civil Engineers), 1953, pp. 25-37 (in English)
9) Rundgren L., : Water wave forces, Stockholm, 1958.
10) Nagai, S. : Research on pressure of the breaking wave upon the breakwater, Transaction of the Japan Society of Civil Eng., No. 65, Dec., 1959, pp. 1-38.
11) Mitsuyasu, T. : Resultant instantaneous pressure upon breakwater, Proceeding of the Sixth Conference on Coastal Engineering (Japan Society of Civil Engrs.) November, 1959, pp. 107-113 (in Japanese).

HYDRAULIC MODEL EXPERIMENT ON THE OSCILLATION OF WATER LEVEL IN SAKAI CHANNEL

*Haruo Higuchi**

SYNOPSIS

This is a report of the preliminary test of hydraulic model experiment on the oscillation of the water level in Sakai Channel, which connects Lake Nakaumi with Miho Bay.

First, in order to examine the scale effect, some experiments for semi-diurnal tide and 130 minutes' oscillation are carried out under constant horizontal scale, 1/500, and five different distortions, that is, 2, 4, 6, 8, and 16. The term "distortion" means the ratio of vertical scale to horizontal. As the result, it is found that the scale effect seems rather large for the oscillaton of longer period as semi-diurnal tide and very small for that of shorter period as 130 minutes' oscillation. In spite of the smaller reservoir and larger amplitude, the state of damping of amplitude in the channel with a reservoir is similar to the prototype when the distortion is 4.

Then, in order to investigate the character of frequency response of the model channel, two series of experiments are carried out for sinusoidal waves of various frequencies, one is that for the the channel with a reservoir and the other without a reservoir. After these experiments it is clarified that the character of frequency response of the channel without a reservoir is considerably different from that with a reservoir; therefore, the effect of the area of the reservoir on the character of frequency response is of much importance.

I. INTRODUCTION

A lake of half salt water named "Nakaumi" is located in the east part of Shimane Prefecture, the area of which is about 102 km^2 and the mean depth of water is 4.6 m. From the north east part of it a channel called "Sakai Channel", 7.5 km in length, 200～800 m in width and 5 m in depth, starts eastward to Miho Bay, Japanese Sea.

As the first step of the reclamation work in Lake Nakaumi, there is a plan to close the channel for making fresh the water in the lake by inflow. After this plan will be executed, it is supposed that hydraulic phenomena in and near the channel and the lake will be largely changed. There are many problems to be solved; for instance, the state of the water level in the lake, the features of surface undulation and flow pattern in the channel, the condition of mixing of water, the state of ground water near the lake especially at the Kyuhin-Hanto Peninsula, etc. Among these, the ocillation of water level in the channel was dealed experimentally. In this paper, the results of preliminary experiments are described as the fundamental data to discuss the scale effect on the oscillation and the effect of the reservoir on the character of frequency response of the system containing a channel and a lake. In the model with a simplified channel and a distorted lake the experiments for the scale effect were carried out with several different water depths, and those for the frequency response are made under the conditions that channel is open and closed.

---

* Assistant Professor, Kyoto University

II. EXPERIMENTAL EQUIPMENTS

The experiments were performed by the "facility for estuary model experiments" of Ujigawa Hydraulic Laboratory, Disaster Prevention Research Institute, Kyoto University. This facility consists of a reinforced concrete basin, a concrete channel and a pneumatic wave generator. The dimension of the basin was 20 m in width, 15 m in length, and 0.6 m in depth, and that of the channel was 2 m in width, 20 m in length, and 0.5 m in depth. In the basin and the channel the model was constructed, the horizontal scale of which is 1/500. As shown in Fig. 1, this model involved a part of Miho Bay, whole of Sakai Channel, and a part of Lake Nakaumi. Because of the dimensions of the basin and the channel the area of Lake Nakaumi in the model was of 48% of the required one.

Side walls of the channel and the coast of Miho Bay were made by concrete blocks of 20×20×40 cm. The cross section of the channel was rectangular for the convenience of the experiments of scale effect. The bottom of the channel was finished by brush horizontally. In

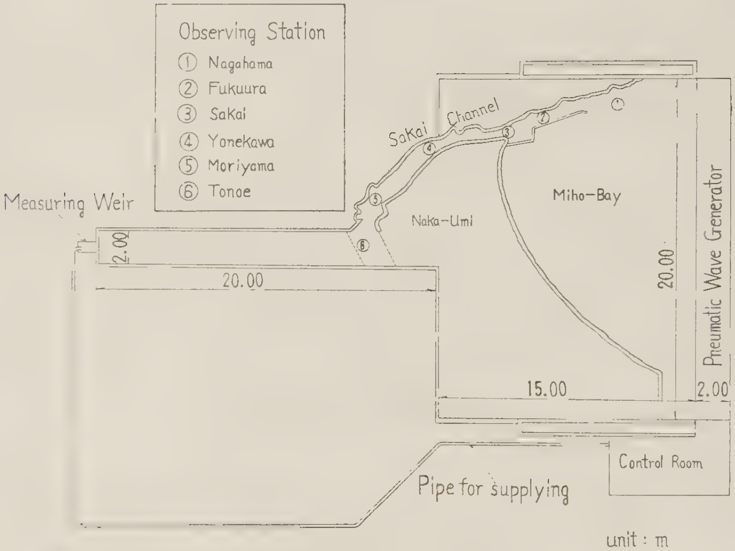

Fig. 1. Experimental facilities and sketch of the model.

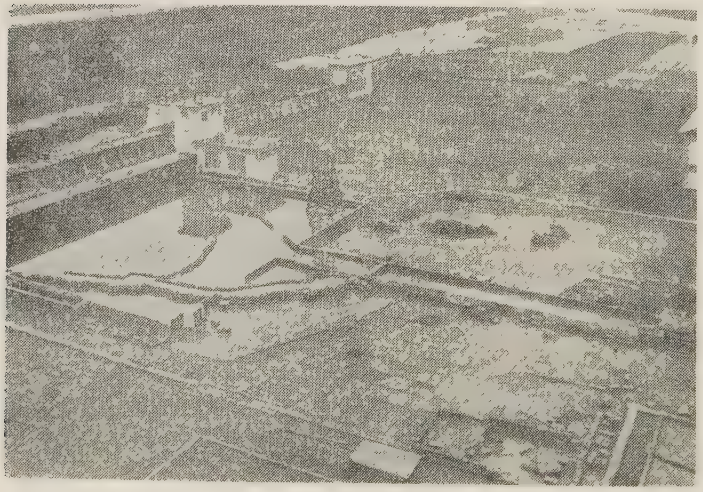

Photo. 1. General view of the model.

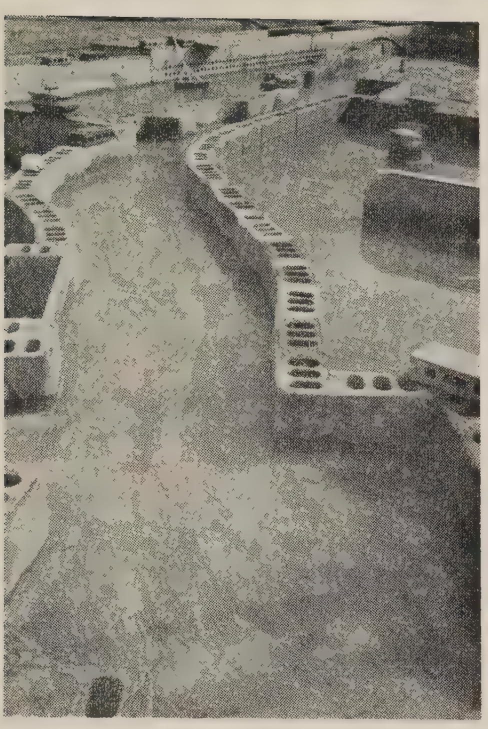

Photo. 2. Model channel with a brushed mortar bottom.

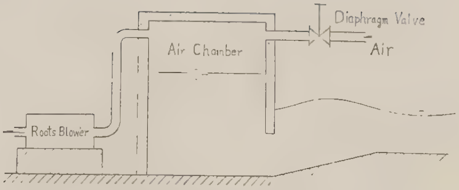

Fig. 2. Schematic diagram of the pneumatic wave generator.

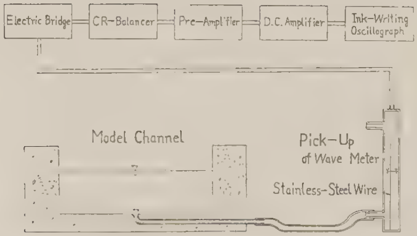

Fig. 3. Block diagram of the wave meter.

the later experiments the channel was closed by concrete blocks near the station ⑥. During the experiments the channel was covered by vinyl plates for protecting from wind. The oscillation was provided by the pneumatic wave generator shown in Fig. 2. The principle of this generator is that, first, by sucking out the air in an air-chamber by the roots-blower of 7.5 HP., the water is sucked up in the chamber, and second, as the diaphragm valve is opened, the water level in the chamber goes down, therefore, that in the basin goes up, and then shutting the valve, the water levels in the chamber and the basin go up and down respectively again. Therefore, the water level in the basin could be controlled by operating the diaphragm valve. There is a pipe for supplying the river flow in this facility. This pipe was used for the experiment to seek the roughness coefficient of the channel.

The water level was measured by the wave meter shown in Fig. 3, which was of electric resistance type.

III. ARTICLES OF EXPERIMENT AND MEASURED ITEMS

Articles of Experiment

1) Roughness of the model
2) Scale effect on hydraulic phenomena
3) Frequency response (1) (with the reservoir)
4) Frequency response (2) (without the reservoir)

Measured Items

1) Water levels at six points
   ① : Nagahama, ② : Fukuura, ③ : Sakai, ④ : Yonekawa, ⑤ : Moriyama, and ⑥ : Tonoe.
2) Velocities of flow at the water surface between ④ and ⑤. By means of float. Some

representative records are shown in Fig. 4 and Fig. 5. Fig. 4 represents the case with the reservoir and Fig. 5 without the reservoir. The marks ∘ represent the surface velocities and full lines show the elevations of water level at Station ⑤.

3) Roughness Coefficient

IV. PROCEDURE AND RESULTS OF EXPERIMENTS

1) Roughness of the Model

The model of Sakai Channel was finished by mortar. Measuring the gradient of the water surface in steady flow, the roughness coefficient was evaluated.

As shown in Fig. 1, the water was circulated through the pipe, the weir, and the channel. The water levels were measured by point gages set at the six stations, from ① to ⑥. In this experiment on the roughness, the flow was steady in the channel having a horizontal bottom and rectangular cross sections. Assuming that the width of the channel is constant between successive stations for simplicity, the following equation is derived from the equation of motion.

$$n^2 = R^{4/3}\left(\frac{A^2}{Q^2}\right)i_w\left[1-\frac{1}{gh}\frac{Q^2}{A^2}\right], \quad \cdots(1)$$

in which, n : Manning's roughness coefficient, R : hydraulic radius, Q : discharge, g : gravity acceleration, and h: water depth. Fig. 6 shows the coefficient calculated by equation (1).

2) Scale Effect

As the existing facility was used for these experiments, the area of the lake was too small. Therefore, the strict similitude was not expected. Then the aim of the experiments of this ar-

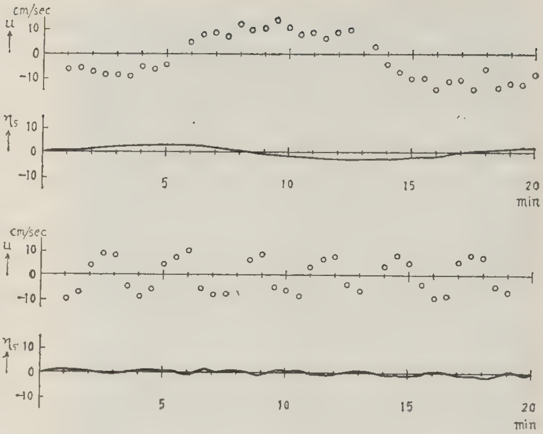

Fig. 4. Velocities of flow u at the station between ④ and ⑤, and water levels (η_5) at Station ⑤ for semidiurnal tide (top) and 130 minutes' oscillation (bottom) in the channel with the reservoir : the depth of water is 4 cm.

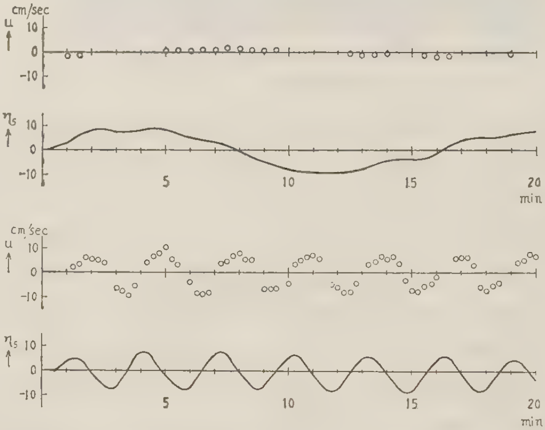

Fig. 5. Velocities of flow u at the station between ④ and ⑤, and water levels (η_5) at Station ⑤ for semi-diurnal tide (top) and 130 minutes' oscillation (bottom) in the channel without the reservoir : the depth of water is 4 cm.

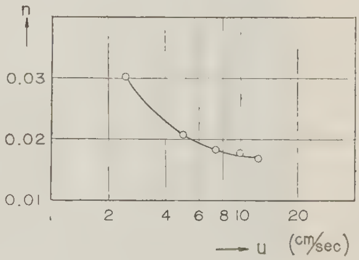

Fig. 6. Relation of Manning's coefficient n of the model channel to velocities of flow u : the depth of water is 4 cm.

ticle was to seek the suitable vertical scale, so that damping state of semi-diurnal tide and 130 minutes' oscillation in the model was similar to those in the prototype. The horizontal scale was always provided as 1/500, and on the other hand, the vertical scale, was chosen for five distortions, which is the ratio of vertical scale to horizontal one, 2, 4, 6, 8, and 16 respectively. Considering Froude number, the hydraulic factors in the model and the prototype are shown in Table 1. When "distortion" is one, the water depth in the model channel is only as small as 1 cm, and therefore it is difficult to carry out the experiment with small error considering the accuracy in constructing the bottom. From this reason, this case was omitted. Since it is also difficult to carry out the experiment for the oscillation of as small amplitude as several millimeters required by vertical scale, the experiments for the oscillation having the amplitude of 1 cm were mainly treated.

Table 1

Distortion of Model	Vertical Scale	Water Depth	Amplitude	Time Scale	Period		Velocity Scale	Velocity
Prototype		5 00 cm	40 cm		130 m	12 h 25 m		40 cm/sec
1	1/500	1	0.08	1/22.4	5′48″	33′12″	1/22.4	1.79
2	1/250	2	0.16	1/31.6	4′07″	23′36″	1/15.8	2.53
4	1/125	4	0.32	1/44.7	2′55″	16′40″	1/11.2	3.57
6	1/83.4	6	0.48	1/54.7	2′23″	13′38″	1/9.13	4.38
8	1/62.5	8	0.64	1/63.3	2′03″	11′46″	1/7.90	5.07
16	1/31.25	16	1.28	1/89.4	1′27″	8′20″	1/5.59	7.15

where "horizontal scale" is 1/500.

There are many oscillations having different periods from tides in the actual channel but it is very difficult to identify each oscillation, especially in the case of shorter period. The semi-diurnal tide and the 130 minutes' oscillation in the prototype were chosen as the representative oscillations with respect to longer and shorter period respectively. In cases of various distortions, some successive sinusoidal waves which have the corresponding periods and the constant amplitudes, 1 cm, were provided by the pneumatic wave generator shown in Fig. 1, and the damping state in the channel were examined. The results are shown in Fig. 7 and

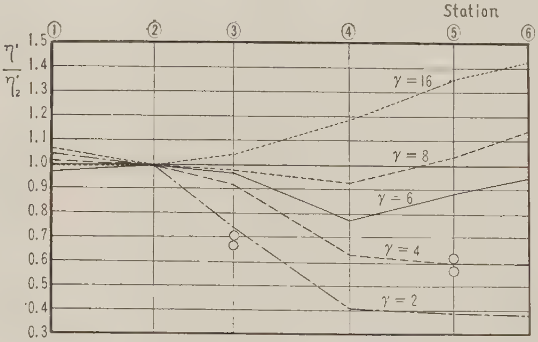

Fig. 7. **Ratios of amplitudes at each station with respect to Station ②, for semi-diurnal tide : γ shows the distortion, and the marks ∘ the values for the prototype.**

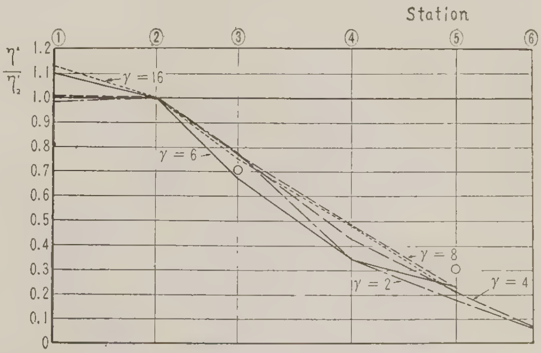

Fig. 8. **Ratios of amplitudes for 130 minutes' oscillation.**

Fig. 8. These show the ratios of amplitudes at each station referring to Station ②. Station ② was chosen as a standard for convenience sake to be compared with the prototype. Fig. 7 for the semi-diurnal tide shows that the smaller the distortion becomes, the more the damping. It is considered as the reason that since the smaller water depth corresponds to the smaller distortion, the effect of friction in the channel becomes larger. In this figure, the marks ∘ show the values for the prototype. Excepting the value at Station ③, the state of damping seems to be similar to the prototype in the case of distortion 4. Fig. 8 shows the state for the 130 minutes' oscillation. From the figure, it is found that the state in each case is almost same. This may suggest that the effect of friction on these oscillations of shorter periods is very small.

Then the effect of amplitude on the state of damping was examined in the case of distortion 4 for both the semi-diurnal tide and the 130 minutes' oscillation. Fig. 9 shows the result for the semi-diurnal tide, and the numerals in the figure show the amplitudes at Station ②. From this it is found that in the case of the larger amplitude, the larger damping appears. This may show the difference of effect of friction. In the case of 130 minutes' oscillation as shown in Fig. 10, it is found that the state is almost as same as Fig. 8.

In conclusion, it was clarified that the scale effect was large for the oscillation of as long period as the semi-diurnal tide but that was small for as short period as the 130 minutes' oscillation, and in the case of distortion 4, the state of damping of semi-diurnal tide was most similar to the prototype. However, it must be noticed that it is correct only when the area of the lake is smaller and the amplitude of oscillation has a particular value.

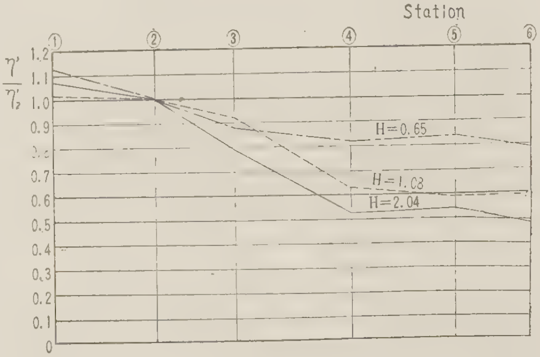

Fig. 9. Ratios of amplitudes for semi-diurnal tide of different amplitude, when $\gamma=4$: H shows the amplitude.

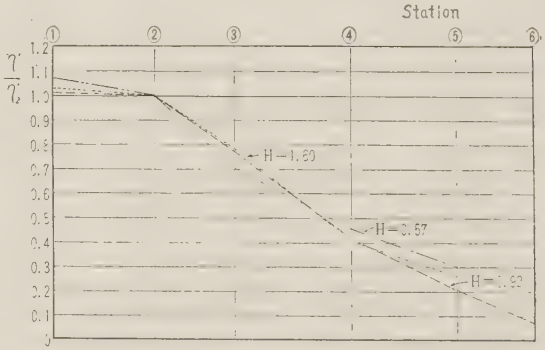

Fig. 10. Ratios of amplitudes for 130 minutes' oscillation of different amplitude, when $\gamma=4$.

3) Frequency Response (1) (with the reservoir)

Since it was clarified that when the distortion was 4 and the amplitude was 1 cm, the state of damping in the model was similar to the prototype, the following series of experiments were carried out under these conditions.

The oscillations of ten different periods from 1 to 32 minutes were provided. The ratios of amplitudes at each station referred to Station ② are shown in Fig. 11 for each period individually. From this figure it becomes clear that, except in the particular case that the period is 1 minute, when the period becomes long, the ratios of amplitudes at each station become gradually smaller till the minimum value about 4 minutes, and then the ratios be-

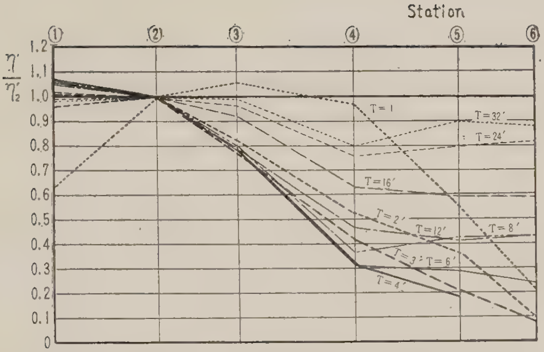

Fig. 11. Ratios of amplitudes for each period from 1 to 32 minutes : shows the period (with the reservoir).

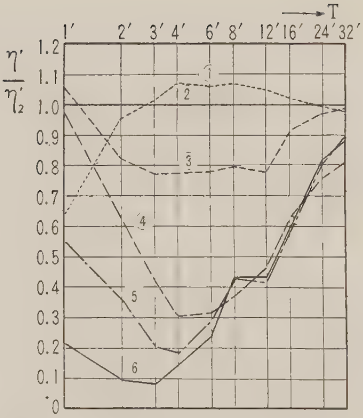

Fig. 12. Experimental frequency response : each curve corresponds each station (with the reservoir).

come large again with increase in the period. To understand this fact more easily, Fig. 12 is shown. The abscissa shows the period in minute, and the ordinate is the ratio of amplitude at each station as the above figure. Each curve in the figure shows the ratio at each station respectively. This figure shows that the values of the ratio take minimum value when the period is between 3 and 6 minutes. The reason why the change in the values of the ratio at Station ① shows an opposite form is that the ratio is referred to Station ②, and Station ① is located in the opposite side of the other stations.

Now the particular form when the period is 1 minute in Fig. 11 and the reason why the minimum values appear in Fig. 12 were examined theoretically.

Considering the uniform channel having a rectangular cross section and a horizontal bottom, and assuming the linear frictional term, the equations of motion and continuity are as follows :

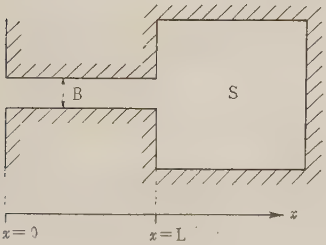

Fig. 13.

$$\frac{\partial u}{\partial t}+\alpha u+g\frac{\partial \eta}{\partial x}=0, \quad \cdots\cdots(2)$$

$$\frac{\partial \eta}{\partial t}+h\frac{\partial u}{\partial x}=0, \quad \cdots\cdots(3)$$

in which, α : coefficient of friction, u : velocity of flow, η : displacement of water level from still water surface, h : water depth, and g : gravity acceleration. In the case as shown in Fig. 13 the solution of the equations under the conditions that $\eta=\eta_0 e^{i\omega t}$ at $x=0$, and $\frac{d\eta}{dt}=\beta u$ at $x=L$ is

$$\frac{\eta}{\eta_0}=\frac{(p+iq)\left(e^{(p+iq)(L-x)}-e^{-(p+iq)(L-x)}\right)+\frac{\beta}{h}\left(e^{(p+iq)(L-x)}+e^{-(p+iq)(L-x)}\right)}{(p+iq)\left(e^{(p+iq)L}-e^{-(p+iq)L}\right)+\frac{\beta}{h}\left(e^{(p+iq)L}+e^{-(p+iq)L}\right)}e^{i\omega t}, \quad \cdots\cdots(4)$$

$$p^2=\frac{\omega^2}{2c^2}\left\{\sqrt{1+\frac{\alpha^2}{\omega^2}}-1\right\},\quad q^2=\frac{\omega^2}{2c^2}\left\{\sqrt{1+\frac{\alpha^2}{\omega}}+1\right\},\quad \omega=\frac{2\pi}{T},\quad c=\sqrt{gh}$$

in which, $\beta=\frac{Bh}{S}$, B : width of the channel, S : area of the reservoir, and T : period. Rationalizing the equation (4), the ratio of amplitude is written as follows :

$$\left(\frac{\eta'}{\eta_0}\right)^2=\Big[(p^2+q^2)\{\sinh^2 p(L-x)+\sin^2 q(L-x)\}+\frac{\beta^2}{h^2}\{\sinh^2 p(L-x)+\cos^2 q(L-x)\}$$

$$+\frac{\beta}{h}\{p\sinh 2p(L-x)-q\sin 2q(L-x)\}\Big]\div\Big[(p^2+q^2)\{\sinh^2 pL+\sin^2 qL\}$$

$$+\frac{\beta^2}{h^2}\{\sinh^2 pL+\cos^2 qL\}+\frac{\beta}{h}\{p\sinh 2pL-q\sin 2qL\}\Big]\cdots\cdots\cdots(5)$$

Now if the frictional term is represented by Manning's formula, the coefficient α may be written as follows :

$$\alpha=\frac{gn^2}{h^{\frac{4}{3}}}u$$

By using the value of α estimated from the measured mean velocity based on the above equation, the equation (5) can be numerically calculated. The result of its calculation is shown in Fig. 14. This corresponds to Fig. 12. As the calculation is carried out for the simplified model, the theoretical value does not coincide completely with the experimental one, but the tendency of the frequency response seems to be considerably similar to the experimental results.

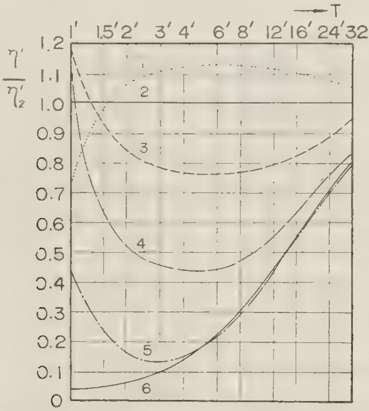

Fig. 14. Theoretical frequency response (with the reservoir).

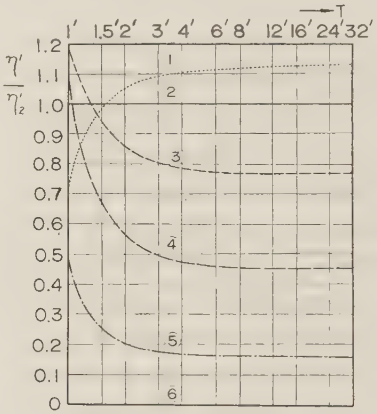

Fig. 15. Theoretical frequency response when $S\to\infty$.

When the area of the reservoir is infinite ($S\to\infty$), β vanishes and the equation (5) becomes as follows :

$$\left(\frac{\eta'}{\eta_0}\right)^2=\frac{\sinh^2 p(L-x)+\sin^2 q(L-x)}{\sinh^2 pL+\sin^2 qL}\cdots\cdots\cdots(6)$$

In this case, as shown in Fig. 15, the ratios become small with increase in the period, and then they approach constant values respectively. On the other hand, when S takes a finite value the minimum value appears. Therefore, it is understood that the minimum values shown in Fig. 12 and Fig. 14 take place because of finite value of S, and then it is concluded that the area of the reservoir plays an important role on the frequency response of the system containing a channel and a reservoir. This effect of the area seems to become larger for a longer period.

Since the effect of the reservoir is little for the oscillation of 1 minute period because of the shortness of the period, and the frictional effect is assumed to be neglisible, it may be written that $\beta=0$, $\frac{\alpha}{\omega}\ll 1$. Therefore, $p=0$, $q=\omega/c$, and the equation (6) becomes as follows:

$$\frac{\eta'}{\eta_0}=\frac{\sin\frac{\omega}{c}(L-x)}{\sin\frac{\omega}{c}L}=\frac{\sin\pi\frac{T_0}{T}\left(1-\frac{x}{L}\right)}{\sin\pi\frac{T_0}{T}}\cdots\cdots\cdots(7)$$

in which, $T_0 = 2L/\sqrt{gh}$, that is the characteristic period of the open channel. The equation (7) shows that if $2T_0 > T > T_0$, the maximum value appears at $x/L = 1 - \frac{1}{2}T/T_0$. As the characteristic period of this model channel is theoretically 48 seconds, the period of 1 minute corresponds to the above mentioned case, that is $2T_0 > T > T_0$, and the occurence of the maximum value is expected between Station ③ and ④. This provides good agreement with the experimental result.

With respect to the velocity of flow, the following solution is obtained.

$$\left(\frac{u}{\eta_0}\right)^2 = \frac{g}{h\sqrt{1+\frac{\alpha^2}{\omega^2}}}\Big[(p^2+q^2)\{\sinh^2 p(L-x)+\cos^2 q(L-x)\}+\frac{\beta^2}{h^2}\{\sinh^2 p(L-x)$$
$$+\sin^2 q(L-x)\}+\frac{\beta}{h}\{p\sinh 2p(L-x)+q\sin 2q(L-x)\}\Big]\div\Big[(p^2+q^2)\{\sinh^2 pL$$
$$+\sin^2 qL\}+\frac{\beta^2}{h^2}\{\sinh^2 pL+\cos^2 qL\}+\frac{\beta}{h}\{p\sinh 2pL-q\sin 2qL\}\Big]. \cdots\cdots\cdots\cdots (8)$$

The result of numerical calculation of the equation (8) is shown in Fig. 16. In this figure the marks ④ and ⑤ show the station numbers for which the velocities of flow were calculated. The experimental values measured at the location between ④ and ⑤ are shown by a full line. In this figure it seems that the theoretical values coincide with the experimental values in spite of the theoretical treatment approximated by the straight uniform channel.

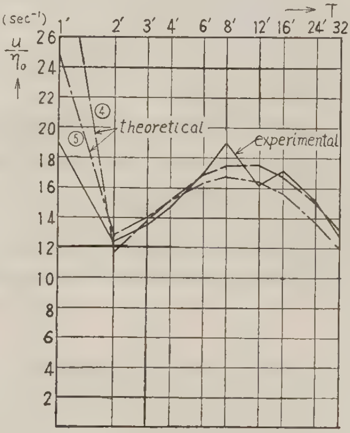

Fig. 16. **Experimental maximum mean velocities at the station between ④ and ⑤, and theoretical values at Station ④ and ⑤ (with the reservoir).**

4) Frequency response (2) (without the reservoir)

This series of experiments was carried out in the channel closed near Station ⑥ shown by the broken lines in Fig. 1. The provided amplitudes were 1 cm as before. The results are shown in Fig. 17 and Fig. 18.

Fig. 17 corresponds to Fig. 11 in the preceding article. From this it becomes clear that the amplitudes of the oscillations of longer period than 2 minutes do not become small but large on the contrary.

Fig. 18 corresponds to Fig. 12. This shows that each curve has maximum value when the period is 3 min-

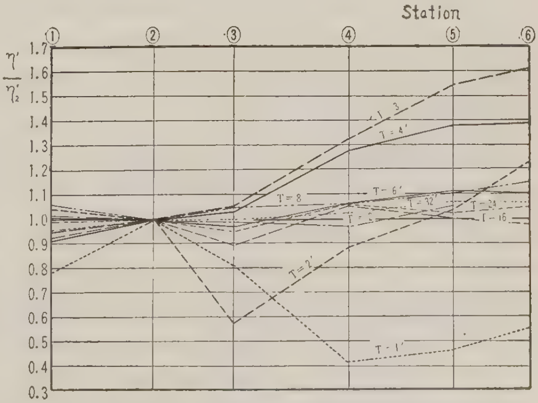

Fig. 17. **Ratios of amplitudes for each period from 1 to 32 minutes (without the reservoir).**

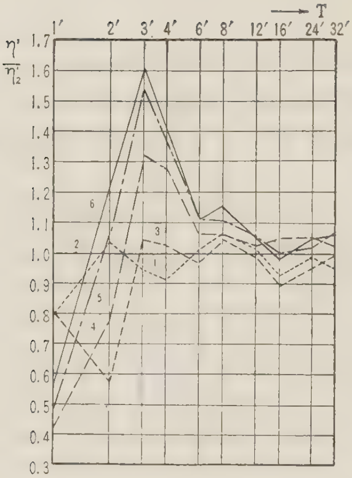

Fig. 18. Experimental frequency response (without the reservoir).

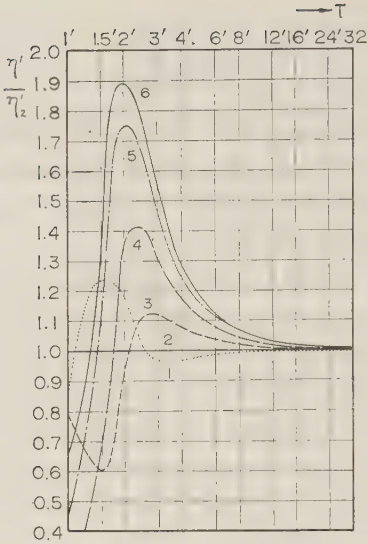

Fig. 19. Theoretical frequency response (without the reservoir).

utes at each station between ③ and ⑥, and each curve approaches unity gradually when the period becomes longer.

The calculated values by the equation (5) are shown in Fig. 19. This figure resembles Fig. 18 in general tendency, but the maximum values appear when the period is 2 minutes. The reason why the theoretical maximums exist at 2 minutes may be that the resonance occurs at this period from the following consideration. That is, since the period is short and the area of the reservoir is small, assuming that $\alpha=0$, and $\beta=\infty$, the equation (5) becomes as follows :

$$\frac{\eta'}{\eta_0}=\frac{\cos\frac{\omega}{c}(L-x)}{\cos\frac{\omega}{c}L}=\frac{\cos\frac{\pi}{2}\frac{T_0}{T}\left(1-\frac{x}{L}\right)}{\cos\frac{\pi}{2}\frac{T_0}{T}}\quad\cdots\cdots\cdots(9)$$

in which, $T_0=4L/\sqrt{gh}$, which is the characteristic period of the closed channel. The theoretical period of the closed channel is 114 seconds. The reason why the experimental characteristic period of the closed channel does not coincide with the theoretical one may be considered that the characteristic period of the channel in the model is elongated by the complexity of the form of the channel, the frictional effect and others.

The theoretical values of the velocities of flow calculated by the equation (8) are shown in Fig. 20. From this it is found that the velocities in the channel without the reservoir become smaller as the period becomes longer. Comparing with Fig. 16, the velocities of flow in shorter period are the same as in the preceding article, but in longer period they become much smaller.

The effects of amplitude for the semi-diurnal tide and the 130 minutes' oscillation were again examined.

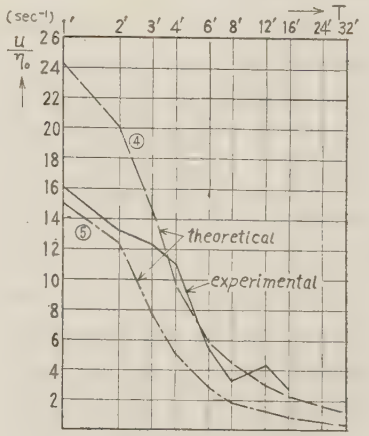

Fig. 20. Experimental maximum mean velocities at the station between ④ and ⑤, and theoretical values at ④ and ⑤ (without the reservoir).

The results are shown in Fig. 21 and Fig. 22. From these it is found that the ratios of amplitudes in this case are much different from those with the reservoir, that is, the ratios of amplitudes of the semi-diurnal tide do not vary throughout the channel for any amplitude, on the other hand those of the 130 minutes' oscillation of small amplitude become larger in the inner-part of the channel than those of large amplitude.

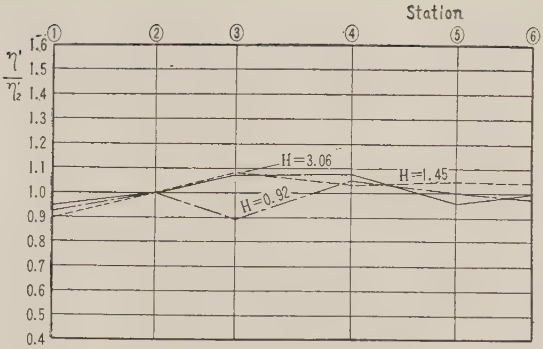

Fig. 21. Ratios of amplitudes for semi-diurnal tide of different amplitude (without the reservoir).

V. CONCLUSION

As the preliminary test for the hydraulic model experiment on the oscillation of the water level in Sakai Channel, the scale effect on the oscillation character for the channel and the difference between two characters of frequency response, one is for the channel with the reservoir and the other without the reservoir, were researched.

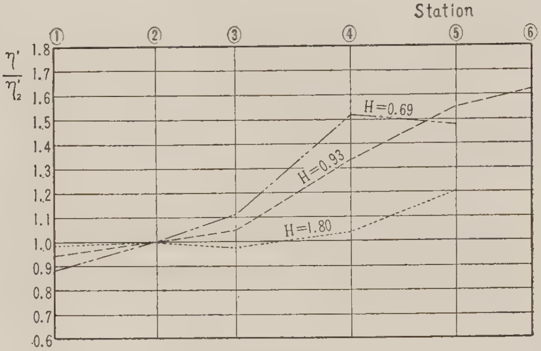

Fig. 22. Ratios of amplitudes for 130 minutes' oscillation of different amplitude (without the reservoir).

As a result, it became clear that

1) the scale effect was large for the oscillation of as long period as the semi-diurnal tide, but that was small for as short period as the 130 minutes' oscillation,

2) the frequency response of the system was largely influenced by existence of the reservoir, that is, in the channel with the reservoir the amplitudes of most provided oscillations were decreased, but for the case of no reservoir those were increased on the contrary, and the oscillation of particular period predominated, and

3) in both cases the velocities of flow for short period were not different, but those for long period became very small for the case of no reservoir.

These experiments were carried out as a preliminary test. Accordingly the area of the reservoir was not sufficiently large and the amplitude of each oscillation was too large. Therefore the obtained results may not be applied quantitatively to the prototype, but those may be correct qualitatively. To discuss quantitatively, it is necessary that a precise experiment is carried out with reference to these results.

We wish to thank Prof. S. Hayami, Mr. S. Adachi and Mr. H. Kunishi for their kind suggestion, and Mr. Y. Tani for his assistance in the experiment.

This work is partially supported by Ministry of Agriculture and Forestry of Japan.

STABLE CONFIGURATION OF COAST LINE

*Yasuo Mashima**

I. INTRODUCTION

In the natural coasts, the material which forms the beach or cliff is incessantly moved by wave action, longshore current and other canses. Some amount of coast material is carried away from the beach along or normal to the shore, while the other amount may be transported into the beach and accumulates there. The beach where the amount of supplied sediment balances with that of removed sediment during a certain period is defined as "equilibrium beach" and its profile normal to the shoreline may be called "equilibrium profile". Wave action and longshore current vary with time, but many coasts are considered to approach to their proper configuration, "ultimate shore line", after a very long lapse of time.

The advance or recess of a beach is resulted respectively from the increase or decrease of beach material in the area. Therefore the stability of a coast scope is related with the equilibrium conditions of supply and removal of sediment in this coast.

Rocky coasts are generally considered to be in equilibrium because there leaves no sediment under wave action and the rock resists to the erosion for a certain period. But even these rocky cliffs may be eroded in a sufficiently long period and approach to the ultimate configurations.

The motion of the coast materials is resulted by the waves which are originated by the winds. Though the wind blows from all directions, the most frequent direction at any situation is usually fixed in a narrow limit. Accordingly, though the motion of the coast materials will change in direction and volume corresponding to the wind, there will be a certain tendency of coastal process during a long period. For a certain length of time the coast will have a portion where the erosion and accretion will be repeated alternatively. This portion is defined as beach prism and its upper surface is produced by the accretion at calm condition and the lower surface is by the erosion at storm conditions. The deformation of the beach prism is affected by grading, specific gravity and shape, etc. of particle of the beach material. The situation of the beach prism relating to the wave action for a short time was reported previously[2]. The short period variation of beach prism is covered under the long time one, and does not affect on the general characteristics of the coast line. The slope and the grading of the particle in the prism face are changed according to the erosion or the accretion. Therefore the properties of beach prism are characterised by its thickness, slopes, grading of the particle of beach material (or the roughness of the prism surface) and the width of the prism. Tanner defined the stable coast as "the stable coast is that have such the coast line configuration and the sand prism characteristics as to produce the longshore processes which have the sufficient energy just to remove the beach materials transported from the upper end of the coast. And the time required to attain to the stable equilibrium is considered a long time".[1]

The beach prism consists of many kinds of materials, such as soft and fine clay or tough and strong rocks, and they are arranged on their situation according to the degree of waves respectively. If the coast material has an uniform property, the stable coast will maintain its situation by its configuration and slopes. When the coast slope is very steep, the important factor to maintain the stable condition is only the configuration of the coast line. Capes, head-lands or strong coast groins resist against the wave action and give influence on their neighbouring coast lines. They are the fixed points on the configuration of shore line. Between the adjoining fixed points, the beach prism has usually an uniform property, so that the coast maintains its coast line configuration and slope. The supply of materials around the fixed point will be related to the depth adjacent the fixed point and the approaching directions of the coast lines. In this report, the configurations of the coast line between the fixed points are described.

---

* Dr. Eng. Prof. of Civil Engineering Institute, Defence Academy, Yokosuka, Japan.

II. WAVE ENERGY DIAGRAM

The waves far offshore are characterised according to the directions, velocities and durations of winds and the fetch, and they propagate in the wind directions. The wave energy for unit width and one wave length is

$$E=\frac{\rho g}{8}H^2\lambda \quad \cdots\cdots (1)$$

where H : wave height (m), λ : wave length (m), T : wave period (sec), ρ : Density of fluid, g : gravity acceleration.

Assuming the waves are uniform, the total energy of continuous wave group is

$$E_t=E\times\frac{\text{duration time}}{T} \quad \cdots\cdots (2)$$

During the times of the development and the decay of waves, the height and length of wave are rather small, so the wave energy in these states may be negligible comparing with the total energy during one storm. Suming up the wave energies of each wind direction for a certain period and plotting them on their wind directions by length respectively, the wave energy distributing diagram during the time will be obtained. Even if the location of wind observation is far offshore, the wave by the land wind is small due to its fetch, and its wave energy is also small. Accordingly the diagram show larger energy for the sea wind direction and smaller for the land wind direction. Now assuming the significant wave to represent the waves in one storm, the factors of the significant wave are expressed as follows,

$$\left.\begin{aligned} H &: 0.0174\,F^{0.423}\,V^{1.154}\\ \lambda &: 0.8273\,F^{0.626}\,V^{0.748}\\ T &: 0.7282\,F^{0.313}\,V^{0.374}\\ F &: 3.6\,t\,V \end{aligned}\right\} \quad \cdots\cdots (3)$$

where V : wind velocity (m/sec), t : wind duration time (hour), F : Fetch (km).

The total energy of unit width is

$$E_t=\frac{\rho g}{8}\cdot\frac{(0.0174\,F^{0.423}\,V^{1.154})^2(0.8273\,F^{0.626}\,V^{0.748})}{0.7282\,F^{0.313}\,V^{0.374}}\,\frac{F\times 3600}{3.6\,V}$$

$$=\frac{\rho g}{8}(0.34396\,F^{2.159}\,V^{1.682})=0.04299\,\rho\,g\,F^{2.159}\,V^{1.682} \quad \cdots\cdots (4)$$

when the wind velocity is V and the fetch F is wind fetch. If F is land fetch, formula (4) represents the total wave energy of the duration time $t=F/3.6\,V$. Introducing wind fetch $F=3.6\,t\,V$ in (4),

$$E_t=0.04299\,\rho\,g(3.6\,t\,V)^{2.159}\,V^{1.682}\,0.68299\,t^{2.159}\,V^{3.841} \quad \cdots\cdots (5)$$

If the ratio of the mean wave height to the significant wave height is about 0.67, and the wave length and the wave period are equal each other, by multiplying $(0.67)^2=0.4489$ to (5), the total wave energy is

$$E_t=0.3066\,\rho\,g\,t^{2.159}\,V^{3.841} \quad\cdots\cdots(6)$$

Formula (6) is the total energy of one group wave produced by the wind fetch F, that is $F=3.6\,tV$.

If F is land fetch, t is duration time and $F=3.6\,tV$, the number of waves is t/T. Then

$$E_t=\frac{\rho\,g}{8}\frac{(0.0174\,F^{0.423}\,V^{1.154})^2(0.8273\,F^{0.626}\,V^{0.748})t\times 3600}{0.7282\,F^{0.313}\,V^{0.374}}$$

$$=\frac{\rho\,g}{8}(1.23826\,F^{1.159}\,V^{2.682})t=0.15478\,\rho\,gF^{1.159}V^{2.682}\,t \quad\cdots\cdots(7)$$

Multiplying the ratio $(0.67)^2=0.4489$ to (7),

$$E_t=0.06948\,\rho\,g\,F^{1.159}\,V^{2.682}\,t \quad\cdots\cdots(8)$$

Formula (8) is the total energy of one group wave produced by the land fetch F which is smaller than $F=3.6\,tV$. The wave energy diagram is obtained by plotting the sum of E_t in each wind direction.

In the wind energy diagram, in which each area between two radial lines includes the wind direction as a center line and represents the total energy ΣE_t of each direction.

Then $$\frac{2\pi}{16}\frac{R^2}{2}=\Sigma E_t$$

Therefore $$R=\sqrt{\frac{16}{\pi}\Sigma E_t} \quad\cdots\cdots(9)$$

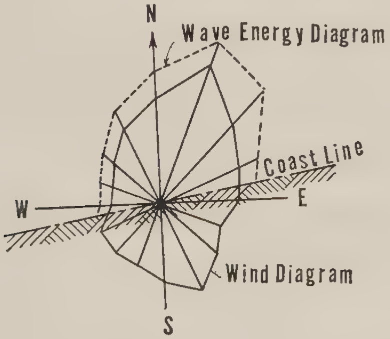

Fig. 1

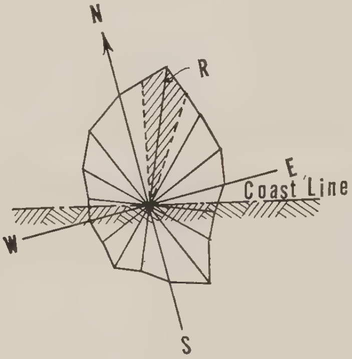

Fig. 2

R is the radial length to be taken on each wind direction line and the area of such diagram will be the wave energy on each direction.

The shape of these wave energy diagram is approximately an ellipse cut by a straight line of coast line direction. These diagram for a long period will include any short time variations of wave energy. The seasonal variation will be indicated in each season diagram.

III. CONDITIONS OF COAST LINE STABILITY

When the offshore waves approach to the coast, its form, velocity and direction are varied by the effect of sea bottom. Therefore the total energy of offshore wave does not always arrive the coast. But when the depth near shoreline is sufficiently large, the most part of the wave energy will be supplied in the direction of wind. When the components of this energy normal and parallel to the coast are designated by E_n and E_p respectively,

the equation $E_p=0$, or constant on any point of the coast ·································· (10)
signifies that the littoral drift of sand is none or constant along the coast. That is, when the littoral drift does not be supplied from the one end of the coast, the condition of the stable equilibrium is $E_p=0$, and when the littoral drift is supplied from one end of the coast and transfered out of the other end, the condition of stable equilibrium is $E_p=\text{const.}$ If the resistance properties of beach prism to the erosion are constant, it indicated in the previous report[3] that the eroded volume is approximately proportional to the wave energy E_t. So if $E_p=\text{constant}$ along the coast, the advance or recess of the coast line will be related with the magnitude of E_n. The coast line will take the location where the resistibility of beach prism is in balance with E_n on that location. The ordinary sandy beach will be eroded at offshore positions where E_n is large, but it will be sufficiently resistible and not be eroded at the interior of a bay where E_n is small. Therefore there must exist E_n that is critical to the erosion corresponding to the properties of beach prism. The problem whether the coast is eroded or not, may be decided by that the actual E is larger or not than the critical E_n, say E_{nc}, of that beach prism.

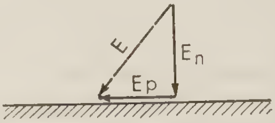

Fig. 3

The coast where the condition

$$E_{nc}>E_n \qquad \cdots\cdots (11)$$

is satisfied, is stable to the actual E_n.

In order to stabilize any coasts artificially, the following methods shall be adopted by one or in combination. Those are to make E_n (right side of (11)) smaller than ever, to increase E_{nc} (left side of (11)) by coast protections, or to supply sediment to the coast in order to maintain its coast position (beach nourishment). Similarly the natural coasts maintain their stability by the decrease of E_n attained by the roughness of sea bottom and the decrease of the water depth, the increase of E_{nc} attained by the slope and sand grading of beach prism, and $E_p=\text{const.}$ by the constant continuous supply of littoral drift to the coast.

IV. CONFIGURATION OF STABLE COAST LINE

As above described, offshore waves vary their magnitudes and directions in the way of their arrival to the coast. But it seems that these variations have only secondary effects. Therefore at first it assumes that the offshore wave energies arrive at the coast in their direction and subsequently the correction deduced from this assumption will be considered. As explained in the section 2, the wave energy diagram at the coast is approximately a half of an ellipse and the wave energy at any direction is the partial area of the ellipse including the direction. Considering a coast between two neighbouring fixed points, the total wave energy at any point between them is expressed by the area of the wave energy diagram cut off by the direction lines connected the point and the two fixed points, If the wave energy diagram is approximately a geometrical circle or ellipse, the wave energy at any point can be calculated mathematically, but if the diagram has an irregular shape, the wave energy at any point will be investigated from the area of the diagram. Generally the wave energy diagram resemble an ellipse. So in order to find the fundamental configuration of general coasts it is assumed that the wave energy diagram can be expressed approximately by a half of a circle or an ellipse.

1. The case when the wave energy diagram is a semicircle.

In Fig. 4, A and B is the fixed points, $AB=l$ is the distance between A and B, and 0 is the origin of co-ordinate axes x and y taking as Fig. 4.

The co-ordinates of any point $p\ (x, y)$ is expressed in dimensionless factors as

$$\frac{x}{\frac{l}{2}}=p \quad \text{and} \quad \frac{y}{\frac{l}{2}}=q \quad \cdots\cdots\cdots\cdots\cdots\cdots (12)$$

The wave energy arrived the point P can be expressed by the area $A'OB'$ of the wave energy diagram cut off by the radial lines parallel to PA and PB.

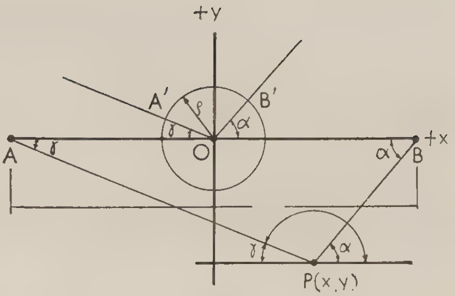

Fig. 4

$$\left.\begin{array}{l} \text{The direction angle of } PB:\ \alpha=\tan^{-1}\dfrac{-y}{\frac{l}{2}-x}=\tan^{-1}\dfrac{-q}{1-P} \\ \text{The direction angle of } PA:\ \delta=\pi+\gamma=\pi+\tan^{-1}\dfrac{y}{\frac{l}{2}+x}+\tan^{-1}\dfrac{q}{1+P} \end{array}\right\} \cdots\cdots\cdots\cdots\cdots\cdots (13)$$

Assuming the radius of the wave energy diagram as, the energy component normal to x axis as A and that parallel to x axis as B,

$$\left.\begin{array}{l} A=\displaystyle\int_\alpha^\delta \frac{\rho^2}{2}\sin\theta\, d\,\theta=\frac{\rho^2}{2}(-\cos\delta+\cos\alpha) \\ B=\displaystyle\int_\alpha^\delta \frac{\rho^2}{2}\cos\theta\, d\,\theta=\frac{\rho^2}{2}(\sin\delta-\sin\alpha) \end{array}\right\} \cdots\cdots\cdots\cdots\cdots\cdots (14)$$

Introducing (11) in (14)

$$\left.\begin{array}{l} A=\dfrac{\rho^2}{2}\left\{\dfrac{1+p}{\sqrt{(1+p)^2+q^2}}+\dfrac{1-p}{\sqrt{(1-p)^2+q^2}}\right\} \\ B=\dfrac{\rho^2}{2}\left\{\dfrac{-q}{\sqrt{(1+p)^2+q^2}}+\dfrac{q}{\sqrt{(1-p)^2+q^2}}\right\} \end{array}\right\} \cdots\cdots\cdots\cdots\cdots\cdots (15)$$

The angle between the coast line at P and x axis is assumed as φ. The direction of propagation of energy in the wave energy diagram is expressed by the direction of the center from the circumference of the energy circle, so that (+) of A and B in formula (15) is the direction in Fig. 5.

The wave energy E_n normal to the coast (this direction is taken (+)) is

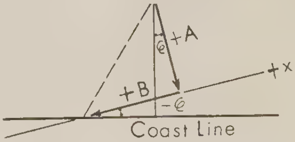

Fig. 5

$$E_n=A\cos\varphi-B\sin\varphi \quad \cdots\cdots\cdots\cdots\cdots\cdots (16)$$

The wave energy E_p parallel to the coast and to the right side facing to offshore (this direction is taken (+)) is

$$E_p=-A\sin\varphi-B\cos\varphi \quad \cdots\cdots\cdots\cdots\cdots\cdots (17)$$

When there are not any flowing in or out of coast materials around the fixed points A and B, it must be $E_p=0$ at the stable coast. Namely $-A\sin\varphi-B\cos\varphi=0$, hence $\tan\varphi=-\dfrac{B}{A}$, so that $\dfrac{dy}{dx}=-\dfrac{B}{A}$.

Accordingly

$$-\frac{dq}{dp}=\frac{B}{A}=\frac{-q\sqrt{(1-p)^2+q^2}+\sqrt{q(1+p)^2+q^2}}{(1+p)\sqrt{(1-p)^2+q^2}+(1-p)\sqrt{(1+p)^2+q^2}} \cdots\cdots\cdots\cdots\cdots\cdots (18)$$

$$\Delta q=\frac{q\sqrt{(1-p)^2+q^2}-q\sqrt{(1+p)^2+q^2}}{(1-p)\sqrt{(1-p)^2+q^2}-(1-p)\sqrt{(1+p)^2+q^2}}\Delta p \cdots\cdots (19)$$

On the curve line that satisfies this formula (18) or (19), the energy component of the tangent direction to the curve is zero and there is no littoral drift. The curve line calculated by the successive numerical integration of (19) is the fundamental form of the stable coast. Fig. 6 is the examples of stable coasts through the points $p=0$ $q=-0.1$, $p=0$ $q=-0.3$ and $p=0$ $q=-0.5$. This coast line is symmetric on account of the circular energy diagram.

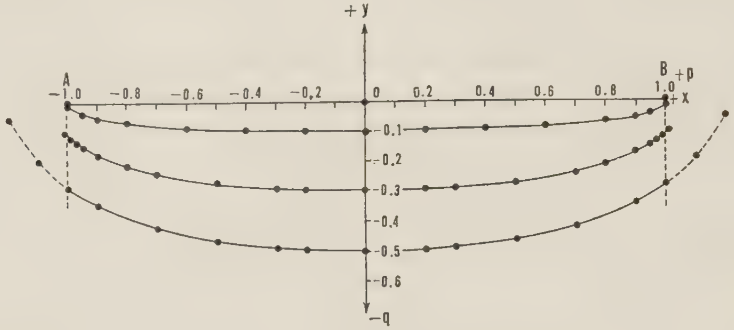

Fig. 6

On the middle point of the coast where $\varphi=0$, the energy component normal to the coast E_n is

$$E_n=A=\rho^2\left(\frac{1}{\sqrt{1+q^2}}\right) \cdots\cdots (20)$$

Even if it is assumed that the wave energy does not damp in the bay, the normal energy component diminishes corresponding to the depth of bay as shown in Table-1 and Fig. 7.

Table-1

q	E_n/ρ^2	q	E_n/ρ^2	q	E_n/ρ^2
0	1.0	−0.5	0.8944	−2.0	0.4472
−0.1	0.9950	−0.6	0.8574	−2.5	0.3713
−0.2	0.9805	−0.8	0.7808	−3.0	0.3162
−0.3	0.9581	−1.0	0.7072		
−0.4	0.9292	−1.5	0.5547		

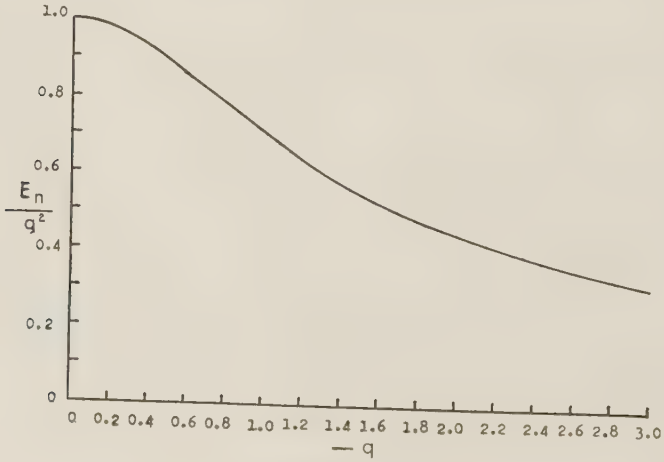

Fig. 7

If the wave energy is consumed more or less by the bottom friction in the bay, E_n will be smaller than Fig. 7. At the interior of the bay where the depth is equal to the width of the bay entrance, E_n is about 0.45 of that at the entrance. The depth of bay will settle at the position where $E_n \leq$Critical E_n of the beach prism.

In the stable coast where the littoral drifts move in around a fixed point and out from another point,

$$-A\sin\varphi - B\cos\varphi = E_p = \text{const.} \quad \cdots\cdots (21)$$

$E_p > 0$ is the case when the littoral drift moves to the right side along the coast facing to offshore.

From (21) $$A\tan\varphi + B + \frac{E_p}{\cos\varphi} = 0$$

Therefore $$\tan\varphi = \frac{dy}{dx} = \frac{dq}{dp} = \frac{-AB \pm E_p\sqrt{A^2+B^2-E_p^2}}{A^2-E_p^2} \quad \cdots\cdots (22)$$

Introducing (15) in (22), the configuration of the stable coast line can be calculated. Here E_p is related to the volume and properties of supplied littoral drift.

From (21) $$E_p = \frac{-A\tan\varphi - B}{\sqrt{1+\tan^2\varphi}} \quad \cdots\cdots (23)$$

When E_p calculated from (23) using $dy/dx = \tan\varphi$ and A and B of actual coast transports the coast materials more than the supplied, the coast will be eroded and when less, it will be deposited, and both coast lines are unstable.

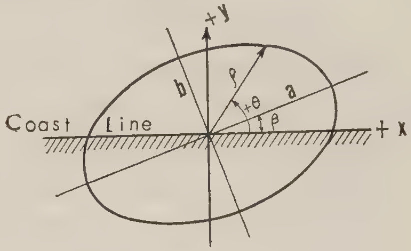

Fig. 8

2. The case when the wave energy diagram is a semi-ellipse.

When it can be assumed that the wave energy dia gram is approximately a semiellipse, a and b represent its major and minor radii on sea wind side respectively, and β is the angle between the major axis of the ellipse and x axis. If the ellipse is represented by polar coordinates in Fig. 8,

$$\rho^2 = \frac{b^2}{1-e^2\cos^2(\theta-\beta)} \qquad \text{where } e = \sqrt{\frac{a^2-b^2}{a^2}} \quad \cdots\cdots (24)$$

Taking the straight line connecting the fixed points as x axis, the wave energy component A normal to x axis, and the component B parallel to x axis are as follows,

$$A = \frac{1}{2}\int \rho^2 \sin\theta \, d\theta = \frac{1}{2}\int \frac{b^2\sin\theta}{1-e^2\cos^2(\theta-\beta)} d\theta$$

$$= \frac{b^2}{4e}\cos\beta \log\frac{y^2-2ey+1}{y^2+2ey+1} + \frac{b^2\sin\theta}{2e\sqrt{1-e^2}}\tan^{-1}\frac{2e\sqrt{1-e^2}}{1+y^2-2e^2} \quad \cdots\cdots (25)$$

$$B = \frac{1}{2}\int \rho^2 \cos\theta \, d\theta = \frac{b^2}{2}\int \frac{\cos\theta}{1-e^2\cos^2(\theta-\beta)} d\theta$$

$$= \frac{b^2\cos\beta}{2e\sqrt{1-e^2}}\tan^{-1}\frac{2e\sqrt{1-e^2}}{1+y^2-2e^2} - \frac{b^2}{4e}\sin\beta \log\frac{y^2-2ey+1}{y^2+2ey+1} \quad \cdots\cdots (26)$$

where $$y = \sqrt{1+\tan^2(\theta-\beta)} - \tan(\theta-\beta) = \frac{1-\sin(\theta-\beta)}{\cos(\theta-\beta)} \quad \cdots\cdots (27)$$

The limits of the integration of (25) and (26) are α and $\pi+\gamma$. Using the co-ordinates of any point in (12), and α and γ in (13), the limit values of y at α and $\pi+\gamma$ are as follows.

$$\left.\begin{aligned} y_\alpha &= \frac{\sqrt{q^2+(1-p)^2} + q\cos\beta + (1-P)\sin\beta}{(1-p)\cos\beta - q\sin\beta} \\ y_{\pi+\gamma} &= \frac{\sqrt{q^2+(1+p)^2} + q\cos\beta - (1+p)\sin\beta}{-(1+p)\cos\beta - q\sin\beta} \end{aligned}\right\} \quad \cdots\cdots (28)$$

Introducing (28) in (25) and (26), A and B can be calculated by subtracting the value used y_α from the value used $y_{\pi+\gamma}$.

Similarly as preceding (1), assuming the angle between the coast line and x axis as φ, the wave energy component E_p parallel to the coast line ((+) is the energy towards the right direction facing off shore) is

$$E_p = -A\sin\varphi - B\cos\varphi \quad \cdots\cdots (29)$$

The wave energy component E_n normal to the coast line ((+) is the energy towards on shore) is

$$E_n = A\cos\varphi - B\sin\varphi \quad \cdots\cdots (30)$$

The configuration of the stable coast where is no littoral drift around the fixed points must satisfy $E_p=0$, namely

$$\frac{dq}{dp} = -\frac{B}{A} \quad \cdots\cdots (31)$$

The configuration of the stable coast where is some supply of littoral drift from one end of the coast must satisfy $E_p=\text{const}$, then

$$\frac{dq}{dp} = \frac{-AB \pm E_p\sqrt{A^2+B^2-E_p^2}}{A^2-E_p^2} \quad \cdots\cdots (22)$$

If the E_p calculated from (23) using A, B and φ of the actual coast cannot transport the supplied materials, it happens there an accretion, on the contrary if it transports more than the supplied, there is an erosion, where both are unstable coasts.

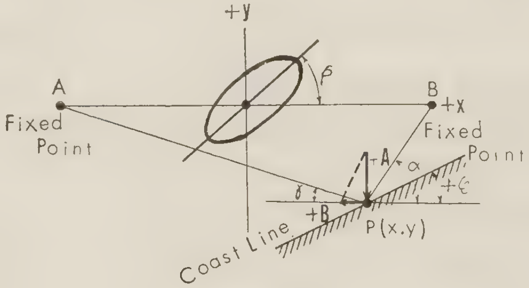

Fig. 9

The results of calculation on Kujukurihama Coast as an example are tabulated in Table-2 and plotted in Fig. 10.

In this calculation, the annual mean wind direction diagrams at Katsuura and Choshi Meteorological Observatories were adopted for the reason of insufficient investigations on the wave data. The diagram has $a=9.45$, $b=3.90$, $e=0.918$ and $\beta=+11°43'$. The values of A,

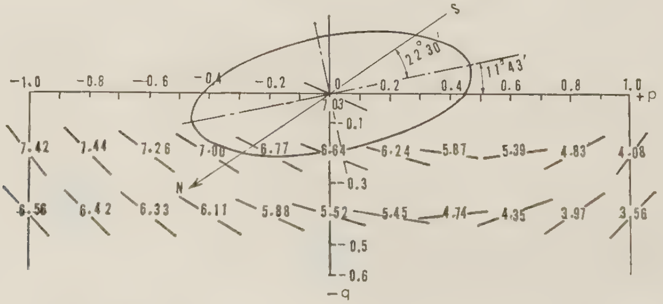

Fig. 10 The distribution of wave energy and the direction of tangents on the stable coast of $E_p=0$.

Table-2

p	q	A	B	$-B/A$	φ	$R=\sqrt{A^2+B^2}$
1.0	−0.2	2.4490	−3.2665	1.3338	53° 8′	4.08
	−0.4	2.4490	−2.5899	1.0565	46 35	3.56
0.8	−0.2	4.2593	−2.2737	0.5338	28 6	4.83
	−0.4	3.2873	−2.2260	0.6771	34 6	3.97
0.6	−0.2	5.3478	−0.6920	0.1294	7 23	5.39
	−0.4	4.1055	−1.4492	0.3529	19 26	4.35
0.4	−0.2	5.8249	0.7302	−0.1254	− 7 9	5.87
	−0.4	4.7167	−0.4464	0.0946	5 18	4.74
0.2	−0.2	6.0210	1.6434	−0.2729	−15 16	6.24
	−0.4	5.4089	0.7219	−0.1334	− 7 36	5.45
0.0	0.0	6.4332	2.8355	−0.4407	−23 47	7.03
	−0.2	6.2243	2.3102	−0.3711	−20 22	6.64
	−0.4	5.3285	1.4426	−0.2707	−15 9	5.52
−0.2	−0.2	6.0990	2.9441	−0.4827	−25 46	6.77
	−0.4	5.4310	2.2697	−0.4179	−22 41	5.88
−0.4	−0.2	6.0265	3.5656	−0.5917	−30 37	7.00
	−0.4	5.2890	3.0712	−0.5806	−30 8	6.11
−0.6	−0.2	5 8857	4.2606	−0.7238	−35 54	7.26
	−0.4	5.0410	3.8297	−0.7597	−37 13	6.33
−0.8	−0.2	5.2925	5.2254	−0.9873	−44 36	7.44
	−0.4	4.5844	4.5000	−0.9816	−44 28	6.42
−1.0	−0.2	4.6556	5.7833	−1.2422	−51 10	7.42
	−0.4	4.5032	4.7698	−1.0592	−46 39	6.56

B and R in Table-2 is multipliers of $b^2/4e$.

The configuration of stable coast calculated by progressive numerical integration of (31) through the point $p=0$, $q=-0.4$ is the dotted line in Fig. 11. And the direction of the stable coast at the actual coast are investigated on the coincidence with the tangent line on the coast in Fig. 11 in which it seems that the right side is nearly stable, but the left is unstable and erosive. The stable coast supported at the both fixed points is the lower dotted line in Fig. 11 which has no erosion even at left side. From above this coast seems to be approaching to the stable state and to maintain its situation on behalf of the resistibility against the erosion in spite of the strong longshore current towards the left side.

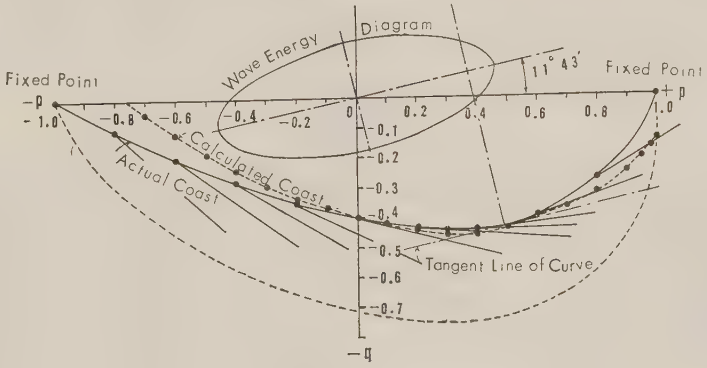

Fig. 11

This configuration of the stable coast is about parabolic on which the tangent direction at the apex of parabola coinsides with the direction of major axis of wave energy diagram and the direction of axis of the parabola with the direction of minor axis. In order to decide whether this characteristics can be applied to the actual coast of general bow shape, it is necessary to investigate the stability of the coast by other data, and the relation between the axes of the wave energy diagram and the axis of the coast parabola.

V. STABILITY OF THE CONFIGURATION OF ACTUAL COASTS

If it is assumed that the general configuration of a bow shape coast is a parabola $y=px^2-b$, the formula of the parabola by the rotation of θ is

$$X\sin\theta+Y\cos\theta=p(X\cos\theta-Y\sin\theta)^2-b \cdots\cdots\cdots (32)$$

The lengths of each part is designated as in Fig. 12.

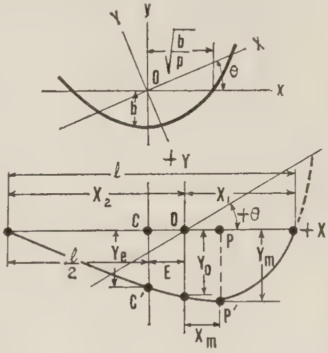

Fig. 12

From X_m-E, l, Y_e and Y_m that can be observed in the plan of the bow shape coast, the values of θ, b, p, E, X_m and Y_e are calculated as follows.

Known values : $Y_m/l=m,\ \ Y_e/l=e,\ \ \dfrac{X_m-E}{l}=\varepsilon.$

Unknown values : $X_m/l=x,\ b/l=\beta,\ l_p=q$, and θ, where p and q are the different factors from those in chapter 4.

The results of calculation are

$$\left.\begin{aligned}
&\tan\theta=\frac{\varepsilon}{m}\\
&x-\varepsilon=\frac{\varepsilon(4e^2\varepsilon^2-m^2)}{8em(m^2+\varepsilon^2)}\\
&q=\frac{4e(m^2+\varepsilon^2)\sqrt{m^2+\varepsilon^2}}{m(4e^2\varepsilon^2-m^2)}\\
&\beta=\frac{\varepsilon}{2\sqrt{m^2+\varepsilon^2}}\left\{\frac{1}{4(x-\varepsilon)}-(x-\varepsilon)\right\}=\frac{1}{\sqrt{m^2+\varepsilon^2}}\left\{\frac{em(m^2+\varepsilon^2)}{4e^2\varepsilon^2-m^2}-\frac{\varepsilon^2(4e^2\varepsilon^2-m^2)}{16em(m^2+\varepsilon^2)}\right\}
\end{aligned}\right\}\cdots(33)$$

Table–3 is the results of calculation on the bow shape coasts of Tokyo Bay, Sagami Bay and Bosō Peninsula of where the plans are the aerial photographs taken by Japanese Maritime Self Defence Force at Tateyama. From Table–3 and Fig. 13, the direction of parabola axis calculated from the assumption that the configuration of the bow shape coast is parabolic, seems to coincide approximately with the direction of the axis of annual wind frequency diagram by the Meteorological Observatory, but the special coasts (such as Kokubo Coast) where are considered the existence of fairly transportation of littoral drift around the fixed points must be investigated far more hereafter.

Table–3

No.	Coast	l	e	m	ε	θ
1	Mabori-Kaigan	1 690m	−0.092 899	−0.111 243	0.235 503	−64°43′
2	Isemachi-kaigan	917	−0.158 124	−0.173 391	0.197 383	−48 42
3	Zushi-Shinjukuhama	1 143	−0.209 781	−0.214 152	0.048 949	−12 52
4	Ōiso-Kugenuma	15 303	−0.067 372	−0.086 519	−0.250 604	70 57
5	Yuigahama	2 258	−0.209 920	−0.222 320	0.111 160	−26 34
6	Shichirigahama	4 516	−0.172 719	−0.265 500	0.277 679	−46 17
7	Enoshima-Koshigoe	976	−0.242 828	−0.254 098	−0.180 328	35 22
8	Ditto (Outer coast)	1 226	−0.305 057	−0.309 135	−0.084 013	15 12
9	Ōiso-Kugenuma (Outer)	14 483	−0.105 434	−0.140 510	−0.304 840	65 15
10	Nanko-Kugenuma	7 721	−0.108 276	−0.124 595	−0.294 262	67 3
11	Futtsu-Kokubo	8 562	−0.113 291	−0.119 822	−0.139 337	49 18
12	Ōsawa-kaigan	4 791	−0.093 091	−0.095 178	−0.015 341	9 9
13	Kokubo (Inner coast)	468	−0.151 709	−0.181 624	0.151 709	−39 52
14	Kokubo (Outer coast)	669	−0.282 511	−0.300 448	0.143 498	−25 32
15	Hirasaura	4 063	−0.109 279	−0.117 401	−0.092 789	38 19
16	Kujukurihama	51 603	−0.204 465	−0.204 988	0.044 823	−12 20
17	Futtsu-Kokubo (Outer)	8 473	−0.152 602	−0.169 715	−0.143 397	40 12
18	Hirasaura (Outer coast)	4 839	−0.137 632	−0.144 451	−0.126 059	41 7

No.	$x-\varepsilon$	q	B	p	$\frac{\sqrt{\beta_q}}{2}$	E	Date of Photo.
1	−0.439 258	−5.642 402	−0.058 721	−0.003 339	0.287 805	742.34m	June 19, 1957
2	−0.341 157	−2.528 102	−0.147 120	−0.002 757	0.304 932	312.84	〃
3	−0.128 240	−0.914 088	−0.202 901	−0.000 800	0.215 331	146.58	Aug. 22, 1957
4	−0.485 077	−9.147 540	−0.014 296	−0.000 598	0.180 813	−7 423.13	〃
5	−0.227 688	−1.227 627	−0.194 603	−0.000 544	0.244 387	514.12	〃
6	−0.314 316	−2.407 509	−0.173 855	−0.000 533	0.323 480	1 419.45	〃
7	0.214 096	−2.032 372	−0.275 948	−0.002 082	0.374 442	−208.96	〃
8	0.100 849	−1.396 275	−0.311 836	−0.001 139	0.329 927	−123.64	〃
9	0.356 389	−7.269 826	−0.156 705	−0.000 502	0.533 671	−5 161.58	〃
10	0.306 063	−9.897 058	−0.235 157	−0.001 282	0.762 785	−2 363.11	〃
11	0.507 622	−1.757 026	(+0.005 724)	−0.000 205	(0.050 142)	−4 346.26	June 19, 1957
12	0.209 110	−0.390 643	−0.078 481	−0.000 082	0.087 547	−1 001.86	〃
13	−0.144 987	−3.753 150	−0.506 168	−0.008 020	0.689 152	67.85	〃
14	−0.159 541	−1.658 793	−0.303 291	−0.002 480	0.354 646	106.73	〃
15	0.539 936	−0.933 121	(+0.023 824)	−0.000 230	(0.074 549)	−2 193.76	Unknown
16	−0.126 560	−0.884 259	−0.197 487	−0.000 171	0.208 943	6 530.87	〃
17	0.376 971	−1.467 236	−0.092 360	−0.000 173	0.184 061	−3 194.08	June 19, 1957
18	0.423 977	−1.366 197	−0.054 475	−0.000 282	0.136 403	−2 051.62	Unknown

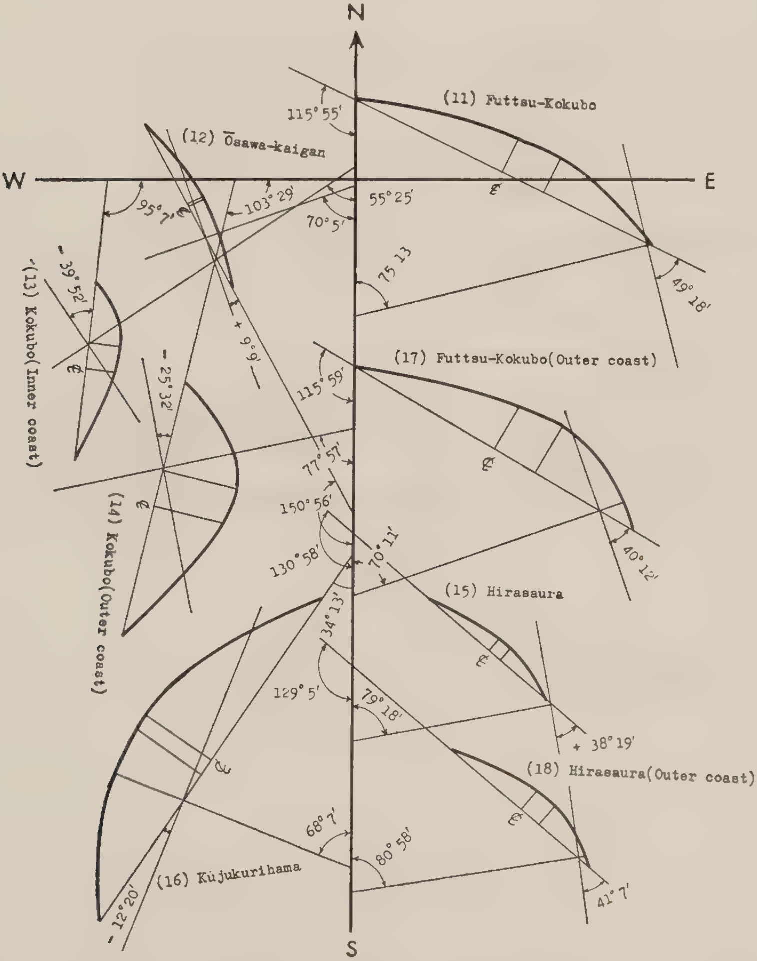

Fig. 13 (a)

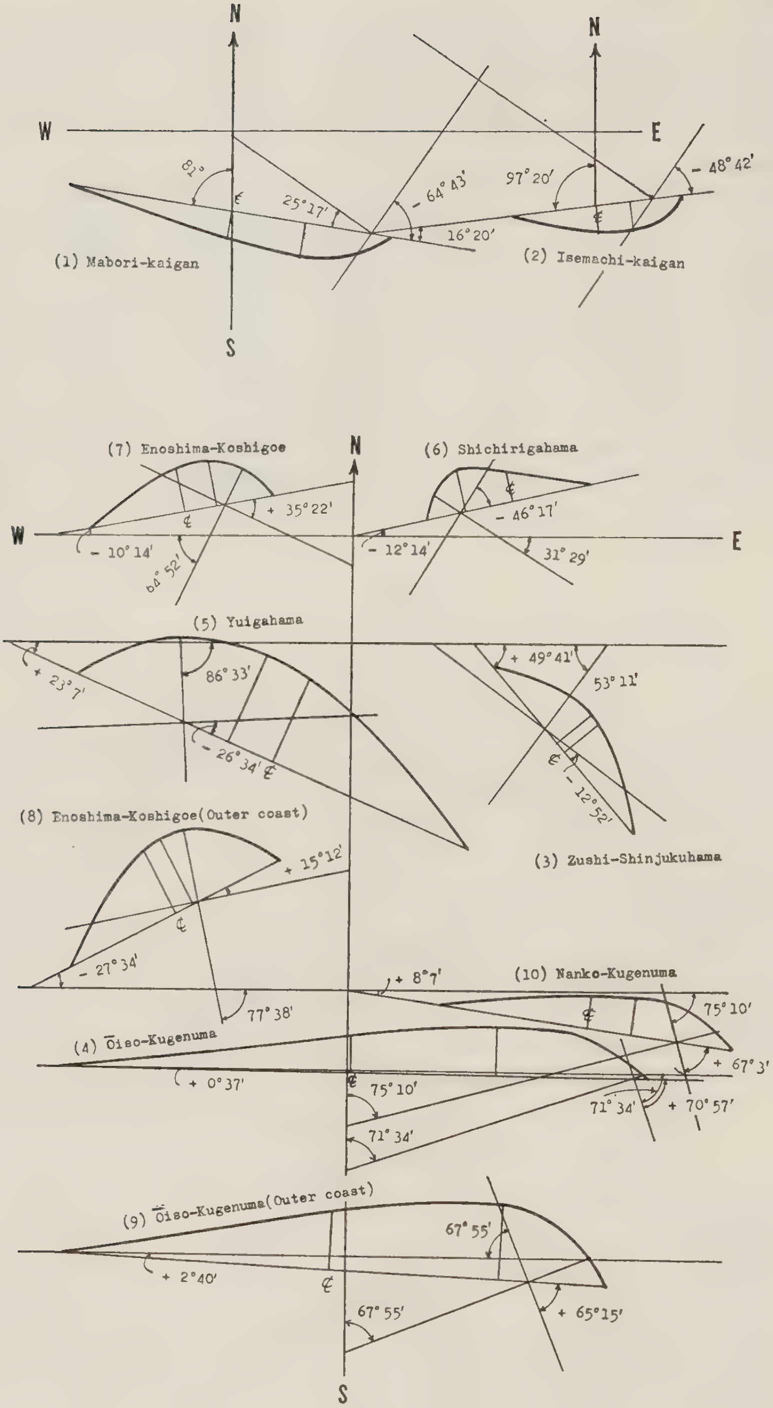

Fig. 13 (b)

VI. CONCLUSION

The calculation methods of the fundamental configuration of movable coast as sandy coasts that satisfies the condition of stable equilibrium, the estimation of stability of the actual coasts and the relation between the position of coast line, the resistibility of beach prism and the wave energies are described in this report. Hereafter it is necessary to research the correction of the effects of sea bottom friction, wave reflection and wave refraction on the relation between the beach prism and wave energy, and the numerical values of wave energy diagram by the observation of actual waves along the coasts.

On this study, the author appreciats heartily to the assistances of the Experimental Research Fund of Ministry of Education, the Yokosuka Headquaters of Japanese Maritime Self Defence Force and the Institute of Civil Engineering of the Defence Academy.

REFERENCE

1) Tanner, W.F. : The equilibrium Beach, Trans. A.G.U. Vol. 39, No. 5, Oct. 1958.
2) Mashima, Y. : Study on Littoral Drift and Longshore Current, Coastal Engineering in Japan, Vol. 1, 1958. (Proceedings of Coastal Engineering Conference, Vol. 2, Nov. 1955, in Japanese).
3) Mashima, Y. : Study on the Volume of Littoral Drift, Coastal Engineering in Japan, Vol. 2, 1960. (Proceedings of Coastal Engineering Conference, Vol. 5, Nov. 1958, in Japanese).

SOME EXPERIMENTS ON BAMBOO SAMPLERS

*Hisao Fukushima,
**Masakazu Kashiwamura

In recent years, present authors have carried out a series of studies on some problems of coastal engineering, such as the measurement of coastal current, sand drift, and the distribution of the size of sediment particles, etc. The main difficulty in pursuing these kinds of studies exists in obtaining proper measuring apparatus. Authors have proposed a use of bamboo samplers vertically set in the sea for the purpose of measuring the distribution of sand drift. Some of the results obtained in this manner are already reported in previous papers. The actual motion of bamboo samplers is very much complicated in the running sea, but when the sea is calm and there is no current, the angle φ, which the bamboo sampler makes with the level is given by

$$\varphi=\sin^{-1}\frac{H}{L}\sqrt{\frac{\rho_0}{\rho}} \tag{1}$$

where ρ_0 is the specifiic weight of the sea water and ρ is the apparent specific weight of the bamboo pole. If the pole is shorter than 1.8 times of the water depth, the pole will stand upright, under the assumption that ρ is 0.3. But in most cases, the pole inclines somewhat due to the coastal current, as is often observed from the shore. However, the relations between the mass of the sediment in the sampler and the density of suspending load in the natural sea water has not yet been directly obtained.

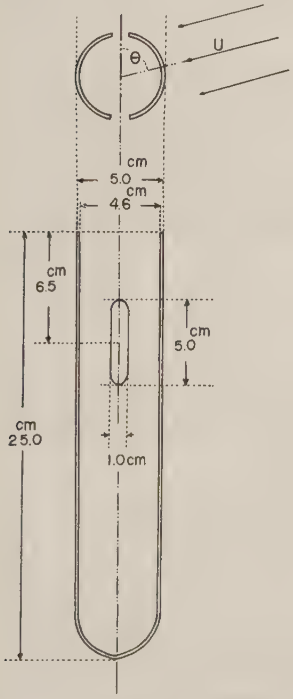

Fig. 1

The mass of the sediment which was gathered through the holes of the sampler may depend upon the following factors :

1) the density or the mass of suspending load per unit volume of sea water in which the sampler is set,
2) the time interval during which the sampler was set in the sea,
3) the size of the holes,
4) the angle θ between the direction of the current velocity and the direction of the holes in the sampler, (see Fig. 1)
5) the relative motion between the sampler and the sea water.

A preliminary laboratory experiment of a sampler tube was carried to obtain the basic data of analyzing the mechanism of the bamboo sampler, though the sampler tube set steadily in a water vessel can not directly be compared with the results obtained in the field observation.

The behavior of stream lines was traced by the method of equipotential line by assuming a two-dimensional ideal flow. The experiment was undertaken by the use of a tin foil of 0.02 mm in thickness. The size of the foil was 30 cm × 23 cm

---

* Dr. Science, Professor of Hokkaido University, Sapporo

** Lecturer of Hokkaido University, Sapporo

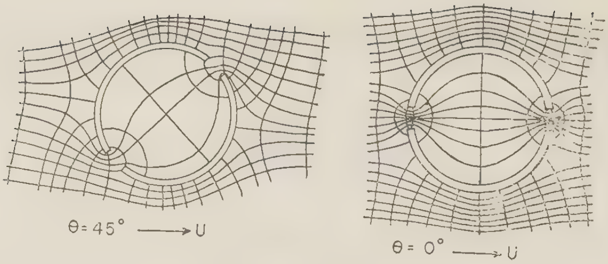

Fig. 2

wide, which was large enough to avoid the edge effect. The stream lines obtained are shown in Fig. 2. From these stream lines, it was found that the relation between the undisturbed velocity and the mean velocity flowing through the holes can be represented by

$$\frac{u}{U} \doteqdot 3\cos\theta \tag{2}$$

where u is the mean velocity of water in the tube, and U is the velocity of water at a point sufficiently far from the tube.

An experiment of the sampler tube was carried out by the use of pulverized coal instead of natural sand. The water vessel has the diameter of 120 cm and the height of 40 cm. The water in the vessel was circulated by a fan which was driven by an electric motor of 1/2 H.P. Several grades of pulverized coal were prepared as are shown in Fig. 4 and Fig. 5. A glass tube of the same size with the bamboo sampler was also tested to observe the motion of the particles captured in the tube.

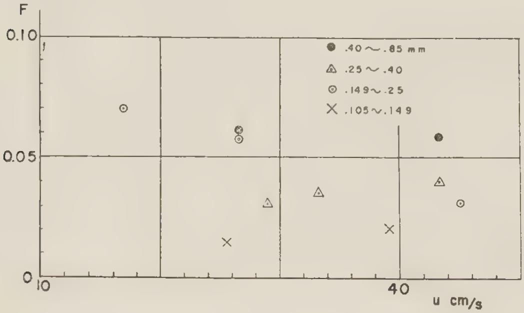

Fig. 4

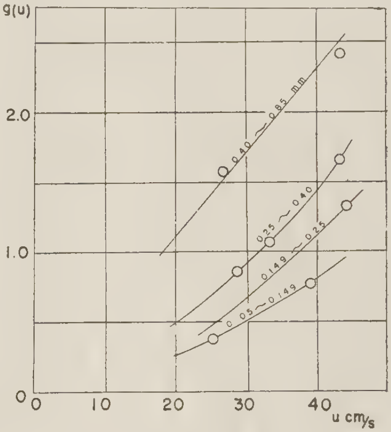

Fig. 5

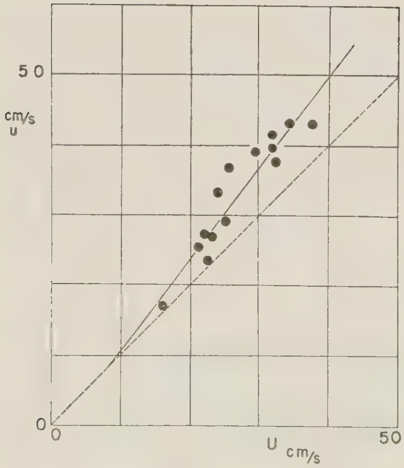

Fig. 3

The length of the tube was 25 cm and the outer and inner diameters were 5.0 cm and 4.6 cm respectively. The dimensions of the hole are given in Fig. 1. The center of the hole is placed at about 6.5 cm from the top of the tube.

The velocity of the current in- and out-side of the tube was measured by a Pitot tube to obtain the relation between u and U which is shown in

Fig. 3. The velocity u is larger than U by about 0~25%, when $\theta=0$. The ratio of the mass of the suspended load (S_i) which flows into the tube per unit time to the mass sedimented in the tube (S_f) gives the efficiency of capture F. Namely,

$$\frac{S_f}{S_i}=F \tag{3}$$

F may be considered as the function of dimensionless quantities of $\frac{\varepsilon}{uD}$, $\frac{b}{D}$, $\frac{a}{D}$ and $\frac{w_0}{u}$, where a and b are the height and the breadth of the hole, D is the diameter of the tube, w_0 is the sediment velocity of particles, and ε represents the austausch coefficient between the part flowing through and the other part in the tube.

For constant values of a,b, and D,ε is a function of u. Then F must be a function of u and w_0. On the other hand,

$$S_i=C_0Au \tag{4}$$

where C_0 and A represent the density of the suspended materials and the area of the hole, respectively, Therefore,

$$S_f=FS_i=FuAC_0=g(u)AC_0 \tag{5}$$

where $Fu(=g(u))$ has a dimension of velocity and is a function of w_0 and u. When U is obtained from the observation in the natural sea, u can be assumed. If the functions $g(u)$ and S_f are known, the density of suspended load in the sea C_0 will be determined.

When S_f and C_0 are measured, the function $g(u)$ can be determined as is shown in Fig. 5. Lager particles and larger u correspond to larger values of $g(u)$, i.e. larger values of S_f.

The values of F are plotted against the value of u in Fig. 4. Though a considerable scattering is indicated in this result, it may by judged that the larger particles are captured easily in the tube.

REFERENCES

1) Fukushima, H. and Y. Mizoguchi (1958) : Field Investigation of Suspended Littoral Drift, Coast. Eng. in Japan, Vol. 1.

2) Fukushima, H. and M. Kashiwamura (1959) : Field Investigation of Suspended Sediment by the Use of Bamboo Samplers, Coast. Eng. in Japan, Vol. 2.

BEHAVIOR OF SAND-SPIT-BAR AT A RIVER-MOUTH

—A Model Experiment of TONDA Fishery Port—

*Masuo Yoshitaka**

I. INTRODUCTION

Tonda fishery port is situated at the Hitotsuse river-mouth, south east coast of Kyushu Island, where the unstable growth of sand bar has prevented navigation facility and made the improvement works of river mouth necessary for the port. The author carried out a model experiment for the planning of these works. This paper presents a part of the result of experiment, concerning the behavior of sand-spit bar.

As the field data on wind, wave and river flow were insufficient, these elements were estimated in the course of experiment by comparing the sand bar growth in the model with that in the fields[1]. The experimental observations were made on the following three items, (A) Behaviour of sand-bar due to various waves, (B) Water surface slope in river mouth under various flow conditions and (C) Other factors under the various conditions of flow and wave.

The test on the sand bar growth should be compared with the researches[2][3][4] on sand transport by littoral current. In this experiment the integral amount of sand transported a certain section was measured, the initial beach slope being about 1/40.

II. MODEL AND MEASURING EQUIPMENTS

In a model basin (sea part : 20×12 m, river part : 8×10 m), the model of Hitotsuse river-mouth was made, using the sand of mean diameter 0.208 mm and specific gravity 2.67. The vertical and horizontal scale of the model were 1/100 and 1/200 respectively. Mean diameter (d_m) of sand of the prototype was 0.4 mm∼1.0 mm. As the standard model bed of the site, the bottom stage in August 1956 (Fig. 1) was chosen which showed the most draw back condition of the sand-bar.

The length of the wave-generating board was 6 m against the model beach of 18 m long (corresponds to 3.6 km in the prototype).

The height of waves was measured by the electric point gauge, and the water levels and the lay of the bed by a measuring stand which moves in parallel along the co-ordinate of Fig. 1. One interval of the co-ordinate was 25 cm in the model, corresponding to 50 m in the prototype. The high-water level, the mean water level and the low-water level are +2 cm, +1 cm and +0.3 cm above datum respectively.

The data of the wave of NE (incised angle of wave : $\alpha_0=45^\circ$) in Test A is shown in Table-1, which includes the dimension of waves and the volume of sand-bar (Q). The breaker angle α_b shown in the table was observed by the photographs and the observation, E and E_{ib} present the energy of the offing wave $\gamma H_0^2 L_0/8$ and the littoral breaker energy per hour $[(n\gamma H_b^2 L_b/8T)\times 3600 \sin\alpha_b \cos\alpha_b]$ respectively.

---

* Assistant Professor, Miyazaki University

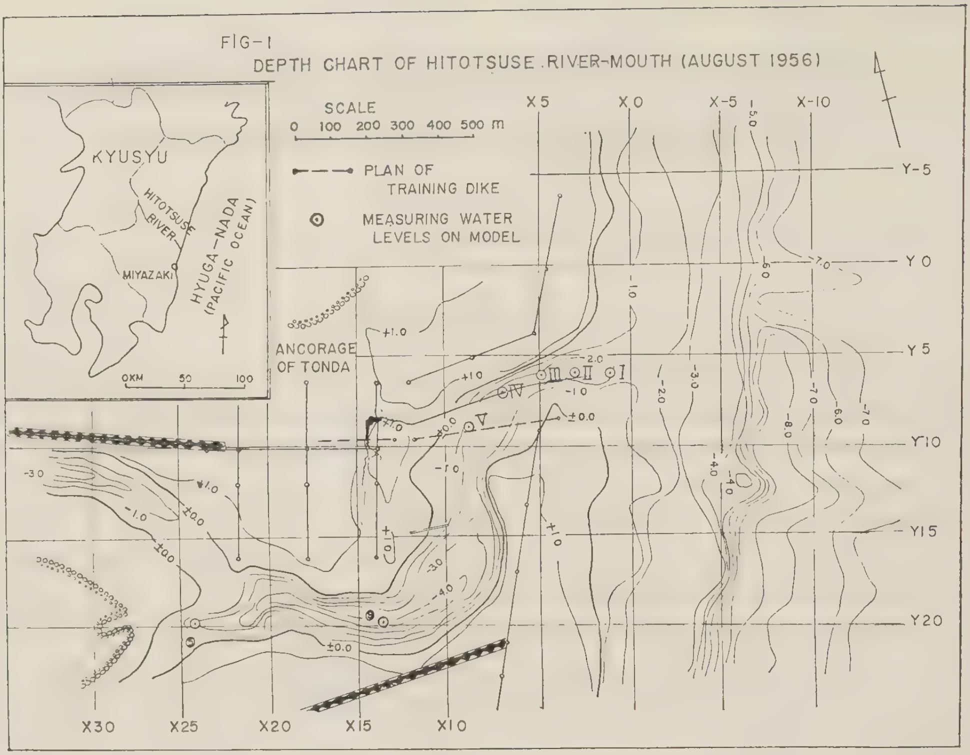

FIG-1
DEPTH CHART OF HITOTSUSE RIVER-MOUTH (AUGUST 1956)

Ⅲ. THE FORM OF SAND-BAR AT A RIVER-MOUTH

1. Feature of sand-bar growth

Under the action of waves in Table–1, the sand-bar grew in various feature. By comparing the test result (Fig. 2) with the field survey (Fig. 3), the movement of the sand-bar is examined. In the case of small steepness (long, low wave), at the outset the waves refract by a large angle and transport sands to the inner part of estuary as shown in Fig. 2 (A 17). After a small growth of the sand-bar, the rate of growth of a head of sand-bar (U_s, Fig. 4) becomes a little rapid. The width of the sand-bar which is wide at the outset becomes narrow more and more. During February to May 1956 (Fig. 3), there were little rain and wind,

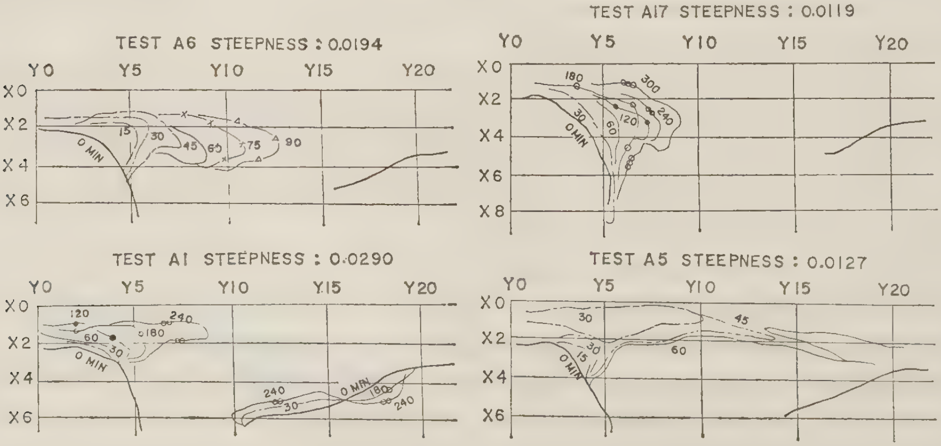

TEST A6 STEEPNESS : 0.0194

TEST A17 STEEPNESS : 0.0119

TEST A1 STEEPNESS : 0.0290

TEST A5 STEEPNESS : 0.0127

Fig. 2 Transformation of sand-bar on test (H.W.L)

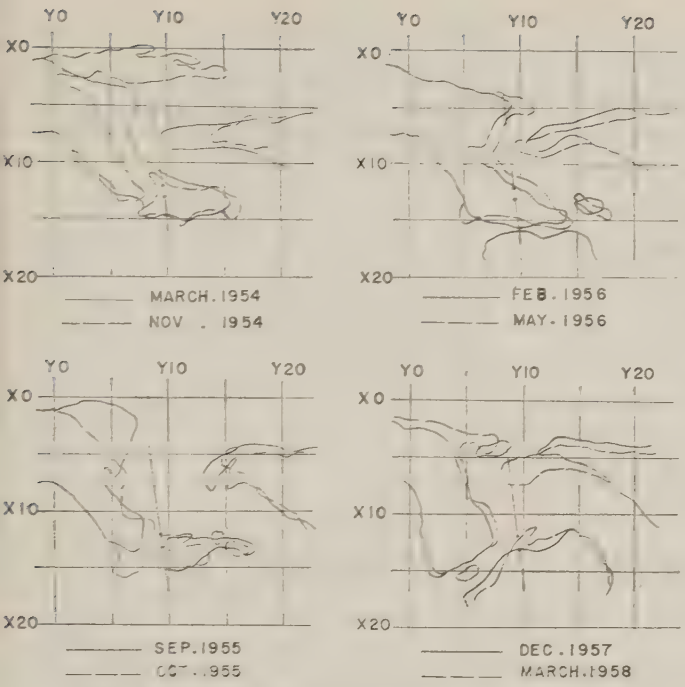

Fig. 3 Transformation of sand-bar on field survey (M.W.L)

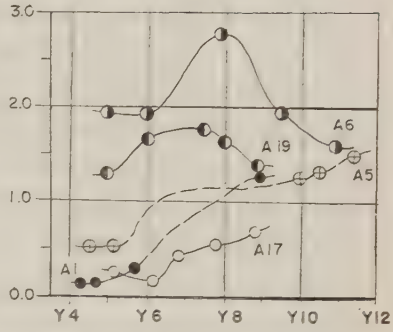

Fig. 4 Littoral of a head of sand-bar

that means it shows the transformation by the waves in spring that have small steepness.

In the A 5 (Fig. 2) that steepness is a little larger than wave of A 17, the sand-bank appears in front of the river-mouth by shoreward movement of sand, while the sand-bar extends itself. Fig. 4 shows the discontinuity in the rate of growth of sand-bar (U_s) in A 5. During December 1957 to March 1958 (Fig. 3), there are small amount of rainfall and weak wind, but sometimes heavy wind. In winter there occurs frequently blockades on the river-mouth, and we know that the test A 5 is equivalent to such stage.

In the case of steepness nearly equal to 0.02 (Fig. 2, A 6), the movement of sand-bar shows the typical one in this district depending on sand drift along the beach. The rate of growth of sand-bar (U_s) is partially affected by the irregularity in topography, but the width of sand-bar is almost uniform. In the period of March to November 1954 (Fig. 3), typhoons passed four times in August and September, so it was supposed that the river-mouth was opened widely by the flood in early autumn and the sand-bar had extended several times by heavy wind from NE. The similar tendency is observed in the result of test A 6.

In the case of steepness nearly 0.03 (Fig. 2, A 1), at the outset the extending rate of sand-bar (U_s) is small. In due time, however the beach profile in front of the river-mouth approaches to the adjacent beach profiles, and the sand bar grows if the river flow is small (Fig. 5). It is supposed that the growth of the sand-bar by a drift along the beach will not appear under the more steepness than 0.03. Because inspite of the rain and hard wind after two floods, the movement of the sand-bar was not observed. (Fig. 3—two typhoons in September∼October 1955).

As mentioned above, corresponding to various steepness of wave, the different tendencies in the feature of movement of the sand-bar were observed. As the result, the wave of steepness about 0.015 seems to have dominant effect upon the rapid blockade on the river-mouth.

2. Beach profile

A example of the results of test on the change of beach profile is shown in Fig. 5. It shows that the change in the offshore part is small and the remarkable change happens in the coastal side from the breaking point (surf zone). It may be found that banking of sand appears at the river-mouth and the profile in front of river-mouth (Y 5, Y 7) approaches to that in the section Y 3. At Y 7 section of A 6 a sand bank similar to offshore bar is observed, and in A 5 it developes in all sections. Fig. 2 shows a sand-bank formed rapidly at the river mouth (A 5).

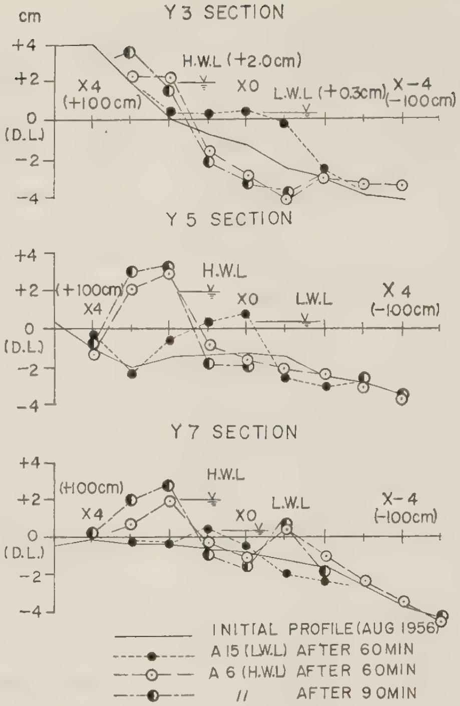

Fig. 5 Beach profiles on test

IV. THE VOLUME OF SAND-BAR AT A RIVER-MOUTH

The volume of sand-bar between the section Y 1 and the head of bar was measured by the change of the sand bed of model. Table–1 shows these results. The volume of sand-bar (Q) may be considered to be equal to the volume of beach drift passing Y 1 section in the period of observation. Fig. 6 shows the relation between the volume of sand-bar (Q) and steepness δ_0, and Fig. 7 shows the relation between Q and the littoral breaker energy E_{ib}. The result of Johnson's experiment[2] is ploted as Fig. 6. (a presumed apparent gravity of sand : 1.6, $d_m = 0.30$ mm, $E = 0.3 \sim 0.7$ kg–m/m)

At first, the technical problems in author's experiment are examined. (1) The beach drift far off from breaking point (offshore) could not be measured from the change of the topography, while it seems that the beach drift which was related only with the movement of sand-bar was investigated. According to the two dimensional experiment by Shinohara[5], the proportion of the sand transport Q_s of shore side from breaking point (surf zone) to the whole sand transport Q_0 is as shown in Fig. 8. The proportion of Shinohara's

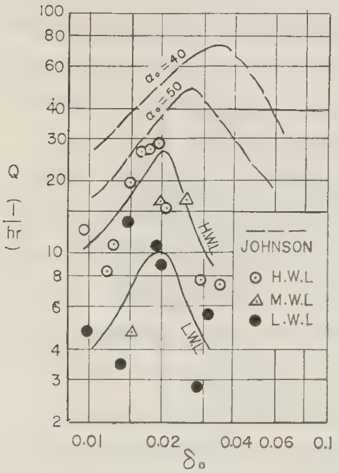

Fig. 6 $Q \sim \delta_0$

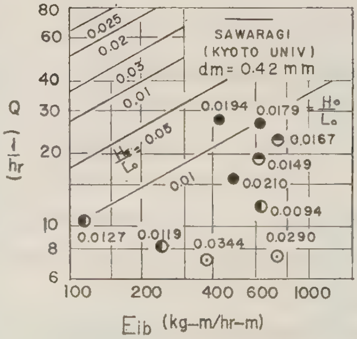

Fig. 7 $Q \sim E_{ib}$

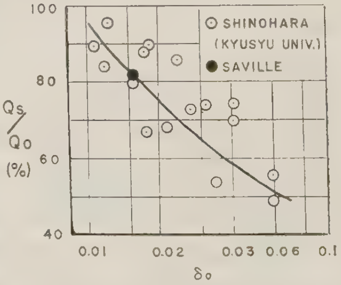

Fig. 8 $Q_s/Q_0 \sim \delta_0$
(Two dimentional experiment)

Table-1 Data of Experiment (Test A)

Test No.	Period (sec)	Sea Water Level	Height H_0 (cm)	Steepness δ_0	Breaker Depth h_b(cm)	Breaker Height H_b(cm)	Breaker Angle α_b	E (kg-m/m)	E_{ib} (kg-m/hr-m)	Q (l/hr) 1 hr	2 hr	3 hr	mean
A 1	0.96	2.00	4.25	0.0290	7.0	6.6	30°	0.326	743	7.1	6.9	8.2	7.4
A 2		2.06	5.02	0.0344	6.5	5.0	25°	0.365	370	6.6	3.4	11.5	7.2
A 3		0.30	4.08	0.0280	5.5	5.7	24°50′	0.240	435	2.0	3.6	1.8	2.5
A 4		0.56	4.50	0.0308	5.2	4.3	24°	0.295	395	5.7			5.7
A 5	1.16	2.00	2.68	0.0127	4.5	3.2	24°	0.152	119	10.6			10.6
A 6		〃	4.10	0.0194	6.2	5.5	25°	0.351	413	24.7	32.0		28.3
A 7		1.70	4.45	0.0210	6.6	5.5	28°	0.415	490	15.3	16.2	16.3	15.9
A 8		2.00	4.52	0.0214	5.0	7.3	(24°)	0.430	650				
A 9		1.64	5.00	0.0237	5.5	6.0	25°30′	0.525	482				
A 10		1.00	3.20	0.0151	5.7	5.4	29°	0.215	432	6.9	4.4	2.6	4.6
A 11		1.06	4.65	0.0220	5.1	5.7	24°30′	0.454	322				
A 12		1.14	5.47	0.0259	7.0	6.5	25°	0.630	635	16.9			16.9
A 13		1.49	6.00	0.0284	6.5	6.0	24°30′	0.752	517				
A 14		0.30	3.10	0.0147	5.0	3.8	24°30′	0.203	178	13.4			13.4
A 15		〃	4.25	0.0200	6.2	6.9	29°	0.380	722	9.0			9.0
A 16	1.48	2.00	3.24	0.0094	6.5	6.3	30°	0.360	622	15.4	8.9		12.2
A 17		〃	4.08	0.0119	6.2	4.3	25°	0.571	250	8.4	7.1	8.2	8.1
A 18		〃	4.90	0.0142	6.8	6.1	(25°)	0.875	547				
A 19		1.95	5.12	0.0149	6.8	4.8	29°40′	0.900	614	17.7	21.0		19.3
A 20		1.90	5.75	0.0167	7.0	6.0	25°	1.130	732	28.6	24.4		26.5
A 21		2.01	6.15	0.0179	6.8	6.2	28°50′	1.290	620	31.0	22.6		26.8
A 22		1 10	6.80	0.0198	7.0	6.5	26°30′	1.590	662	16.1			16.1
A 23		0.30	3.40	0.0099	5.8	5.3	20°	0.316	310	4.7			4.7
A 24		〃	4.67	0.0136	7.4	6.5	20°	0.750	550	3.8	2.9		3.4
A 25		0.00	6.70	0.0195	7.0	7.0	21°40′	1.525	655	10.0	11.1		10.6

experiment may be a little different from that of three dimensional experiment. But in an approximation, applying this proportion, it seems that the volumes of sand-bar Q ($\delta_0=0.01\sim0.03$) are about 90~60% of the beach drift. (2) The observed breaker angle was too large in comparison with the predicted breaker angle (Fig. 9). The littoral breaker energy E_{ib} seems to be over estimated about 20~50% from measuring error of the breaker angle α_b. (3) In the left beach of the standard section Y 1 in the model no sand was supplied, and the model bed was unsteady. But it seems that the error by the steadiness of the model bed is not notable, because the hourly values of the volume of sand-bar (Q) are nearly equal (Table-1).

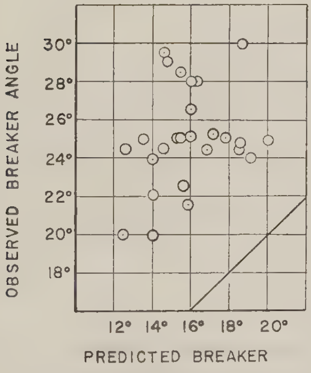

Fig. 9 Comparison between observed and predicted values of breaker angle.

Fig. 6 should be examined again in consideration of the facts mentioned above, the volumes of sand-bar (Q) have a same tendency to Johnson's experiment provided that δ_0 is less than 0.02, but it differs from Johnson's provided that δ_0 is more than 0.02. This result has been presumed from the fact that the proportion of the sand transport of surf zone to the whole sand transport has decreased with the increase of δ_0. However, provided that δ_0 is 0.01~0.02, the proportion Q_s/Q_0 which decreased with the increase of δ_0 has no influence on the volume of sand-bar, and provided that δ_0 is more than 0.02, Q has decreased rapidly.

These facts may show that the volume of sand-bar can not be presume only by the sand transport of surf zone, and may be caused by the initial slope which is about 1/40 in this experiment.

Q measured at L.W.L. has the same tendency to that measured at H.W.L., but the former is less in volume than the latter (Fig. 5).

As is stated above, it is known that, for the wave stage of δ_0 approximately 0.02, the volume of sand-bar is the largest and this sand-bar has an dominant influence on the blockade and changing stream in a river-mouth.

In Fig. 7, there are some differences between Sawaragi's experimental results and the authors'. It may be caused by the difference in the initial slope.

In the tests A 6, A 7 and A 25 the wave steepness is nearly 0.02 and the hourly values of the volume of sand-bar are nearly equal. On the other hand, the hourly values in A 1, A 2 which have waves of larger steepness the volume of sand-bar are unequal, and it shows the irregularity of the growth of sand-bar.

V. THE SURFACE SLOPE AT A RIVER-MOUTH AND THE LIMIT LINE OF VELOCITY

Fig. 10 shows a data of the water levels at the river-mouth (Fig. 1). Fig. 11 shows a data of the limit line of velocity (where velocity of river water vanishes), which was observed by making a sketch of the line that paper floats gather at the sea surface of the model.

The surface slope becomes steep with the increase of the discharge of flow, and at the flow with the wave motion (Test C) the reversed slope is observed (broken line in Fig. 10). The limit line of velocity has a regular tendency to the various values of discharges and sea water levels. The types of the limit line may be similar

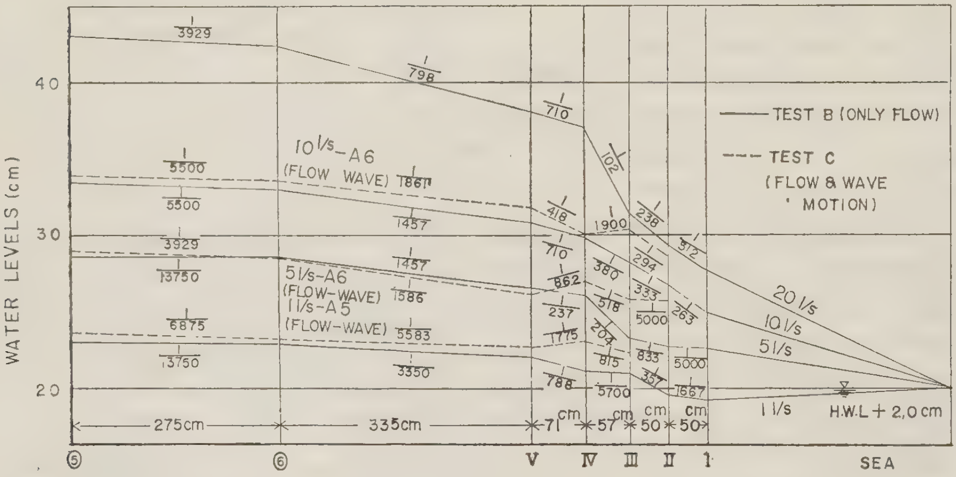

Fig. 10 Water surface slope of river-mouth (H.W.L.)

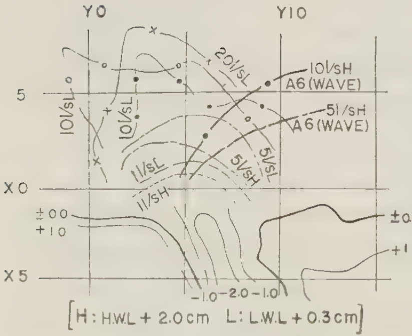

[H: H.W.L + 2.0 cm L: L.W.L + 0.3 cm]
(HEAVY LINE—TEST C)

Fig. 11 The limit line of current velocity (Aug. 1956)

to the results that Sato[6] had investigated the river water to flow into sea by the change of specific gravity of sea water (Fig. 11).

The continuity equation on the movement of sand-bar at a river-mouth may be expressed as follows :

$$\frac{\partial q_x}{\partial x}+\frac{\partial q_y}{\partial y}=\int_T \frac{\partial h}{\partial t}dt$$

where, q_x and q_y is each component of the volume of the sand transport in x and y directions, h is height of the each point on sand-bar above the datum. At the head of sand-bar, q_y may be mainly the sand transport by wave, q_x may be river sediment. It is presumed that q_y is equal to the preceding volume of sand-bar Q, but q_x connot be determined when the water surface slope at a river-mouth is not difinite. In this purpose the water surface slope at a river-mouth and the limit line of velocity had been observed, but the sufficient results have not been obtained. The theoretical and experimental researches on this problem are left for the future.

VI. CONCLUSION

Examining the form and the volume of sand-bar at a river-mouth, the following conclusions were obtained; (1) the volume of sand-bar was maximum at a steepness of 0.02, (2) the wave had the dominant effect on the blockade in a river-mouth at a steepness from 0.015 to 0.02.

This experiment was carried out by using the model of the Hitotsuse river-mouth, and the results may be applicable to the beaches of the foreshores slope which is nearly to slope 1/40. However, there are still some uncertain points concerning the volume of sand-bar, the author is intending to try a more accurate and improved experiment.

ACKNOWLEDGEMENTS

This experiment was done on consignment of Miyazaki Prefecture. The author expresses his gratitude to Prof. Kawakami of Miyazaki University, and Dr. Tsubaki of Yamaguchi University who guided this research.

REFERENCES

1) Kawakami, K., M. Yoshitaka : The Model Experiment of Tonda Fishery Harbour, Bulletin of the Faculty of Eng. Miyazaki University. No. 6 (1959).

2) Johnson, J.W. : Sand Transport by Littoral Currents, Proc. of 5th Hydraulics Conference, Bulletin 34, State Univ. Iowa (1953).

3) Saville T. : Model Study of Sand Transport along an Infinitely Long, Straight Beach, Trans. A.G.U. Vol. 31, No. 4 (1950).

4) Sawaragi, T., M. Murakami : Estimation of the Rate of Littoral Drifts, Proc. 4th Conf. Coast. Eng. Japan (1957).

5) Shinohara, K., T. Tsubaki, M. Yoshitaka, and C. Agemori : Sand Transport along a Model Sandy Beach by Wave Action, Coast. Eng. in Japan Vol. 1 (1958).

6) Sato S. : Kakōheisoku to sono Bōshisaku ni tsuite (On the Prevention of the Blockade at River-mouth), Proc. 2nd Conf. Coast. Eng. Japan (1955).

RECENT COASTAL PROCESSES IN NIIGATA PREFECTURE

*Tadao Haruta**

1. INTRODUCTION

The coast of Niigata Prefecture is exposed to the winter monsoon of Japan sea which has the predominant direction from N.W. to N. and is the most important factor affecting the beach erosion or sand drift in this coast. The most parts of the coast are sandy beaches nourished by sediment from the rivers as shown in the map (Fig. 1).

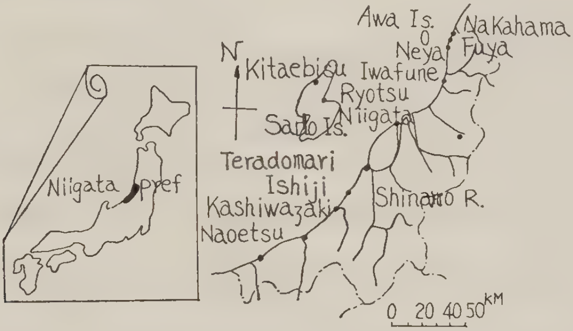

Fig. 1 The location of ports in Niigata Prefecture

Along this coast there are some harbours and a number of small fishery ports. The construction of breakwaters, groins or jetties in these harbours or ports caused certain changes in the patterns of wave, current and sand drift around them. Thus beach erosion or sand deposit recently took place in many parts of the coast. This paper presents several examples of such coastal process with the description on the protection works applied in some places.

II. SOME ASPECTS IN NATURAL CIRCUMSTANCES

1. Topographical Features of Coast:

The most parts of Niigata coast are monotonous beaches except the north and south districts where small indentations, cliffs, reefs and collapses of precipices exist successive each other. There lie notable sand dunes along the shore line stretching about 70 km long between the port of Iwafune and the western district of Niigata City. In the coasts of Kashiwazaki and Naoetsu, west part of the prefecture, there also lie gentle sand dunes.

The features of rivers which pour at this coast are much different each other. Some of them supply fine sand to the beach, while others flow out coarse gravel from its mouth.

2. Wind and Wave:

Fig. 2 contains the wind diagrams for the winter season observed in the western part of Niigata City. The direction diagram shows that the wind of N.W. or S. appears frequently, while in the velocity diagram the wind of N.N.W, N.W. or W.N.W. prevails.

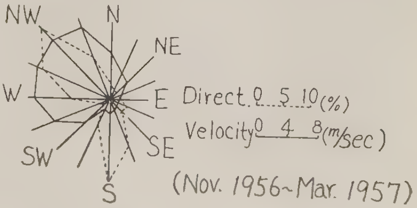

Fig. 2 Frequency in the direction of wind and the average velocity of wind

According to the observation for 35 years by the Niigata Weather Bureau, the wind of more than 10 m/sec comes from W.N.W. most frequently.

---

* Japan Port Consultant Co.

In general, the wind of the direction between N. and N.W. prevails in this whole coast through winter season as already described.

The winter monsoon in this coast is caused by the migrating low atomospheric pressure moving from west to east over the Japan Sea. According to the path of the low, the wind shows various characters. J. Takahashi classified them into five patterns A. B. C. D and E,[1] with respect to the origination of low, the direction and velocity of the moving low, the minimum pressure at the center of low and the location of high atmospheric pressure. The duration of wind is usually 20–40 hours, but sometimes it continues to blow over several days (Fig. 3). The direction changes with the eastward advance of the low.

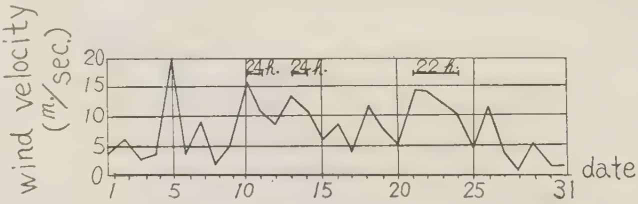

Fig. 3 Daily change of wind velocity (in Dec. 1956)

During the season from spring to autumn, the south wind is common, but its velocity is not high except in the case of sudden gusts which sometimes appear.

The wave near the coast rises with the wind over the sea. The highest wave is generally observed after the highest velocity of wind has passed and high wave continues for a while after the wind became weak.

The Fig. 4 and 5 are the weather charts on December 12 and 13 of 1957 when a low atmospheric pressure brought the instantaneous wind of 41 m/sec at the Niigata coast and caused the high tide damage on the port facilities. This storm may be defined as the type B according to J. Takahashi. The average wave heights observed during this storm were as follow.

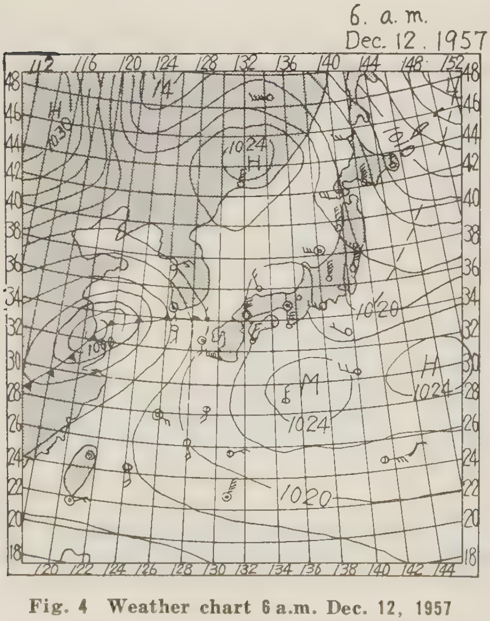

Fig. 4 Weather chart 6 a.m. Dec. 12, 1957

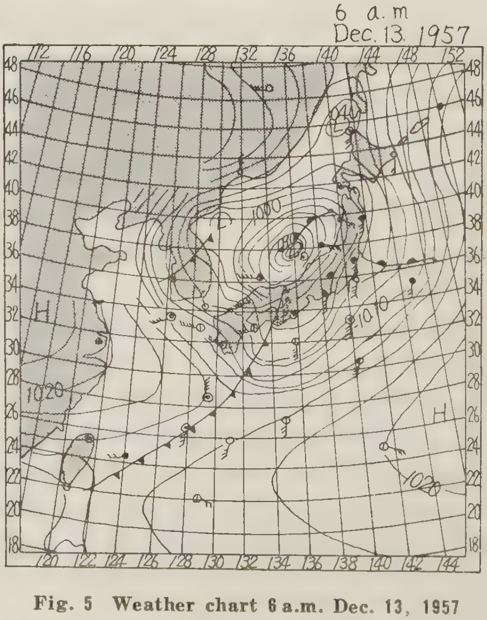

Fig. 5 Weather chart 6 a.m. Dec. 13, 1957

Iwafune	Niigata	Teradomari	Naoetsu
4–5 m	3–4 m	3–3.5 m	4.5–5.5 m

The wave in the west coast of the prefecture and that in front of Niigata area are smaller than that in other parts of the coast, because of the shelter by Noto Peninsula and Sado Island.

3. Tide

In this coast the range of astronomical tide is very small, being 10–30 cm. The mean sea level is higher in summer than in winter, the difference between them being about 30 cm. The figure 6 shows the monthly variation of mean sea level in the port of Kashiwazaki.

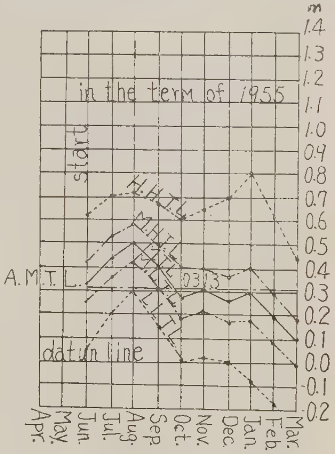

Fig. 6 Monthly change of tide at Kashiwazaki

III. COAST EROSION

1. The Easten Coast of Niigata

A number of reports has already been published on the erosion in the west coast of Niigata. The author shall describe here on the recent recession of the eastern coast of Niigata.

As shown in Fig. 7, this coast has been eroded remarkably in the recent 10 years and

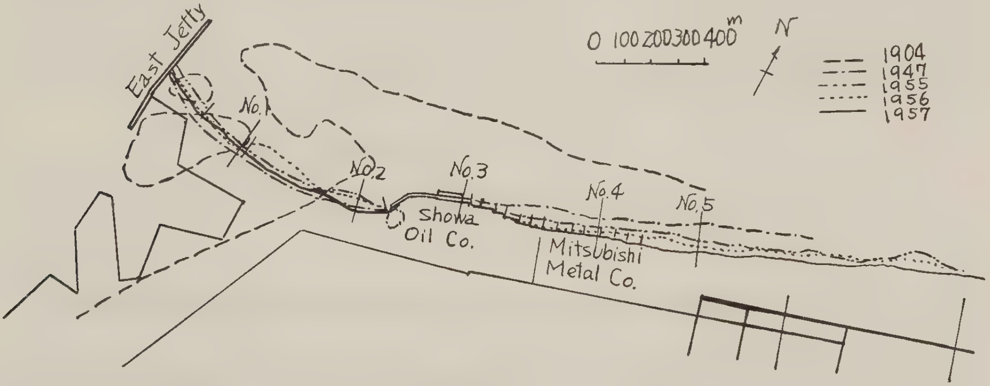

Fig. 7 Shore-line changes along th eastern coast of Niigata

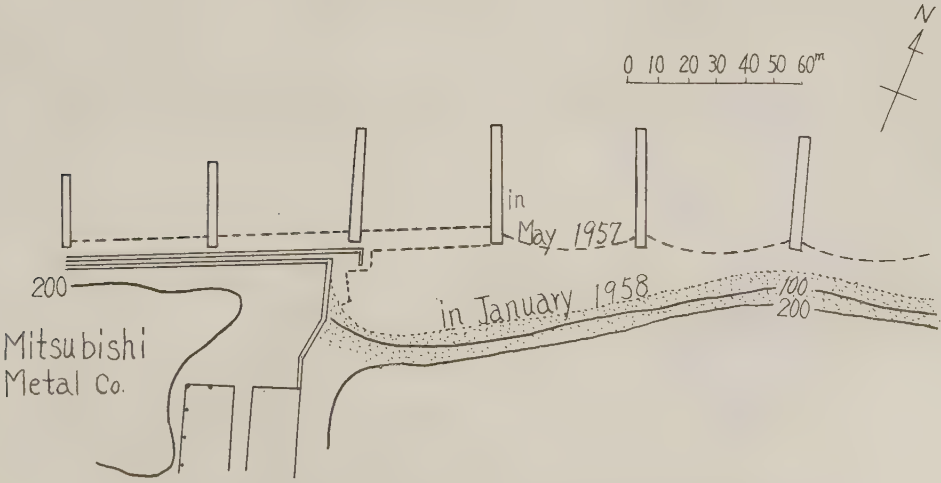

Fig. 8 Shore line along the eastern coarst of Niigata

the loss of sand from this coast was estimated to be about 300,000 m^3 a year. Several years ago the beach between the east jetty of port and the Showa Oil Co. (Fig. 7) was neary fixed by the construction of protection works, but owing to the recent land subsidence in this area the shoreline began to recede again very rapidly. The amount of recession in the winter season of 1957 was nearly 20 m.

The beach between Mitsubishi Metal Co. and Agano river mouth has been eroded little by little, and the recent land subsidence accelerated this tendency. The Fig. 8 shows the erosion at the beach east of the Mitsubishi Metal Co. took place in winter of 1957. The rigid revetment around the factory is considered to be responsible for the local erosion. The bottom profiles of this coast are shown in Fig. 9. The general bottom profile in this area has the slope of 1/70–1/100.

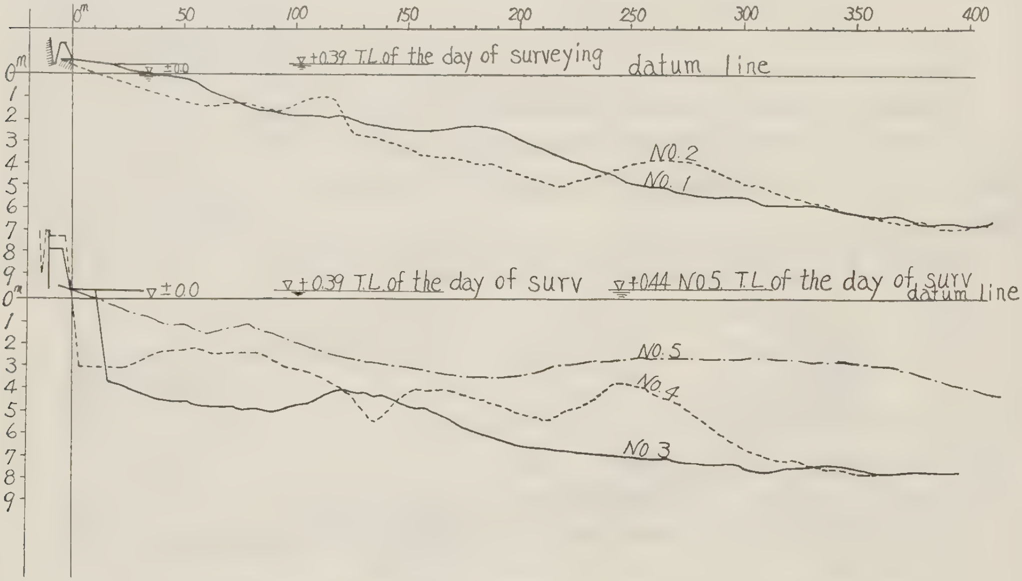

Fig. 9 Bottom profiles at the Eastern Coast of Niigata (Surveyed in June 1958)

2. Nakahama Harbour

This fishery harbour is located near the northern limit of the prefecture and is next the Nezugaseki harbour in Yamagata Prefecture. The breakwater of 34 m long was constructed in 1956 about 40 m off the shoreline (the cross-section of the breakwater is shown in Fig. 11.). The beach of coarse material has not shown any remarkable recession or growth of tombolo after the completion of breakwater. This fact manifests that the shoreline was stable under the influence of longshore current.

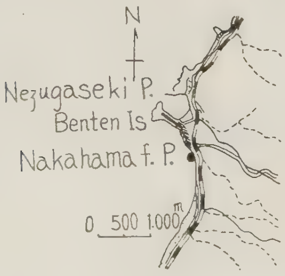

Fig. 10 Location map of Nakahama fishery harbour

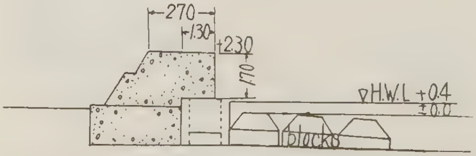

Fig. 11 Section of breakwater at Nakahama fishery harbour

Recently the south jetty of Nezugaseki, which connects the coast and the Benten Island, was constructed. Since its completion the southward longshore current became stronger and beach sand was gradually flushed away. At the storm in December of 1957, the beach of 800 m long between Nezugaseki and Nakahama was badly eroded, the shoreline recession being 5–10 m in average, and some of the houses along the coast are now in dangerous stage.

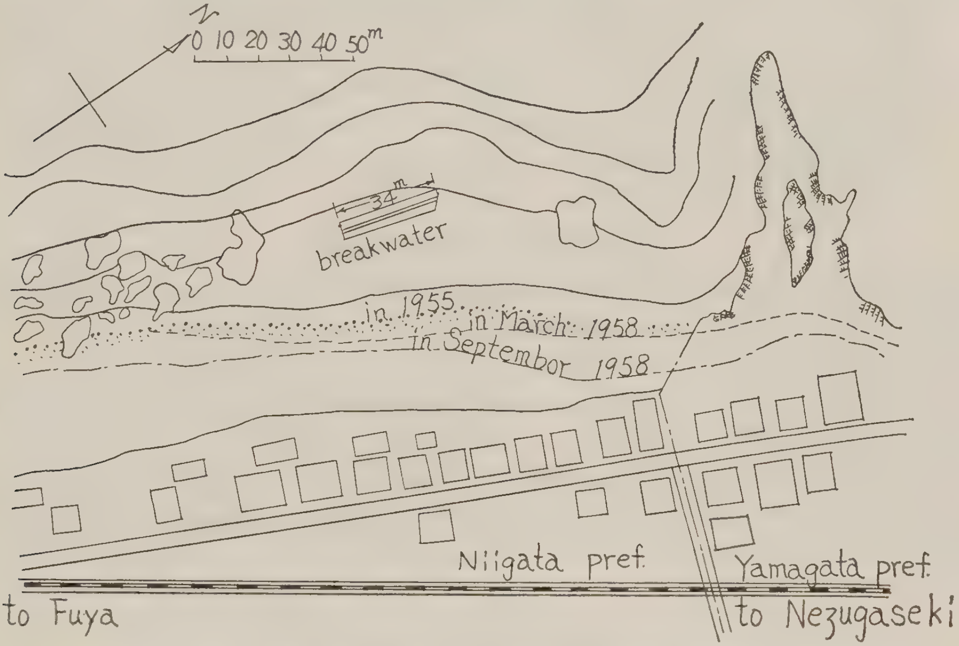

Fig. 12 Shore-line change at Nakahama fishery harbour

IV. THE COAST WITH LOCAL MOVEMENT OF SAND

1. Kitaebisu Harbour

This fishery harbour is located in the north-west part of Sado Island and faces the open sea which is exposed to the north wind in winter. According to our observations the prevailing direction of wind is N.W. and the maximum velocity of wind takes place in the direction between N.W. and W.N.W. in winter. The bottom slope of sea near the shore is about 1/20 and violent wave attacks surging upon the beach.

Figs. 13 and 14 show the cross-section and the location of breawater in this harbour. With to progress of the construction of breakwater the influence of it came to appear. The

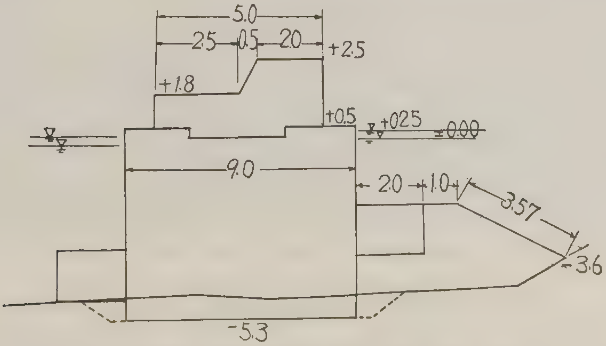

Fig. 13 Cross-Section of breakwater at Kitaebisu fishery harbour

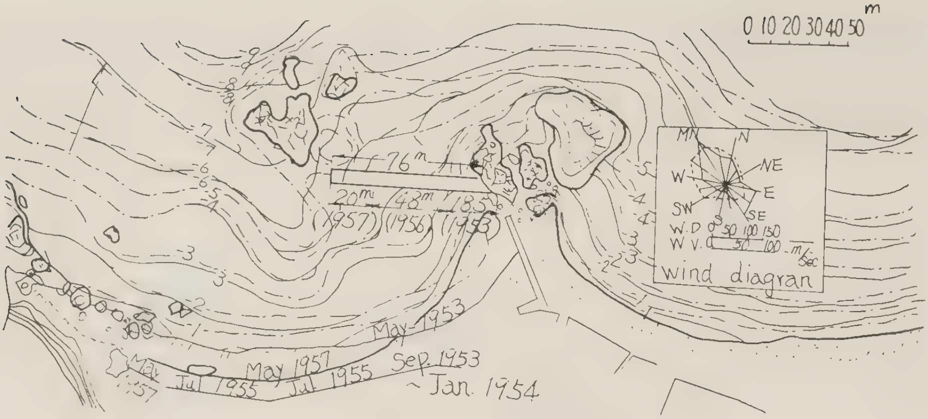

Fig. 14 Kitaebisu fishery harbour

shore line in western coast began to recede, while the beach shaded by the breakwater advanced. The revetment was damaged, especially in winter of 1957.

2. Ishiji Harbour

Ishiji fishery harbour is situated 16 km north of Kashiwazaki and between them sand dunes lie along the coast.

Three rubble mound breakwaters were constructed in 1935. In 1955 the fourth breakwater was built and in 1956 the east breakwater was repaired. The height of them is not sufficient to check the overrun of high wave.

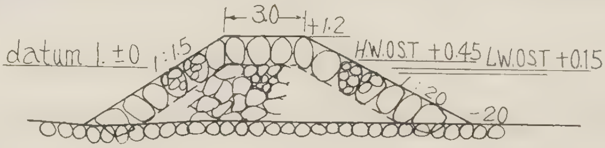

Fig. 15 Section of breakwater at Ishiji fishery harbour

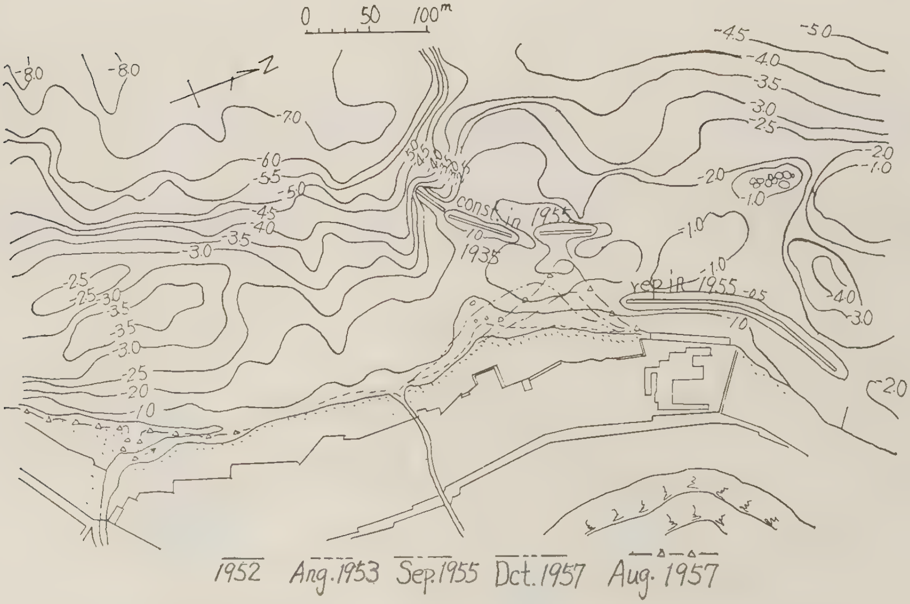

Fig. 16 Ishiji fishery harbour

After the construction of the fourth breakwater the tombolo began to growth and shift to east. The shape of tombolo chages with the seasonal variation of wave and at the same time, the western coast began to recede a little.

3. Neya Harbour

The fishery harbour of Neya is located in a small bay near the north limit of the Prefecture. The narrow sandy beach stretches between the mountain and sea. The Fig. 17 shows the location of breakwaters and groin.

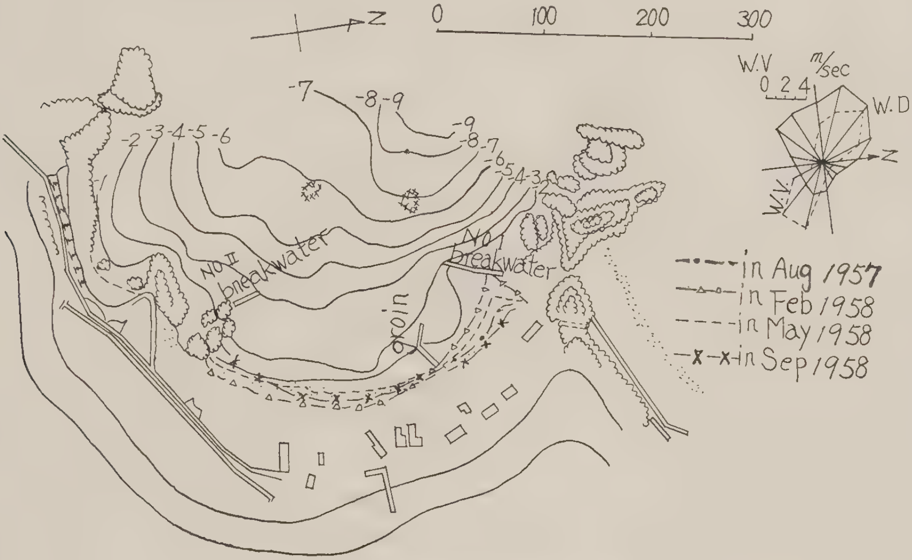

Fig. 17 Neya fishery Harbour

In winter season the wave of N.W. direction invades the bay.

It diffracts by the existence of No. 1 breakwater (northern breakwater) and causes northward longshore current which transports shore sand over the groin into anchoring basin because the height of groin is not sufficient to check the sand movement. Thus a tombolo behind the No. 1 brekwater is easily built.

In the season of spring and summer the south wind prevails and wave from the south flushes the tombolo away. These phenomena are repeated every year.

In Fuya port which is situated 4 km north of the port of Neya, the similar phenomena are observed.

Photo 1 Fuya fishery Harbour

V. SAND DEPOSIT

1. Yoshizumi beach in the port of Ryotsu

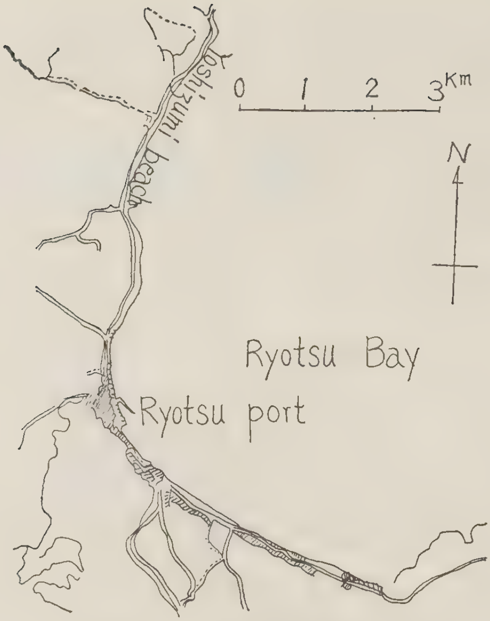

Fig. 18 Yoshizumi beach

Yoshizumi beach is the northern part of the coast of Ryotsu bay in Sado Island (Fig. 18).

The northeast wind invades the bay directly and attacks the revetments. While in winter season N.W. wind prevails and causes southward longshore current along the Ryotsu coast. After the damage by winter wave. the new coastal groins were constructed at the Yoshizumi coast in the autumn of 1957. The rubble mound groins 15 m long were built at interval of 30 m, and remarkable sand deposit took place in the area between the groins, as shown in Fig. 20.

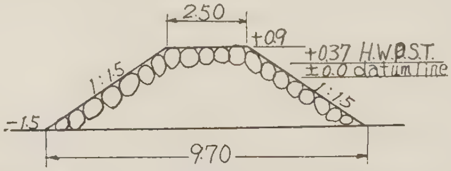

Fig. 19 Section of jetty along Yoshizumi beach

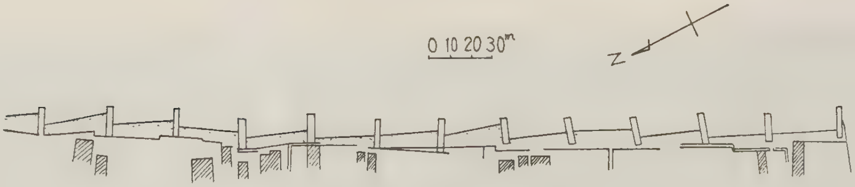

Fig. 20 Yoshizumi beach

2. Iwafune Harbour

Iwafune is located about 45 km north of Niigata City and about 5 km south of the mouth of Miomote River. It was 1913 when the first jetty was built in this harbour. Since that time this harbour has been incessantly suffered from the shoaling sand. With the construction or elongation of breakwater or groin, sand deposit advanced and river mouth was blocked. The dredging was repeated for the maintenance of mooring area. The Figs. 22-25 are frequency diagram of strong wind (more than 10 m/sec) in this area observed by the author from January 21 to April 20 in 1957. It may be noticed that the direction of strong wind changes from N.W. to W. with the progress of time.

The features of wave were observed from the observation station on the sand dune. Fig. 26 is the distribution of wave direction in offshore.

The most frequent direction is 10 degree north of the line of east groin. The measurement of offshore waves is difficult, but the wave height is estimated to be 3–4 m in rough stage about 150 m off the end of groin.

The wave length and period differ according whether the wave is swell or wind wave. As a whole it may be said that maximum period is 7–10 sec. and maximum wave length is 60–100 m. In December and January wave is generally steeper than in March and April.

The shoreline between Miomote river mouth and Iwafune has the direction 24° east from north, while the direction of winter wave is N.W.–W.N.W. That is, the angle of incidence of wave is from 65–90 degree to the beach. But the shoreline near the foot of breakwater is about 15° east to south (Fig. 21) and the wave of the direction N.W.–W.N.W. makes the incidence angle of 30°–50°. Thus the remarkable southward current may occur along this shore in

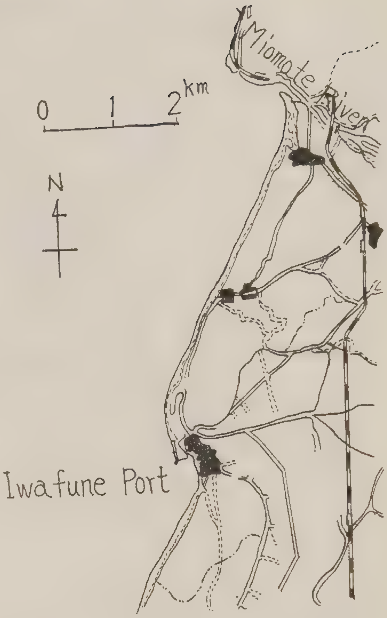

Fig. 21 Location of Iwafune Harbour

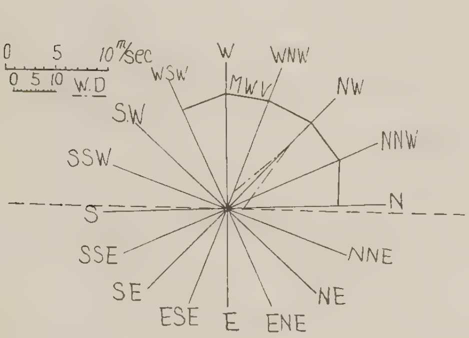

Fig. 22 Diagram of the strong wind (in Jan.)

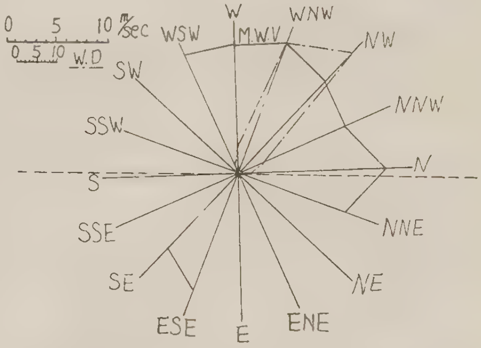

Fig. 23 Diagram of the strong wind (in Feb.)

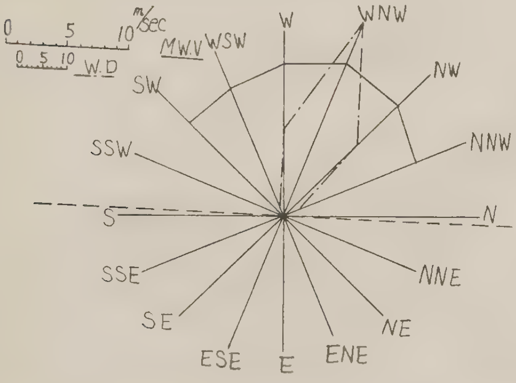

Fig. 24 Diagram of the strong wind (in Mar.)

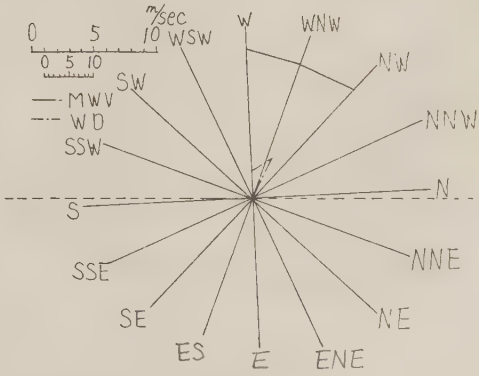

Fig. 25 Diagram of the strong wind (in Apr.)

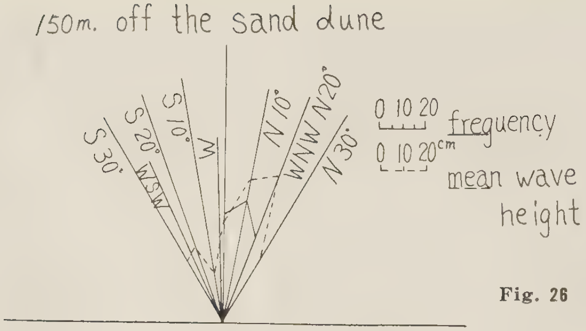

Fig. 26 Diagram of distribution in the wave direction

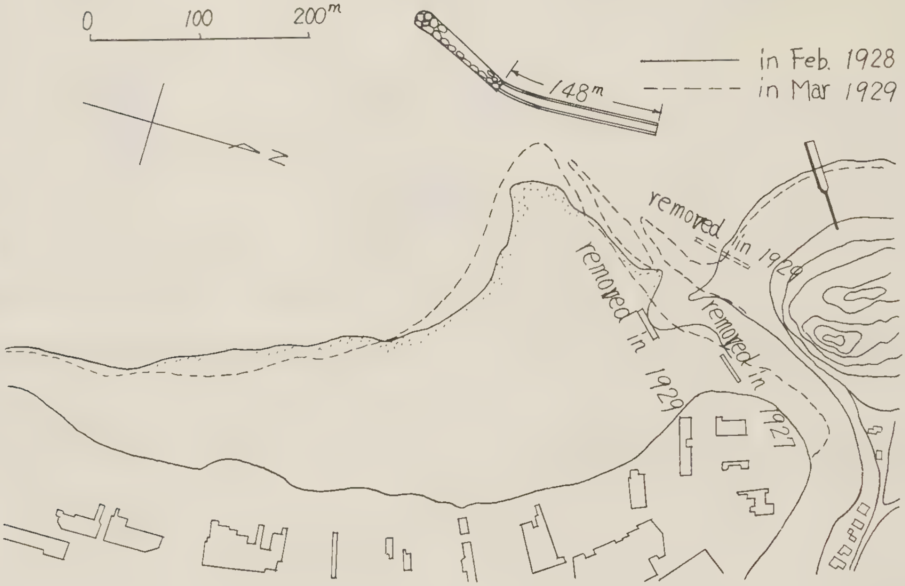

Fig. 27 Map of Iwafune port

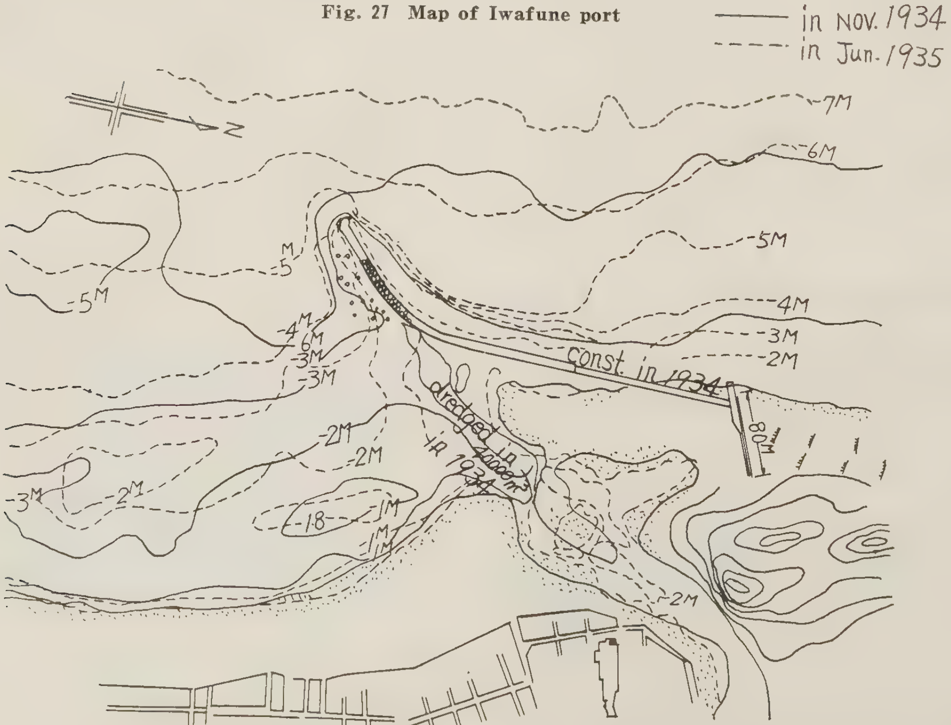

Fig. 28 Map of Iwafune port

winter. Really a lot of sand and gravel is considered to be carried southward from the mouth of Miomote River. Since the first construction of breakwater, sincere struggle was continued against invading sediment which was carried around the breakwater by current or was thrusted into the basin over the breakwater and groin by wave and wind. Fig. 27 s, 28 and 29 show the progress of preventing works and the succeeding shore process. In the stage of Fig. 27, the tombolo developed and after the stage of Fig. 28 the basin of harbour was rapidly filled by sand. The amount of litteral drift is estimated to be about 40,000 m³ a year. The bed slope of near shore (of depth less than 7 m) in this coast is 1/50–1/80 and that of offshore (deeper than 7 m) is 1/170–1/250.

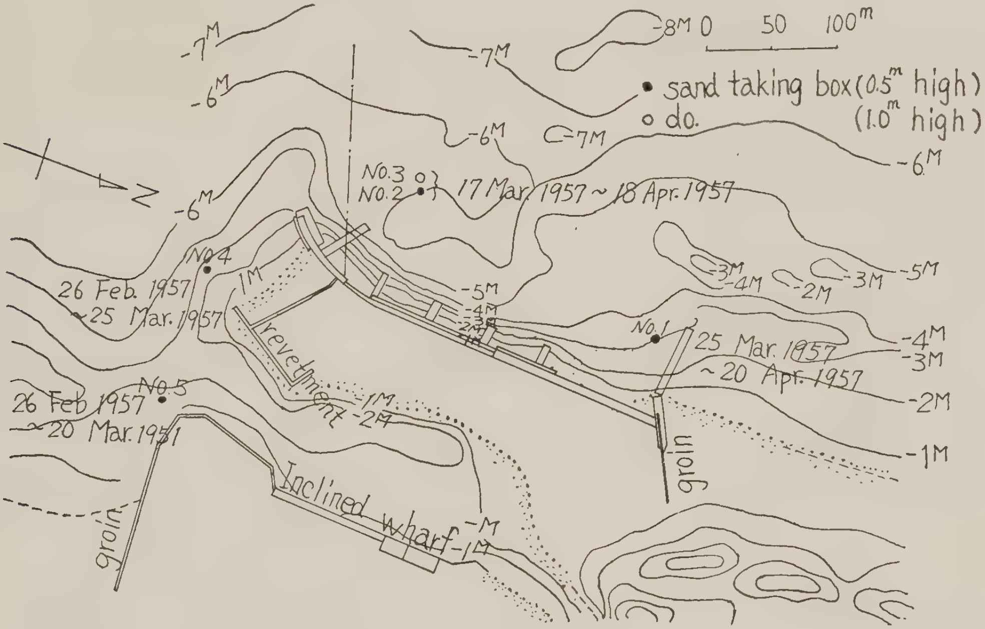

Fig. 29 Map of Iwafune port

REFERENCES

1) Takahashi, J. : Wave and Current in the Niigata Coast, Proceedings of Coastal Engineering in Japan, 1956 (In Japanese)

A STUDY ON SUBMERGED BREAKWATERS

*Masashi Hom-ma**
*Kiyoshi Horikawa***

I. INTRODUCTION

1. Functions of Submerged Breakwater

A submerged breakwater is a kind of offshore structures, with its top at or below sea water and is usually constructed parallel to the shoreline in shallow water. The main function of this structure is of protecting the shoreward area of the breakwater from the severe wave actions by way of attenuating the incoming waves. A part of wave energy is reflected to offshore area at the submerged breakwater, and some part is dissipated due to the breaking of waves at the crown of structure. The remainder, which may occupy small fraction of the incoming wave energy, is transmitted to the inshore zone of the structure. A part of the transmitted wave energy becomes the potential energy for elevating the water surface of the inshore zone in establishing the balance between the inflow due to the mass transport of wave motion and the outflow of return current, and the other is dissipated at the final breaking of waves. The nearshore sediment materials will be less disturbed by the transmitted waves than by the original waves because of the attenuation of wave height.

The function of the submerged breakwater mentioned above is really good enough for letting engineers practically apply the submerged breakwater as one of the shore protection works at several coasts in Japan. At Niigata coast the tidal range is about 30 cm, and this fact is quite favorable for expecting good functions on this device.

On the other hand the maritime structures such as the submerged breakwater will disturb artificially the delicate balance of shore processes established along the coast and produce numerous difficult problems. The slump of the submerged breakwater into the bottom sand at Niigata west coast, for example, is one of the typical new born difficulties.

In this paper the authors will study the functions and maintenance devices of submerged

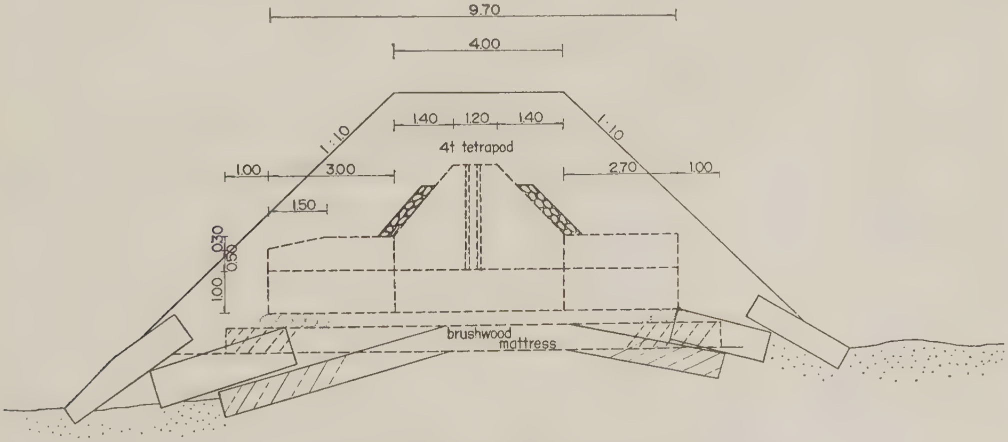

Fig. 1 Cross section of submerged breakwater reinforced with tetrapod blocks

---

* Dr. of Engg., Professor of Civil Engineering, University of Tokyo
** Assistant Professor of Civil Engineering, University of Tokyo

breakwaters experimentally, comparing always with the results of the field observations conducted at Niigata west coast.

T. Hamada considered two possible locations for setting the submerged breakwater at Niigata west coast, that is; (1) 6 m depth location, 300~350 m apart from shoreline, which is a slightly offshore zone from bars, and (2) 2~3 m depth location, 100~150 m apart from shoreline. The former is better for expecting good results of submerged breakwater but costs too much. While the latter is cheaper but is quite dangerous to be destroyed by severe scouring action of waves. According to his opinion, the determination should be established by considering the amount of possible sediment supply from the Shinano River, which is the

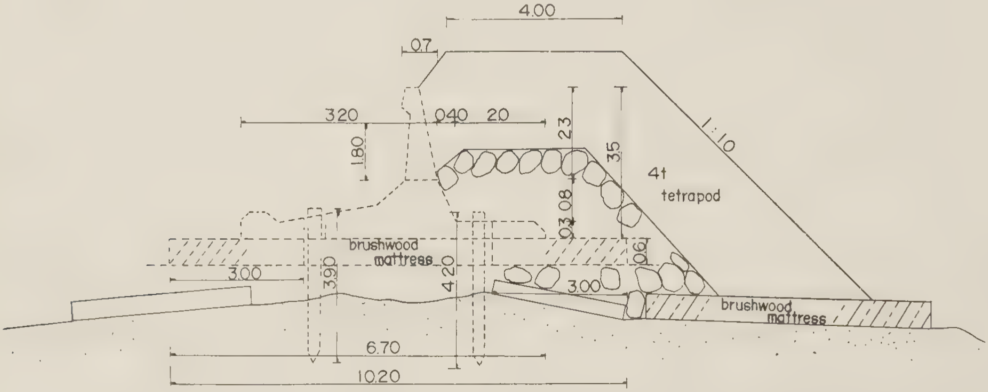

Fig. 2 Cross section of submerged breakwater reinforced with tetrapod blocks

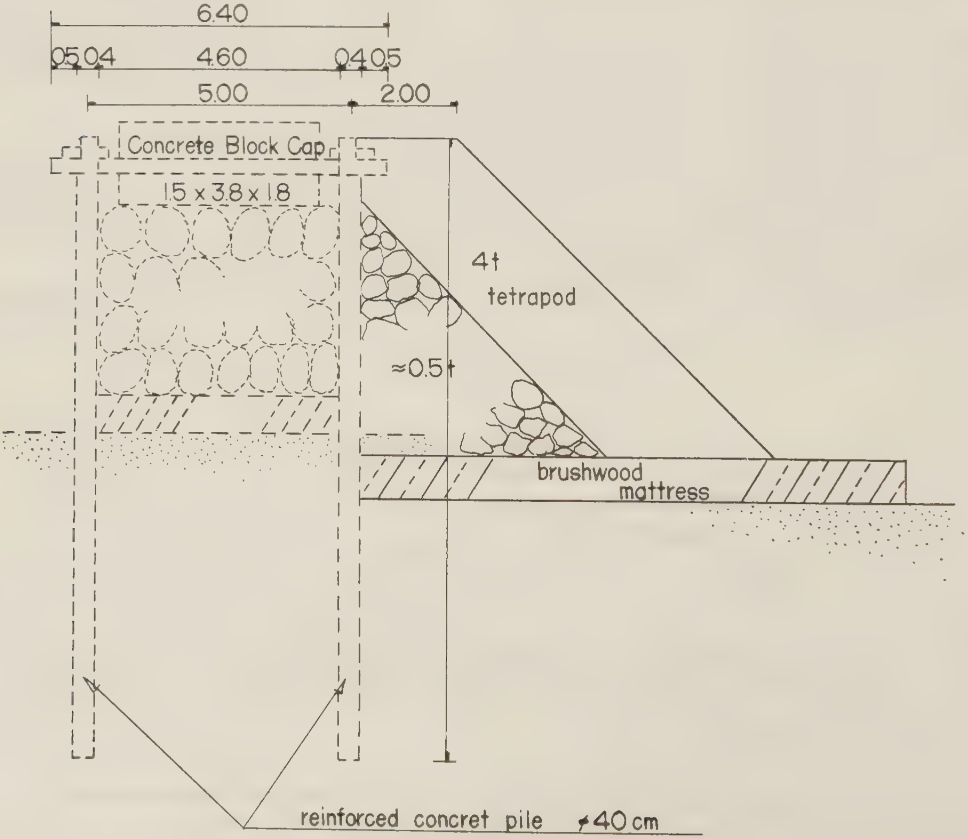

Fig. 3 Cross section of submerged breakwater reinforced with tetrapod blocks

only source to this coast[8].

Actually the latter location was selected and the construction works of submerged breakwaters have been conducted since 1950. In the process of the above project, there have been evidenced a lot of problems, which have an important influence on the functions and maintenance devices of submerged breakwaters.

The first is the structural problem of the submerged breakwater practically used at the Niigata west coast. The wind waves, the steepness of which is fairly large, are mostly breaked prematurely and attack the structure with strong action. Therefore the structure of the breakwater has been improved step by step, and now been maintained by mounding the 4 ton tetrapod blocks. (Figs. 1, 2, 3)

The second is the severe scouring around the structure mainly due to the large disturbance of both the plunging of the waves over the structure and the compensating offshore ward current through and over the body of structure.

The third problem is the slumping of the structure into the bottom sand, the amount of which is practically large enough even though in subtracting the effect of land subsidence in this area. Decreasing the height of submerged breakwater, decreasing tremendously the damping action of the structure; this fact is really evidenced in the field in a way of the large retrogradation of shoreline at the place where the slump of the submerged breakwater is severe. According to the results of previous experimental studies, under the condition that the height of submerged breakwater is less than 70 to 80% of the water depth where the structure is located, the damping action against the incoming waves can not be expected very much. At Niigata west coast 4 ton tetrapod blocks have been mounded on the structure for maintaining its original function. Here are two questions; that is, (1) Why such a slumping occurs? and (2) How many blocks we have to supply in order to keep its original function of submerged breakwater?

The final problem is the variation of the hydraulic conditions in shallow water area owing to the construction of submerged breakwater. The elevation of water surface in the nearshore zone due to the breakwater mentioned above induces the compensating offshoreward current, and also strengthen the longshore current velocities in resulting with the strong return current to offshore zone concentrating at the gaps of breakwaters. Therefore the agitation of waves to the beach sediment seems to be still active. At Niigata west coast the above problem was practically overcome by the ways of (1) extending the groins and connecting them with breakwater and (2) filling the gaps with 4 ton tetrapod blocks.

At the natural beaches the offshore and onshoreward movements of beach sediments are used to be quite active. That is, some amount of beach sediments are transported to offshore zone as suspended and bed load sediments due to the steep wind waves, but most of them will be returned to nearshore zone as bed load sediment by flat swell. If there is a submerged breakwater, the bed load sediment will be checked at the structure, therefore the loosing amount of sediment from nearshore zone will be reduced, but at the same time the sediment supplied from offshore zone can not reach to the shore. It must not be over-lookedt hat the absolute variation of beach profiles inside the structure will be awfully small compared with that at the open beaches. In order to maintain the beach stability at Niigata west coast, most of the materials dredged at the mouth of the Shinano River has been supplied continuously.

2. Review of Previous Studies

Most of the studies previously done have mainly treated the damping action of submerged breakwaters in relation with the height, width, and shapes of structures.

In abroad since Lamb treated a preliminary problem[1], Dean[4], Ursell[5], Jeffreys[3], etc. have done the theoretical studies. The assumptions introduced in these theories are too far from our practical conditions. From the practical stand point, the Beach Erosion Board[2] in the United States has done primal model investigations, and later on Johnson, Fuchs and Morrison[6] presented numerous valuable suggestions through the results of their experimental studies concerning the effects of height, width of submerged breakwater and depth of water where the structures were located, on the damping action against the waves. The important results are, (1) the steeper waves are easily damped and (2) the structures with higher height and wider width are more effective on damping action against waves. In France Delage[7] published his study.

T. Kubo and T. Yamamoto[9] conducted on experimental study concerning the shape effect of submerged breakwaters on damping action, and obtained the result that the trapezoidal section with gentle slope is better than the rectangular section. Unfortunately the scale of the experimental facilities seems to be too small to obtain the reliable results. T. Ishihara and T. Sawaragi[12] studied the effectiveness of submerged breakwater on prevention of overtopping of waves.

The authors[10],[15] have conducted the study on the hydrodynamic characteristics in the vicinity of submerged breakwaters by using the fixed horizontal or sloping bottom of wave channel. The main results are summarized as follows : (1) The height of structure, h, should be larger than 70∼80% of the water depth, d, where the structure is located, in order to get enough damping action. (2) If the ratio of h/d is larger than 90∼95%, the incoming waves will be broken at the crown of structure. (3) The Fourier analysis for the transmitted wave characteristics shows that increasing the structure height, reducing the ratio between the amplitude of basic frequency and the half of wave height (wave amplitude), and increasing that between the amplitude of four-fold or five-fold frequency and the wave amplitude. This agrees qualitatively with the results observed at Niigata west coast such as the decrease of wave period inside the submerged breakwater. (4) The rise of water surface level at the inshore zone of breakwaters will be rapidly increased at the condition of $h/d > 0.7$. At the actual coast the longshore current is generated in nearshore zone as a slope current and may reduce such a high rise of water level. And the permeable structure of submerged breakwaters actually used at the Niigata west coast may also reduce the above tendency. But the phenomena of rising the water surface level will be noteworthy in relation with the slumping action of structures as explained in Chapter 3 of this paper.

II. DAMPING ACTION OF SUBMERGED BREAKWATERS

1. Attenuation of Wave Characteristics

The experimental studies by using uniform wave characteristics have been conducted at several institutions as stated in the previous chapter. But there seems not to be any available datum of field observation except that at Niigata west coast. The Niigata Prefectural Office has been conducting the wide range field observations. As a part of the above project the wave observations had done at the following two stations simultaneously; one was Ojoin Beach, protected without submerged breakwaters, and the other was Kasoba Beach, protected with submerged breakwaters. The above two stations are located at a distance of about 6 km, and 3 km, respectively, from the outlet of Shinano River.

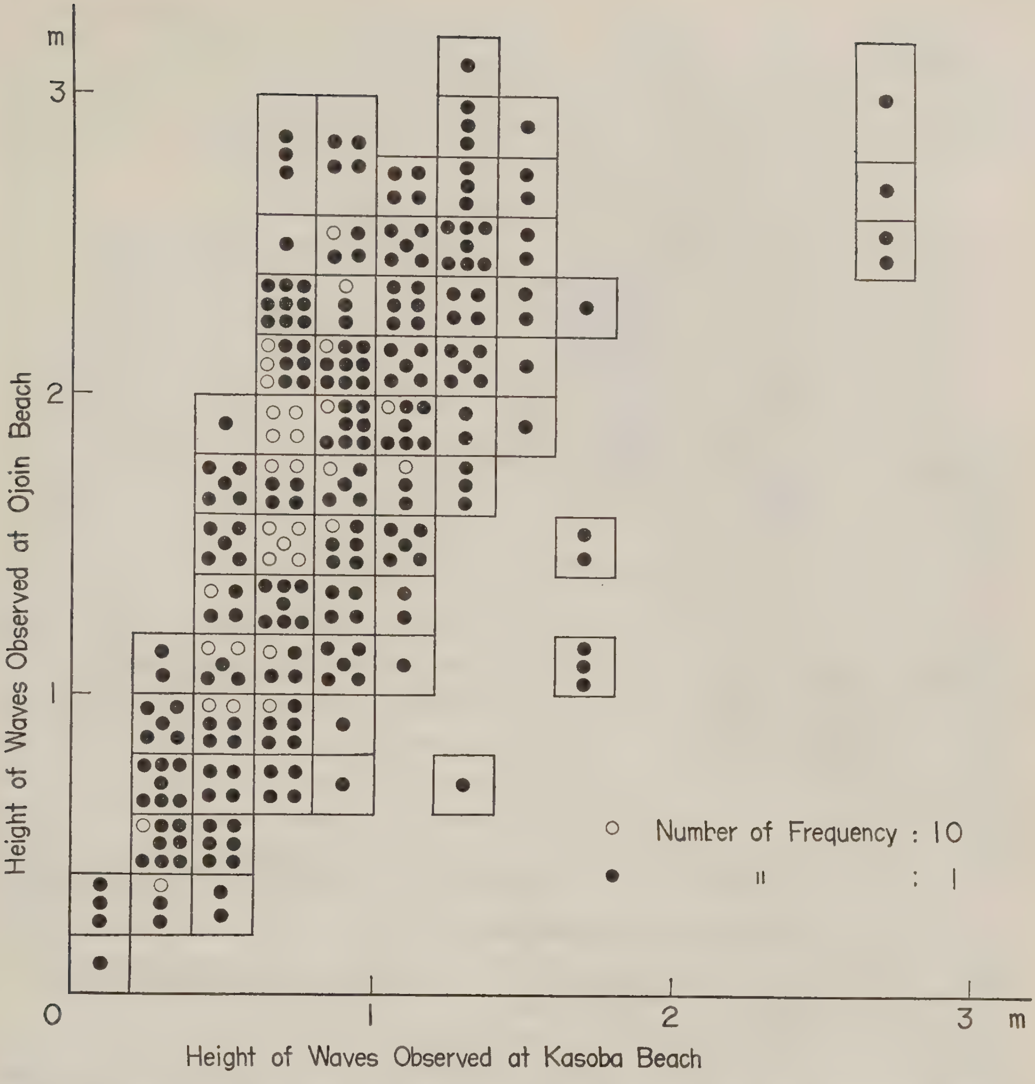

Fig. 4 **Relationship between the wave height at 150 m offshore from Ojoin beach and Kasoba beach (Nov. 1956～Mar. 1959)**

In comparing the wave characteristics observed at 300 m offshore from the seaside revetments, the incoming waves seems to be practically the same at two stations within some limited scattering. While the wave characteristics at 150 m offshore are evidently different depending upon the condition of either sheltering with submerged breakwater or non sheltering. In Figs. 4 and 5 are shown the following evidences; that is (1) the height of waves damped by submerged breakwaters are about 30～70% of that of original waves, (2) the steepness ratio of waves damped by breakwaters is about 10～70% of that of original waves, and (3) the attenuation of waves is larger for steeper waves. The submerged breakwaters are more effective for steeper waves which are responsible for severe beach erosion at Niigata west coast, the fact shows the success of this project at this coast[14).

2. Variation of Beach Profiles

Experimental Procedures

In this section the authors try to investigate the variation of beach profiles induced by the presence of submerged breakwaters through both the experimental and field observations.

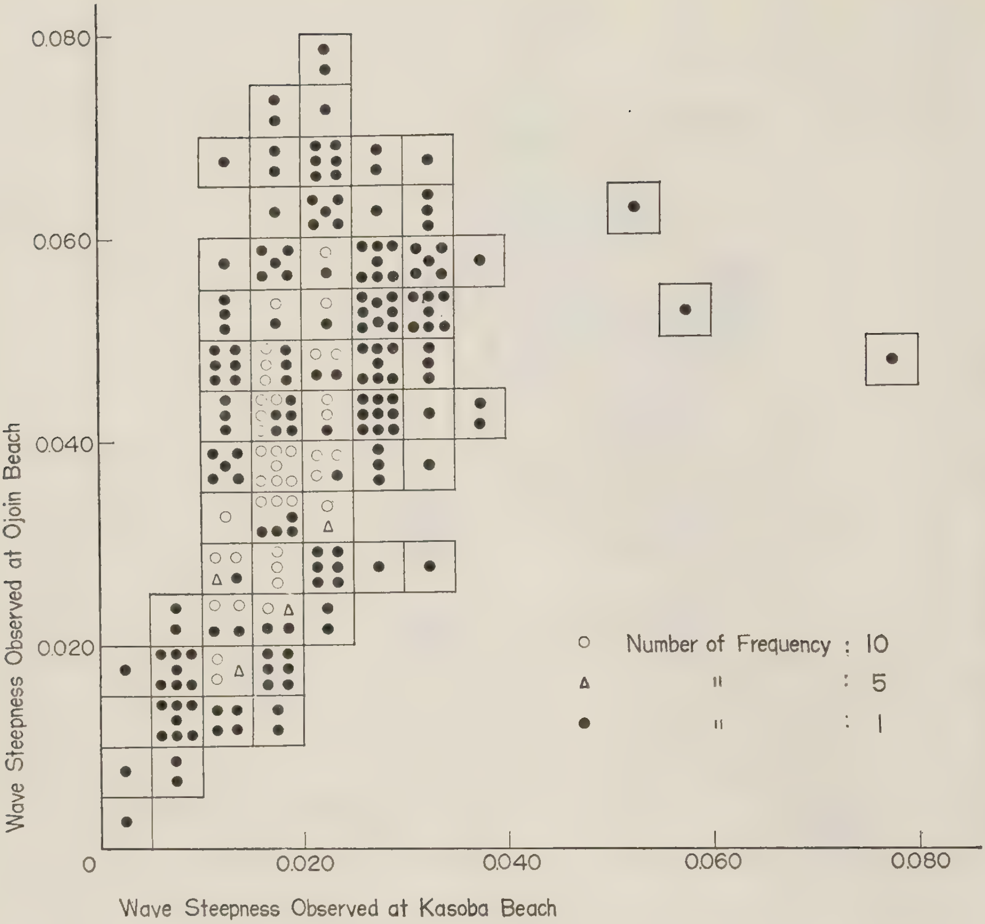

Fig. 5 **Relationship between the steepness ratio of waves at 150 m offshore from Ojoin beach and Kasoba beach (Nov. 1956~Mar. 1959)**

The laboratory experiment consisted of two parts; one was conducted under the fairly simple condition such that the model of submerged breakwater was a vertical impermeable wall extended downward till the bottom of wave channel; the other was conducted by using the exact models of submerged breakwaters (hollow block type and L type) practically constructed at Niigata west coast. Therefore the latter part of experiments could advent the

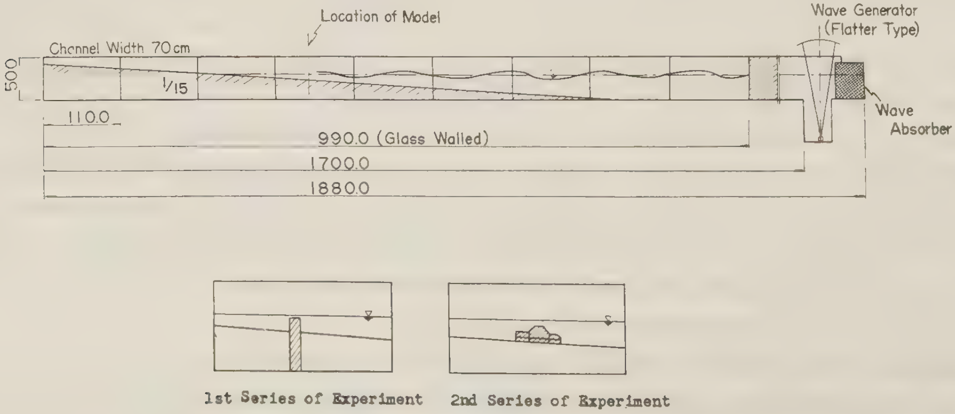

Fig. 6 **Experimental equipment**

similar condition to the actual phenomena.

The wave channel, 17 m long, 0.7 m wide and 0.6 m high, used for both experiments, was sloped in 1/15 at one end with the marine sand (mean diameter of about 100 μ) as shown in Fig. 6. The wave characteristics tested at both experiments are given in Tables 1 and 2.

Table-1

No.	T (sec)	H_0 (cm)	L_0 (cm)	H_0/L_0	db (cm)	H_{35}(cm)	L_{35}(cm)
A-I	1.80	10.4	506	0.0205	13.0	10.1	195
A-II	1.40	12.8	300	0.0427	14.7	11.8	220
A-III	1.15	10.1	206	0.0490	11.3	9.2	170

Table-2

Prototype Wave Condition			1/20				1/40			
H_0 (m)	T (sec)	H_0/L_0	No.	H_0 (cm)	T (sec)	H_{35}(cm)	No.	H_0 (cm)	T (sec)	H_{30}(cm)
3.26	11	0.018		—	—	—	G-1	8.3	1.74	8.2
3.50	7	0.046		—	—	—	G-2	8.8	1.11	8.1
1.57	7.8	0.017	G-6	7.8	1.74	8.7	G-3	3.9	1.23	3.6

Local Scouring around Submerged Breakwaters

The detail of this experiment has been published in the previous paper[13], but the important results will be summerised here. Figs. 7, 8, and 9 show a part of the experimental results, from which the presence of severe scouring around the submerged breakwater will be recognized especially when the location of the structure coincides with the breaking point of waves. The scouring depth is also depending upon the ratio of h/d. When the breakwater is situated at breaking point or in surf zone, the higher structure has tendency to cause greater scouring, while for breakwater at offshore zone the lower structure rather produces greater scouring. The above results will be explained as follows. In the former case the wave current produced by breakers is accelerated downward at the structure, and the above ten-

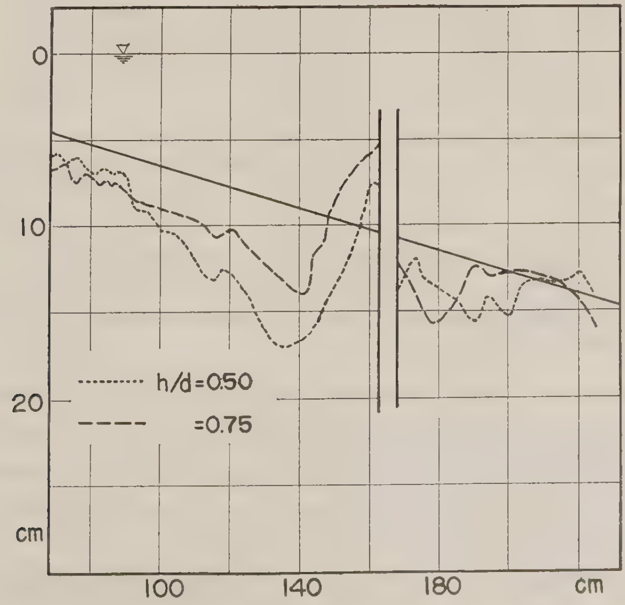

Fig. 7 Variation of beach profile in the vicinity of submerged breakwater set landward the breaking point (wave A-II)

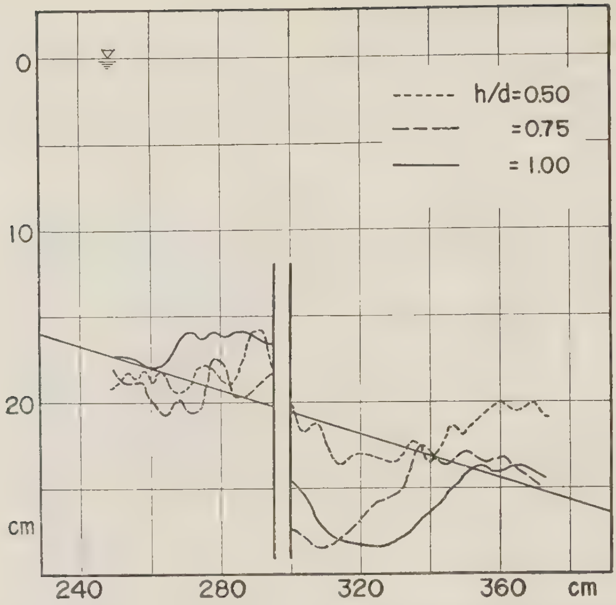

Fig. 8 Variation of beach profile in the vicinity of submerged breakwater set at the breaking point (wave A-II)

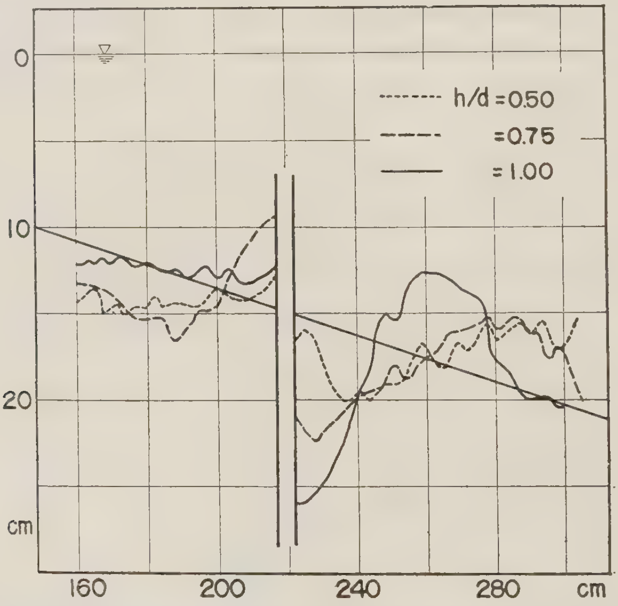

Fig. 9 Variation of beach profile in the vicinity of submerged breakwater set seaward the breaking point (wave A-II)

dency is strengthened by the higher structure. (Fig. 10 a) While in the latter case the waves are apt to be reflected at the structure and the compensating current overflowing the structure is mainly responsible for the scouring, therefore the above current over the lower structure (the height must be at least high enough to produce the rise of water surface) has much more chance to touch with the bottom. (Fig. 10 b)

Looking at the shoreward region from breakwater, there is accretion in stead of erosion in any case, and the variation of beach profile is rather slow. The above facts verify the important function of submerged breakwater such as to stabilize the bottom profile of

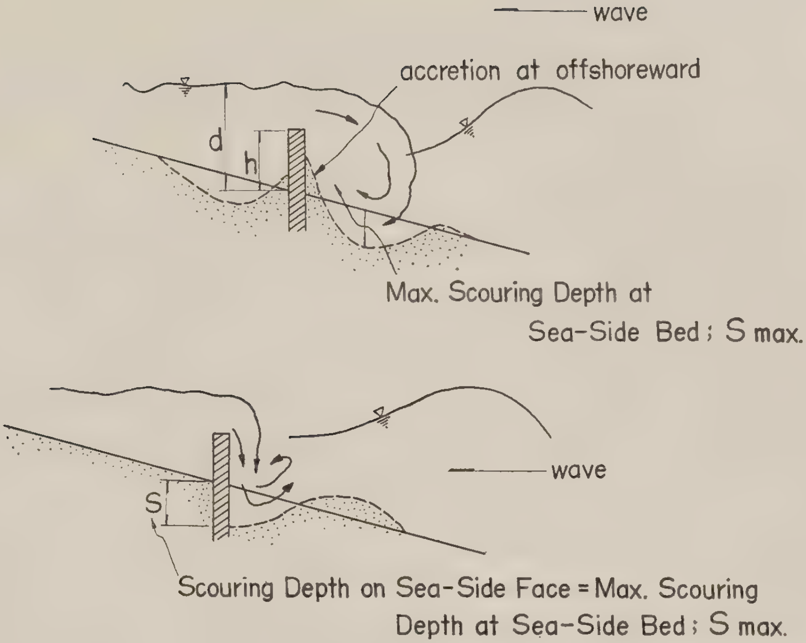
wave
accretion at offshoreward
d
h
Max. Scouring Depth at
Sea-Side Bed ; S max.
wave
S
Scouring Depth on Sea-Side Face = Max. Scouring
Depth at Sea-Side Bed ; S max.

Fig. 10 Scouring in the vicinity of submerged breakwater

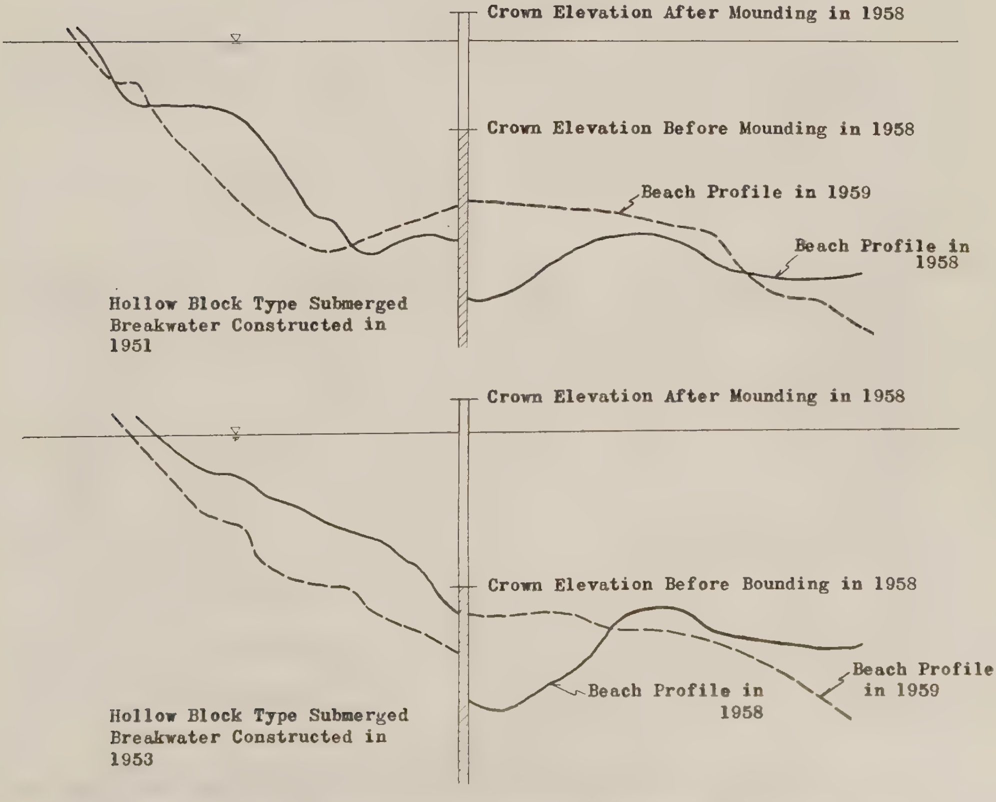

Fig. 11 Bottom profiles in the vicinity of submerged breakwater, Niigata west coast

beaches surrounded by the structures.

Fig. 11 shows the actual beach profiles sounded in the vicinity of submerged breakwaters at Niigata west coast. The solid lines, obtained before rising the height of the slumped breakwaters, are quite similar to that of the experiments conducted under such a simple condition as stated above.

Variation of Bottom Profiles

The daily sounding of beach profiles by far 300 m distance from seaside revetments were conducted in the period between November 1957 and March 1958 at three stations namely Ojoin, Kasoba and Hiyori beaches, Niigata west coast. Using the data obtained by the above soundings, the mean beach profiles and the standard deviation of water depth changes were calculated as shown in Fig. 12. From these results, the following two facts seem to be certain; that is, in comparing with the beach profile at Ojoin beach protected without submerged breakwater, (1) the beach faces protected by breakwaters are steeper, and (2) the variation of beach profiles at the same locations is considerably small.

In the second series of experiments the time variation of beach profiles was measured for several wave conditions with and without a submerged breakwater. In Figs. 13 and 14 the vertical scale upward positive shows accretion of beach sand on the initial profile (slope of 1/15). The hatch indicates the effectiveness of submerged breakwater on decreasing the

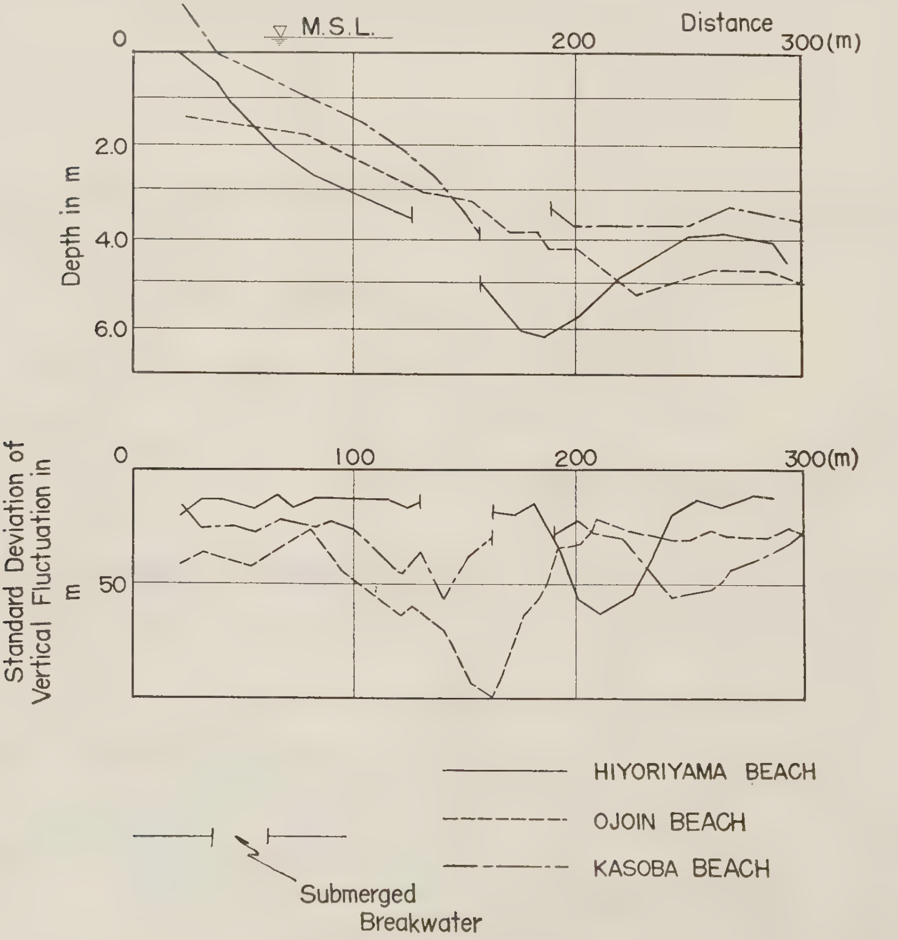

Fig. 12 Variation of beach profiles in the bicinity of submerged breakwater comparing with that at the natural beach

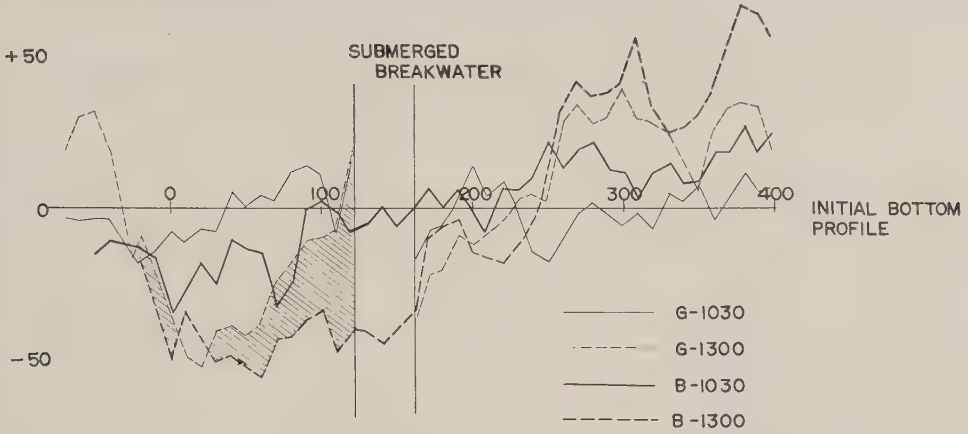

Fig. 13 Variation of bottom profiles in the vicinity of submerged breakwater (second experiment wave G-1)

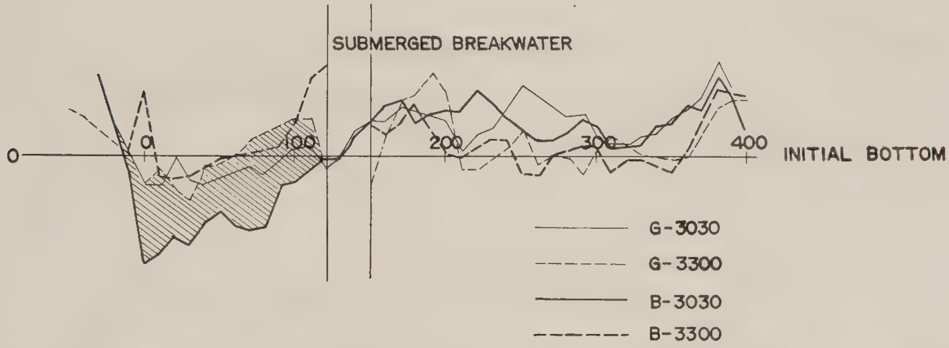

Fig. 14 Variation of bottom profiles in the vicinity of submerged breakwater (second experiment wave G-3)

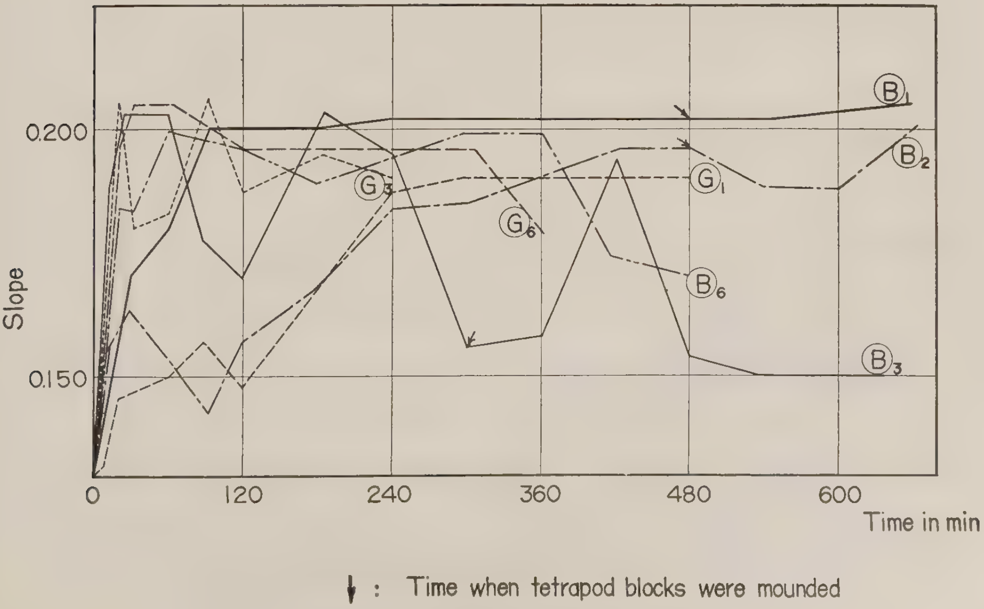

Fig. 15 Time variation of foreshore slope

active movement of sand. Fig. 15 shows the time variation of foreshore slope, the tendency of which is generally speaking agree with the result of field observations.

III. SLUMPING OF SUBMERGED BREAKWATERS AND MAINTENANCE PRACTICE

1. Experimental Purpose and Procedures

The submerged breakwaters have been constructed at Niigata west coast since 1950, and at the same time the numerous improvements have been done step by step. Among the several problems which have to be overcome, the slumping action of submerged breakwaters has recently been picked up as one of the most important problems. As it is stated in the previous chapter, the height of structure is essentially important in order to determine its effectiveness. In the process of slumping the structure is gradually losing its function, therefore the project for maintaining the submerged breakwater has been conducted since 1957.

Now it is necessary to make clear the mechanism of the slumping and also to establish the most effective and economical devices concerning the above project. The authors are

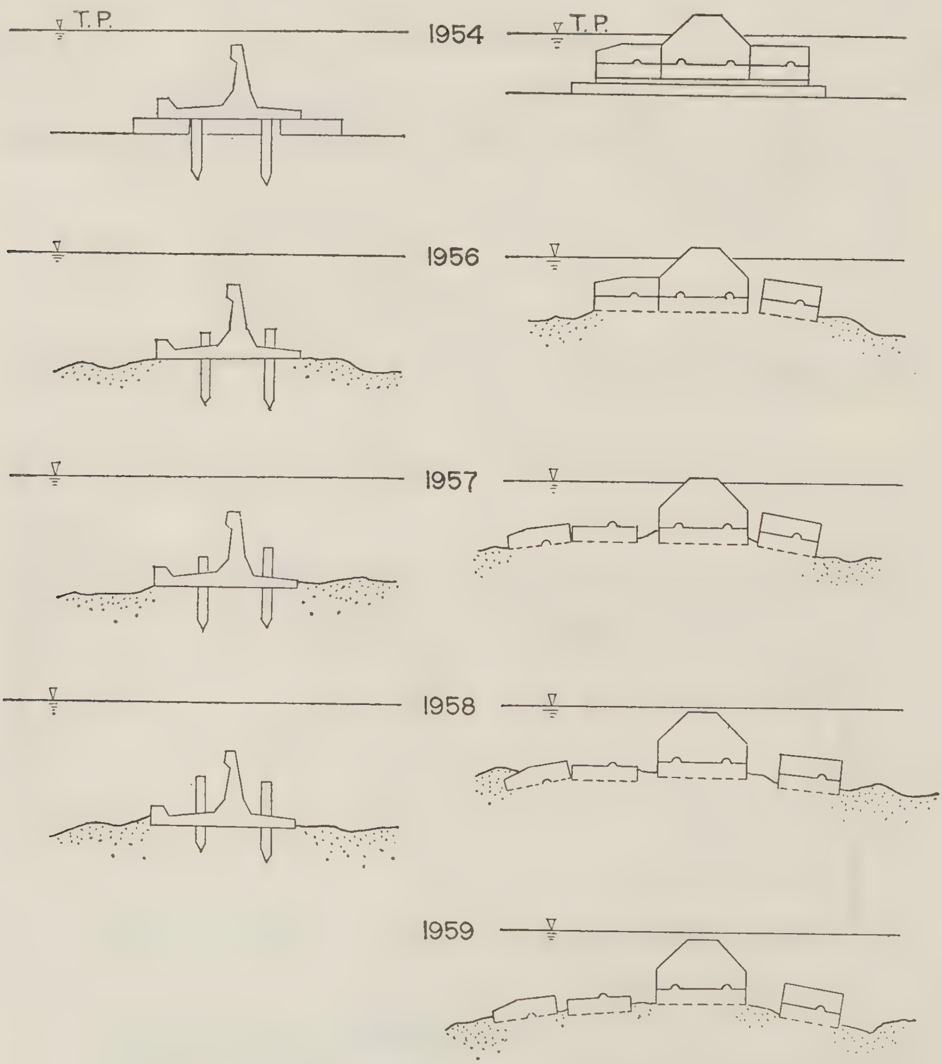

Fig. 16 Slump of submerged breakwaters constructed in 1954

continuing the experimental study on these problems, by using the same channel and the same wave conditions mentioned as the second series of experiments in Chapter 2. The scale of models was chosen of 1/40 and 1/20 of the prototype. In determining the wave characteristics the Froude model law was applied, and the experimental results were carefully compared with the field data in order to check the reliability of the experiments.

2. Mechanism of Slumping

The following three factors will be considered as possible reasons of slumping of submerged breakwater; that is (1) scouring, (2) vibration of structure caused by wave action, and (3) sand movement along the bottom of structure.

It may be quite difficult to find out the main reason among the above through only the investigation of field data as shown in Fig. 16. According to the visual observation in the laboratory, the process of slumping will be as follows; first of all each block of structure is released by the strong wave action, next the sand particles move under the structure from inshore zone to offshore as a pulsative sand flow, and also the offshore side of structure is scoured.

Fig. 17 clearly shows the rise of water surface level in the region shoreward of the submerged breakwater. The difference of water level between at shoreward and at offshoreward locations is largest, hence the velocity of current flowing over the structure to offshore zone is strongest, at the moment when the wave trough approaches to the submerged breakwater. At that time the hydraulic gradient along the base of structure is strong enough to induce the piping phenomenon. But the rise of water level mentioned above is negligible under the

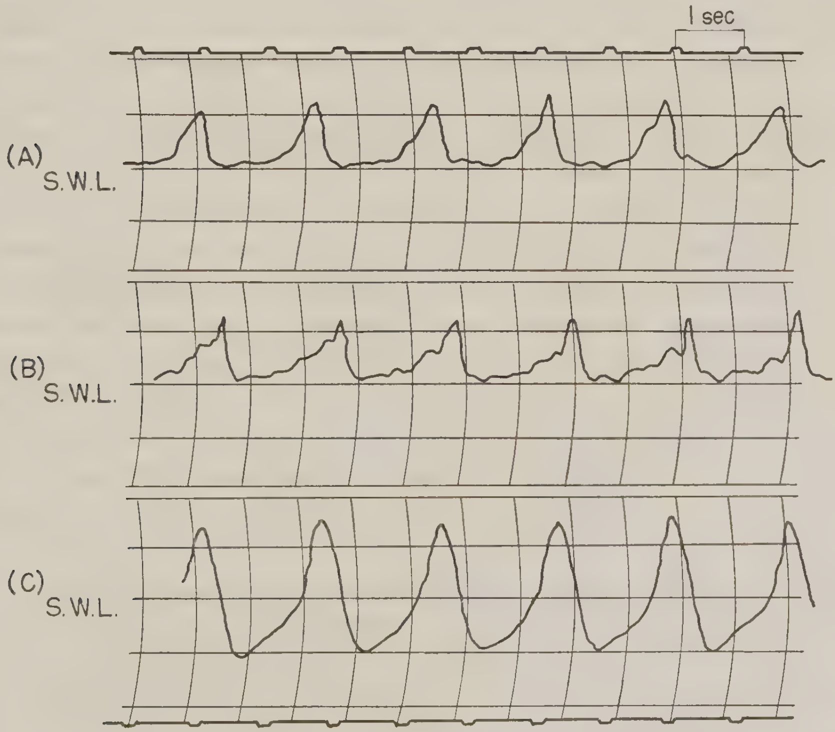

(A) Wave record at 53cm inshore of submerged breakwater
(B) Wave record at 15cm inshore of submerged breakwater
(C) Signifecant wave (d=30cm)

Fig. 17 Comparison of wave records

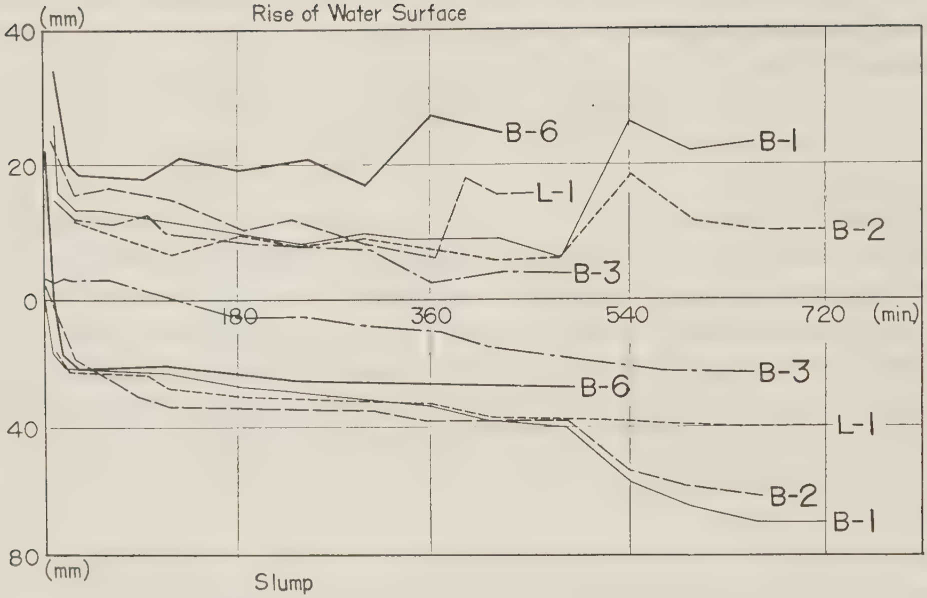

Fig. 18 **Relationship between the slump of the structure and the rise of water surface in the region of submerged breakwater**

condition of $h/d < 0.7$[10].

Therefore there must be a close relationship between the slump of the structure and the rise of water surface, as it is evidenced in Fig. 18, which shows a part of the laboratory experiments. The tendency that the slump is gradually approach to certain state is also clearly shown in that figure. The bigger waves seem to cause larger slump of structure, but the difference of the type of structure such as hollow block type and *L* type seems not to have any particular influence on the slumping action. The amount of slump shown in the figure is a mean value of each block.

The authors will try to consider the mechanism of slumping action in more detail. When the hydraulic gradient becomes larger than the critical value which is depending upon the specific gravity, S, and the void ratio, λ, of bed materials, the sand begins to move along the base of structure. If the difference of water level is the same, the shorter base structure induces more active sand movement. Hence in accordance with the process of structure's slump, the amount of water rise gradually decreases and the effective length of structure increases, therefore the structure is approaching to its stable state. The above process will be occurred even by the waves which are not so strong enough to disorder the blocks. The strong waves cause more active slump of structures because both of the scattering of the blocks, and of scouring at the foot of structure.

According to the studies by K. Terzaghi, and S. Awazu[11] the critical hydraulic gradient H/L is approximately $0.76 \sim 1.09$ assuming $d_m = 0.1$ mm and $\lambda = 0.52$. Actually the submerged breakwaters tested in the experiment have a lot of junctures between each block, which are favourable for seepage, hence the local seepage velocity may vary considerably. It means that the local critical hydraulic gradient must be fairly smaller than the calculated value.

On the other hand the junctures of each block beeing gradually filled with sand in the process of slump, the lower part of structure is buried under the bed materials. Therefore the slump of structure finally stops at certain limit.

If the scale ratios of water depth, size of structure, wave height and rise of water level in the prototype and model were maintained as a same value, the mean hydraulic gradients of both cases are exactly the same. Hence the seepage velocity is determined by the grain size and the juncture size of blocks. If the grain size of model is the same as that of prototype, the seepage phenomenon in the sand layer must be similar in both cases, but the seepage through the juncture of blocks is larger in the prototype ; that is, the sand movement in the prototype is more active than that in the model. On the other hand the rise of water surface is strictly appeared in the model as explained previously. Owing to the above circumstances the estimated amount of slump by using the scale model of 1/20 is not always equal to that by using the scale model of 1/40.

The actual slump of structures is considerably irregular as shown in Fig. 19. Using the above data obtained from 1954 to 1959, the mean value of slump was calculated for each group of structures except the part of filling with tetrapod blocks. (Fig. 20)

Fig. 20 also shows the curve of ground subsidence which was estimated by the surveying data of the bench marks set along the Niigata west coast. In comparing the slope of the slump curves with the slope of the subsidence curve, the submerged breakwaters seem to have stopped the slumping process caused by wave action by 1957~1958. After then the structures seem to be slumping with a fairly quick speed due to the ground subsidence.

The experimental results show the estimated slump of 0.6~1.5 m prior to mounding the tetrapod blocks over the structure, while the field data show the amount of 1.5~2.0 m.

3. Maintenance Practice

In order to reinforce the body and maintain the height of submerged break-water, the mounding of 4 ton tetrapod blocks over the structures has been applied at Niigata west coast since 1958. In the laboratory the same process has been repeated as shown in Figs. 15, 18, and 21. As a result of re-rising of water level due to the recovery of structure's height, the structure is again slumping until it is stabilized. Finally the structure will not slump any more after several times of mounding.

Another thing which is quite interesting is that the tetrapod blocks are quite effective to prevent the severe scouring, and also have a tendency to bury the deeply scoured portion. The aboundant laboratory data evidence the above tendency and the field data verify it too. (See Fig. 11.)

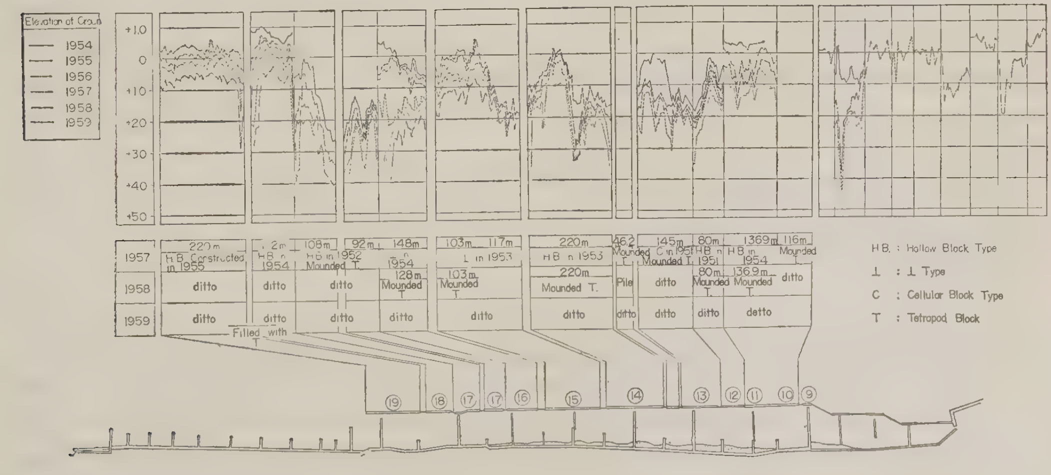

Fig. 19 Location and slump of various submerged breakwaters

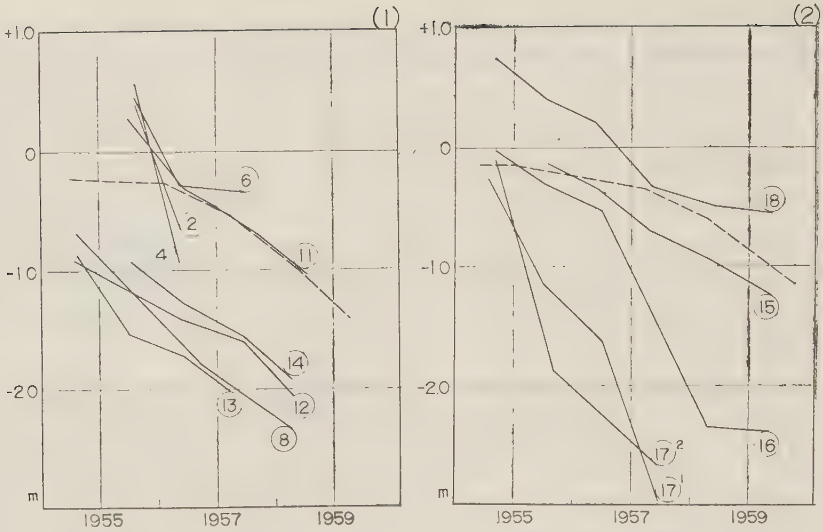

Fig. 20 Slump of submerged breakwaters at Niigata west coarst

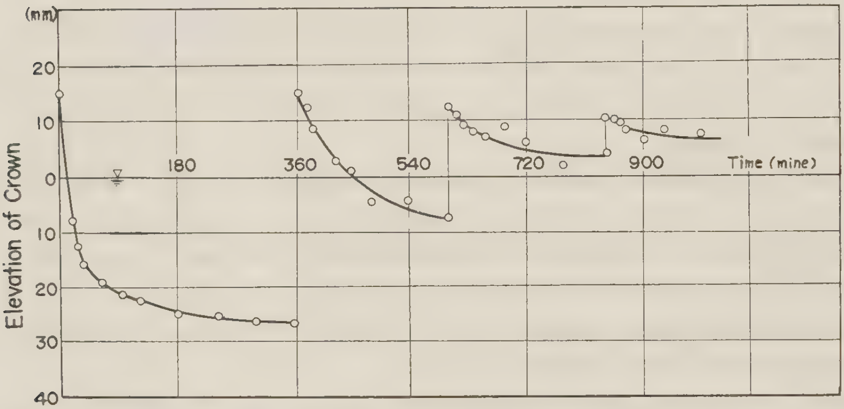

Fig. 21 Variation of crown elevation of submerged breakwater (Hollow block type)

4. Comparison of Several Types of Submerged Breakwater

There are several types of submerged breakwater which have been practically constructed and tested at Niigata west coast. All of them are permeable structures in order to absorb a part of wave energy. The types are as follows; (1) mound of broken stones shaped to rectangular section with iron net, (2) mound of broken stones, (3) cellar block type, (4) two raws of concrete piles filled with broken stone, (5) hollow blocks, and (6) *L* type. But the hollow block type occupies the main part of the present submerged breakwaters. Here the three types, namely (1) hollow block type, (2) *L* type, and (3) tetrapod mound type, will be discussed through the experimental observations.

Hollow Block Type

Prior the scattering of each block by wave, the return current to offshore zone through hollow blocks is favourable to reduce the rising of water level in the shoreward region of structure, therefore to reduce the slump of structure. But the side blocks are too small to resist the severe wave action. They are lifted and moved forward by wave action, hence the blocks are separated into isolated pieces. At this stage the sand movement along the base of the blocks is accelerated to induce the remarkable slump of structure, while the scouring around

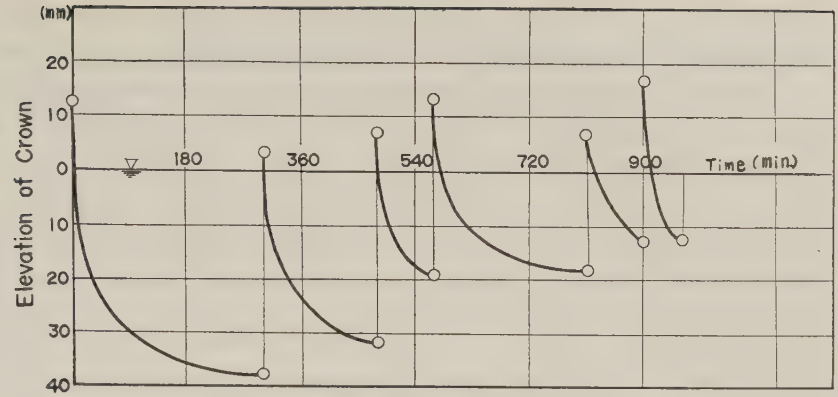

Fig. 22 Variation of crown elevation of submerged breakwater (Tetrapod type)

the structure is progressed by waves and current. The slump seems to be also dependent on the weight of blocks, therefore the slump at central part of section is most severe.

L Type

The damping action of this type must be a little worese than the others theoretically because of the narrow width of its crown. But this has no disadvantage, such as the scattering of blocks, which the hollow block type has. It seems to be fairly difficult to expect the sand deposit on the structure owing to the strong current resulted from the downward current along the body of structure and the horizontal current to offshore zone through the hole of the structure. Each block is supported by 4 piles, this condition is quite helpful to prevent the to and fro movement of structure. On the other hand it is posible to make a big room between the bottom of structure and the beach bed, because the structure itself is supported by 4 piles, and can not settle down following the variation of bed condition.

Tetrapod Block Type

This type has never been applied in the field, but the authors tried to find out the effectiveness of this type on the beach profile and on the maintenance practice in the laboratory. The permeability is quite large compared with other types, hence this type is supporsed to have less damping, but less slump. According to the experimental results this structure will also slump as much as other type, (Fig. 22), but as mentioned previously the scouring action of waves is almost completely diminished. Another advantage is that the construction and maintenance of this structure are fairly easy.

As a result of the comparison of each type the authors believe that the tetrapod block type might be the best one among the above three.

IV. CONCLUSOINS

In this paper the authors have studied the functions and maintenance devices through comparison of the experimental results obtained by the authors with the field data at Niigata west coast.

One of the most important functions of the submerged breakwater, that is the damping action, is really remarkable, hence this structure is taking an important role as a protection work at Niigata west coast. The slump of structure, which was overlooked at the early stage of construction, is becoming a very important and difficult problem. The authors found the following facts; (1) The main reason of the above phenomenon is the sand movement along the base of structure due to the large hydraulic gradient between the inside and outside regions of structure. (2) The slumping of structure may be stopped at certain state, but it starts again by mounding of tetrapod blocks. Finally the slumping may be completely finished after repeating the above process several times. (3) The maintenance device by filling tetrapod blocks seems to result in a good end.

Finally the authors will present here one idea of practice; that is, to construct another raw of submerged breakwater distanced a little shoreward from the present structure. It is really necessary to investigate carefully the advantage of this plan from the view points of its effectiveness and the economical consideration.

ACKNOWLEDGEMENT

Studies described herein were made by the Coastal Engineering Laboratory, University of Tokyo, under the guidance of the present authors. Special acknowledgement is made to the Harbor Section and the Shinano River Construction Office, Niigata Prefecture, for lending numerous data of field observations at Niigata coast.

REFERENCES

1) Lamb, H. : Hydrodynamics, 6 th ed. 1932.
2) Beach Erosion Board : A Model Study of the Effect of Submerged Breakwaters on Wave Action, Tech. Memo. No. 1, 1940.
3) Jeffreys, H. : Note on the Offshore Bar Problem and Reflection from a Bar, Grt. Brit. Ministry of Supply, Wave Report, No. 3, 1944.
4) Dean, W.R. : On the Reflection of Surface Waves by a Submerged Plane Barrier, Grt. Brit. Ministry of Supply, Wave Report, No. 8, 1945.
5) Ursell, F. : The Effect of a Fixed Vertical Barrier on Surface Waves in Deep Water, Proc. Cambridge Phil. Soc., Vol. 43, 1947.
6) Johnson, J.W., R.A. Fuchs and J.R. Morrison : The Damping Action of Submerged Breakwaters, Trans. A.G.U., Vol. 32, No. 5, Oct. 1951.
7) Delage, G. : Lutilissation dum Brise-Lomes pour la Defense dune Plage, Proc. Vth Conf. on Coastal Engg., 1954.
8) Technical Committee for Niigata Harbor : On the Beach Erosion at Niigata Coast, Dec. 1949. (In Japanese)
9) Kubo, T. and T. Yamamoto : Experimental Study on Shape of Submerged Breakwater, Proc. J.S.C.E., Vol. 39, No. 10, Oct. 1952. (In Japanese)
10) Horikawa, K. and C. Sonu : Experimental Study of a Submerged Breakwater, J.S.C.E. 12 th Annual Convention, June 1957. (In Japanese)
11) Awazu, S. : Fundamental Study on Scouring Mechanism, Thesis for Dr. Engg., University of Tokyo, July 1957. (In Japanese)
12) Ishihara, T. and T. Sawaragi : On the Prevention of Overtopping by a Submerged Breakwater, J.S.C.E. 13 th Annual Convention, May 1958. (In Japanese)
13) Hom-ma, M. and T. Sakou : An Experimental Study on the Submerged Breakwater, Coastal Engineering in Japan, Vol. 2, 1959.
14) Shiraishi, N., A. Numata, and N. Hase : Functions of Submerged Breakwaters Field Observations at Niigata Coast—Proc. 5th Conf. Coastal Engineering in Japan, Nov. 1958. (in Japanese)
15) Sakou, T. : A Study of Wave Actions in Relation with a Submerged Breakwater, Thsis for M. S., University of Tokyo, March 1959. (In Japanese)
16) Hosoi, M. and M. Tominaga : On the Wave Attenuation due to a Submerged Breakwater, Proc. 6 th Conf. Coastal Engineering in Japan, Nov. 1959. (In Japanese)
17) Hom-ma, M. and K. Horikawa : An Experimental Study on Submerged Breakwaters, (II), —Mechanism of Slump and Reinforcement of Structures—, Proc. 6 th Conf. Coastal Engg. in Japan, Nov. 1959. (In Japanese)
18) Sugiyama, M. : On the Beach Erosion at Niigata West Coast, Proc. 6 th Conf. Coastal Engg. in Japan, Nov. 1959. (In Japanese)

BEACH EROSION AND PROTECTION WORKS IN IMAZU-SAKANO BEACH

*Masafumi Kubo
**Nobuyuki Iwasa

I. INTRODUCTION

The location of Imazu-Sakano Beach in the east coast of Shikoku is shown in the general map (Fig. 1). It is exposed to the wave from Pacific Ocean through the mouth of Kii-Channel.

At the south limit of the beach spills the Naka River which is 105 km in basin length and has the basin area of remarkable rainfall (the annual rainfall is 2,800∼3,000 mm). The discharge of flood of the Naka River is very large (the design flood is 85,000 m^3/s), and a large amount of sandy sediment is transported to the river mouth. But the amount of trans-

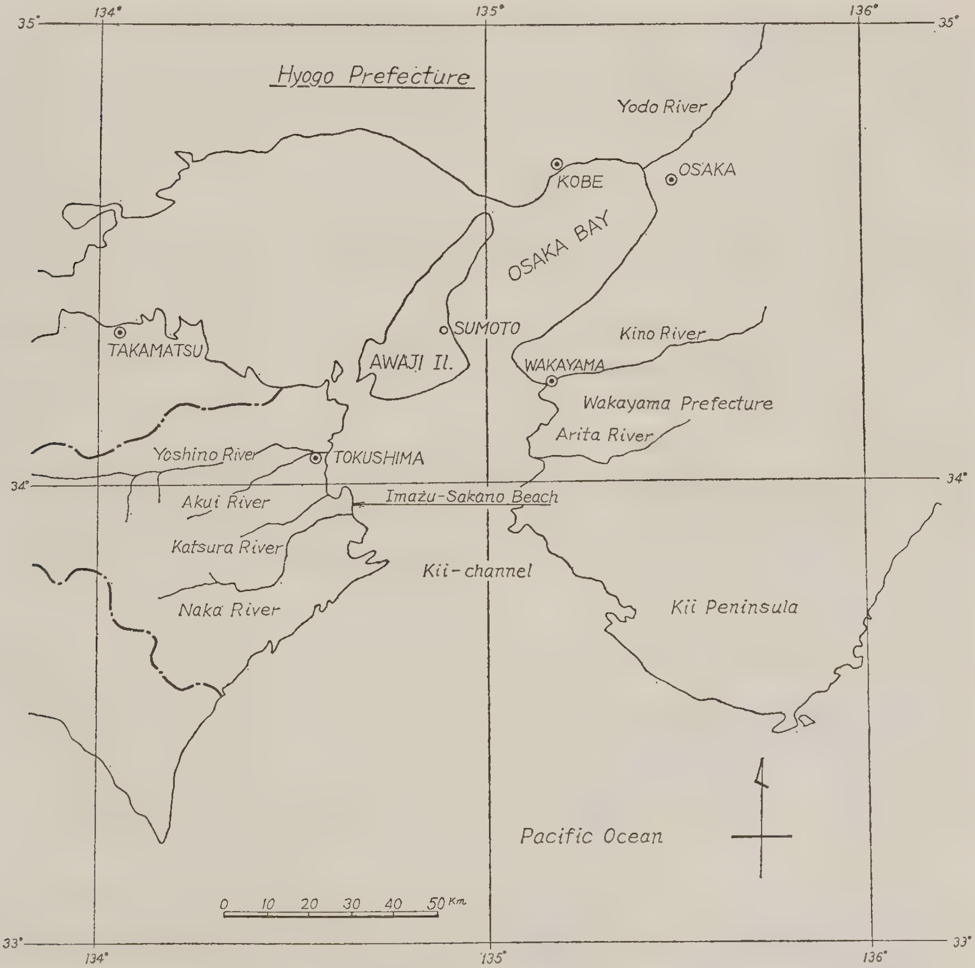

Fig. 1

---

* Dr. of Engr., Professor of Nihon University

** President, Gikenkogyo Ltd., Co.

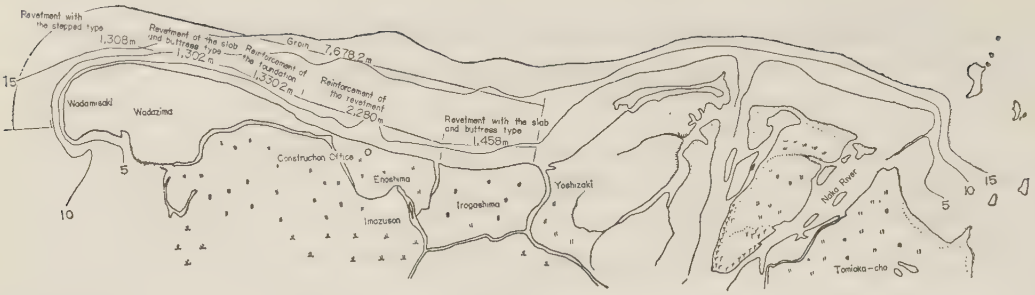
Revetment with the stepped type 1,308m
Revetment of the slab and buttress type 1,302m
Groin 7,678.2m
Reinforcement of the foundation 1,3302m
Reinforcement of the revetment 2,280m
Revetment with the slab and buttress type 1,458m
15
Wadamisaki
Wadazima
5
10
Construction Office
Enoshima
Imozuson
Irogashima
Yoshizaki
Naka River
Tomioka-cho
5
10
15

Fig. 2

ported sediment is not yet sufficient to keep balance with the amount of sand taken off from the beach by storm wave. Thus the shore line of this area recedes every year.

The protection works for the beach has been executed for about 7.5 km length after the typhoon on September, 1954 (No. 12). The general project and the result of these works are reported in this paper.

II. RECENT PROCESS OF THE SHORELINE

Imazu-Sakano Beach has been remarkably scoured lately by the wave attack and the beach erosion has caused directly disasters in the coast. The alluvial plane of this part consisted of sand from the Naka River in old age, and the Naka River formed a sandy spit which was called Wadamisaki. Enojima, Nakagawa-cho was 250 m distance far from present shoreline in 1870 roughly, and there were 60 peaceful houses on the land with dark blue pine-trees rounding. Sites of the old revetment of bank remain 500 m distant from the sand spit in Wadajima south-ward, and this position is about 150 m far from the present coastal line. And in 1850 or so stones of groin (or jetty) in the estuary of the Naka River had been being transported by a large barge, and simple groins were executed at Imazu-Sakano Beach in about 1890. A great typhoon attacked this beach on the 25th of July, 1896. And the tsunami on that typhoon made the sand bar and the forest of pine-trees collapse, and it caused great disasters on that district. Therefore enbankment of stone mounds were executed owing to the government subsidy. People in Tokushima Prefecture made effort such as above mentioned works, but they found it difficult to confirm the bank. And the shoreline recessed by beach erosion, the work of enbankment obliged to go backward against the land, with the result that the present bank is 300 m far from that of old.

The recession of shoreline progressed notably after the subsidence caused by Nankai Earthquake on the 21st of December, 1946. Thus the rate of the beach erosion increased, the sand bar disappeared, the foundation of the revetment of bank was deeply scoured, and the coastal dike was overtopped by wave or destroyed in many places.

The rate of growth of the sand spit was about 400 m per 60 years at the estuary of the Naka River, and that of recession in Imazu-Enojima was about 250 m per 60 years. The sandy beach 500 m distant from Wadamisaki to the Naka River was nourished about 2.0 km distance, but the shoreline recessed about 10 km on the other part. Water level rised about 70 cm, shoreline went backward against the land about 10～15 m owing to the sinking of ground on Nankai Earthquake. Thus the wave force increased and the beach was naturally eroded.

III. THE LATEST DISASTER

Imazu-Sakano Beach was unexpectedly much eroded 40 years ago, and the inclination angle of sea-bed confronting the revetment suddenly increased. Both Jane and Kijia Typhoon in September, 1950 caused much more disaster than Muroto Typhoon (in 1934) with result that the function of facilities on the coast was almost vanished. On observating the place in December, 1952 it was found that 56 sets of groins in 64 sets were destroyed. Misfortunately No. 12-Typhoon in September, 1954 left much disasters under such condition.

IV. WIND AND WAVE

1. Wind.

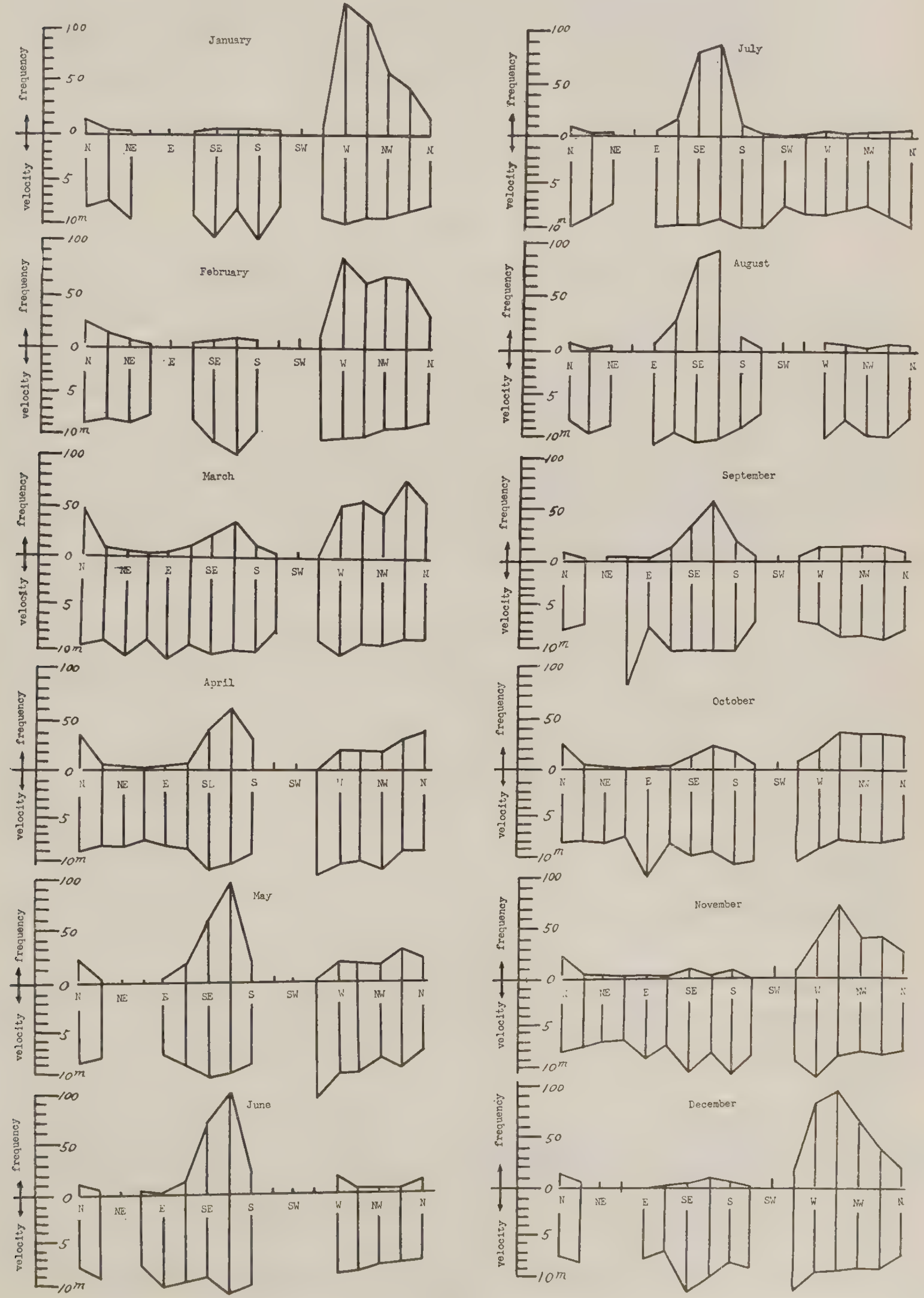

Fig. 3

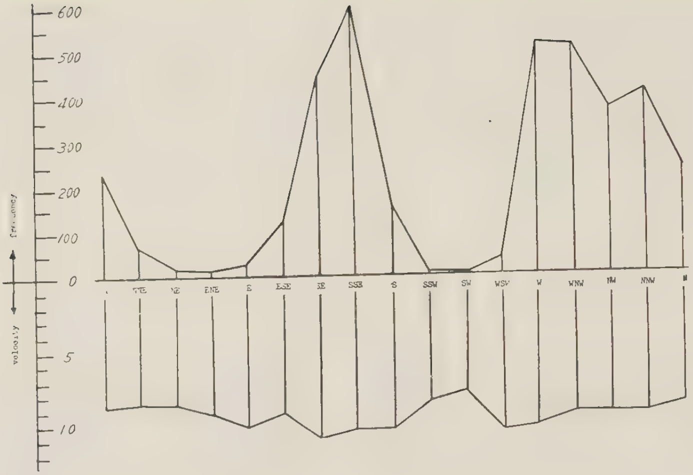

Fig. 4

The wind around Sakano-Imazu Beach has not been recorded, but the observation area of Tokushima Weather Bureau is similar enough to this beach for the use of the data of wind. From the record of wind over 7 m/sec in the period of 1932～1951, the frequency diagrams of wind direction for each month and the corresponding velocity are obtained as shown in Fig. 3. Fig. 4 shows the frequency curve of the direction of strong wind and the corresponding velocity through this period. From those figures it is obvious that SSE wind prevails through a year, while SE and NE winds prevail in summer and winter respectively. The fetch distance is extremely large in SE and NE directions, and the exposed angle is 45° toward Pacific Ocean. Thus the typhoon advancing in these direction will occur heavy disasters.

2. Water Level

As the water level records observed in this beach are very poor, we used the records observed by Tokushima Weather Bureau in Komatsujima Harbour in the period of 1951～1953 which give the following,

Mean level at the new and full moon of flood tide	0.817 m
Mean level of ebb tides at the new and full moon	−0.972 m
Mean water level	0.035 m
The highest water level	1.432 m
The lowest water level	−1.498 m
The largest tidal range	1.798 m

above the mean sea level of Tokyo Bay

As the highest water rises in No. 15-Typhoon is estimated as 0.6 m at 5 : 40 p.m., the 26th of September, 1954, the highest level may be calulated 0.817+0.6 m=1.417 m. This value approximately coinsides with 1.432 m, the observed highest water level.

3. Wave

There are no reliable data of wave observed in this beach, therefore the waves are estimated from the calculation of refraction theory by using the records of wind and sounding survey. Two examples of refraction diagram are shown in Figs. 5 and 6.

From this procedure the distribution diagram of wave height is estimated as Fig. 7. The height in this figure coinsides considerably with the actual height of wave at several places.

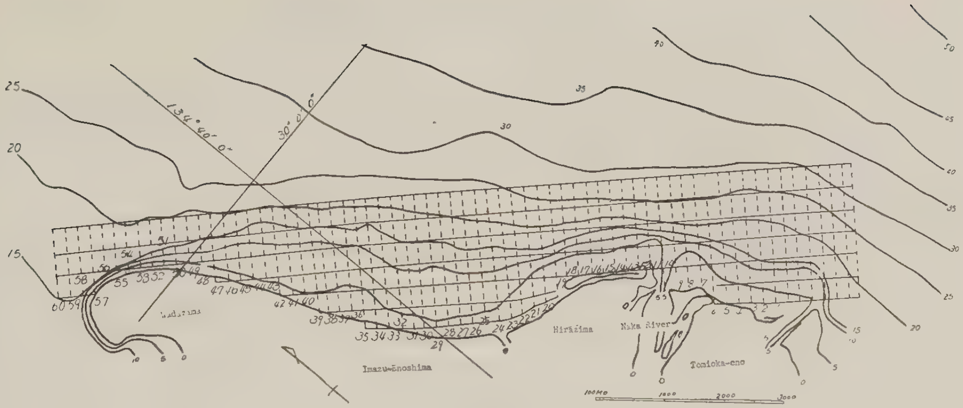

Fig. 5

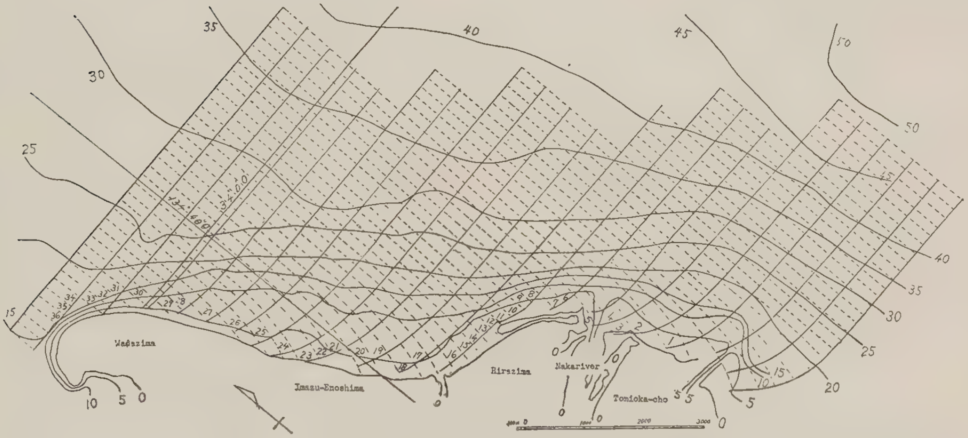

Fig. 6

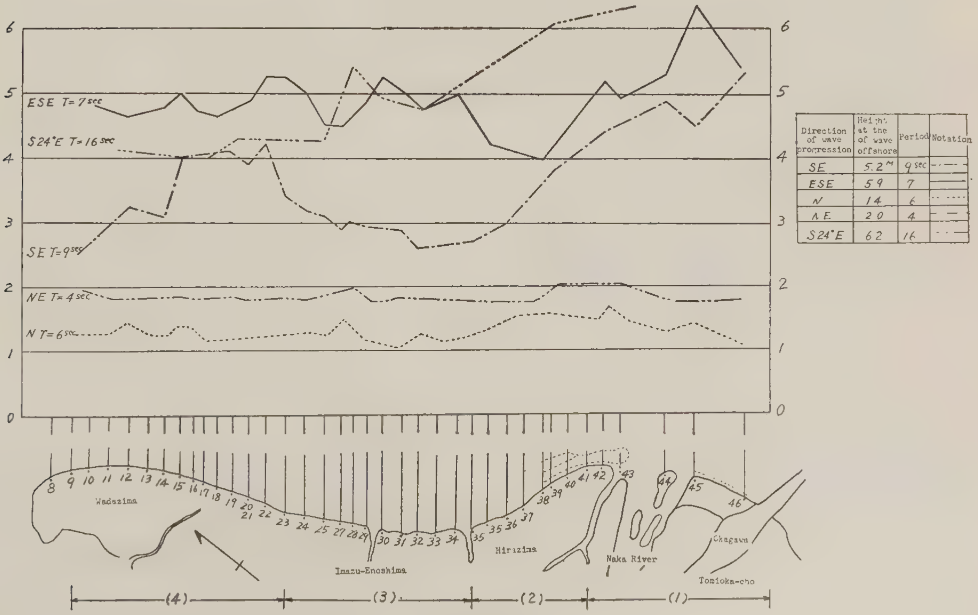

Direction of wave progression	Height at the of wave offshore	Period	Notation
SE	5.2^{M}	9^{sec}	-·—·-
ESE	5 9	7	——
N	1 4	6	·· ····
NE	2 0	4	- —
S24°E	6 2	16	··—

Fig. 7

V. RECENT COASTAL WORKS

1. No. 12-Typhoon in September, 1954

In the two typhoons in 1950 and No. 12-Typhoons in 1954, wave overtopping and the scouring of the foundation of revetment caused the collapse of coastal dike in many places. Here some details on the No. 12-Typhoon will be described.

Meteorological View (Fig. 8)

This Typhoon appeared in 4th of September, 1954 on the ocean east of Mariana Islands and advanced in west-ward direction, growing gradually the pressure in its center was 910 mb, the highest wind velocity around the center was 60 m/s, and the wind velocity in the circumference of 400 km radius was larger than 25 m/s on 8th of September. After that the typhoon took the route as shown in Fig. 8, passed through the Kyushu Island and advanced into Japan Sea. The date and barometric depth at the center at some positions on the route are also shown in the figure.

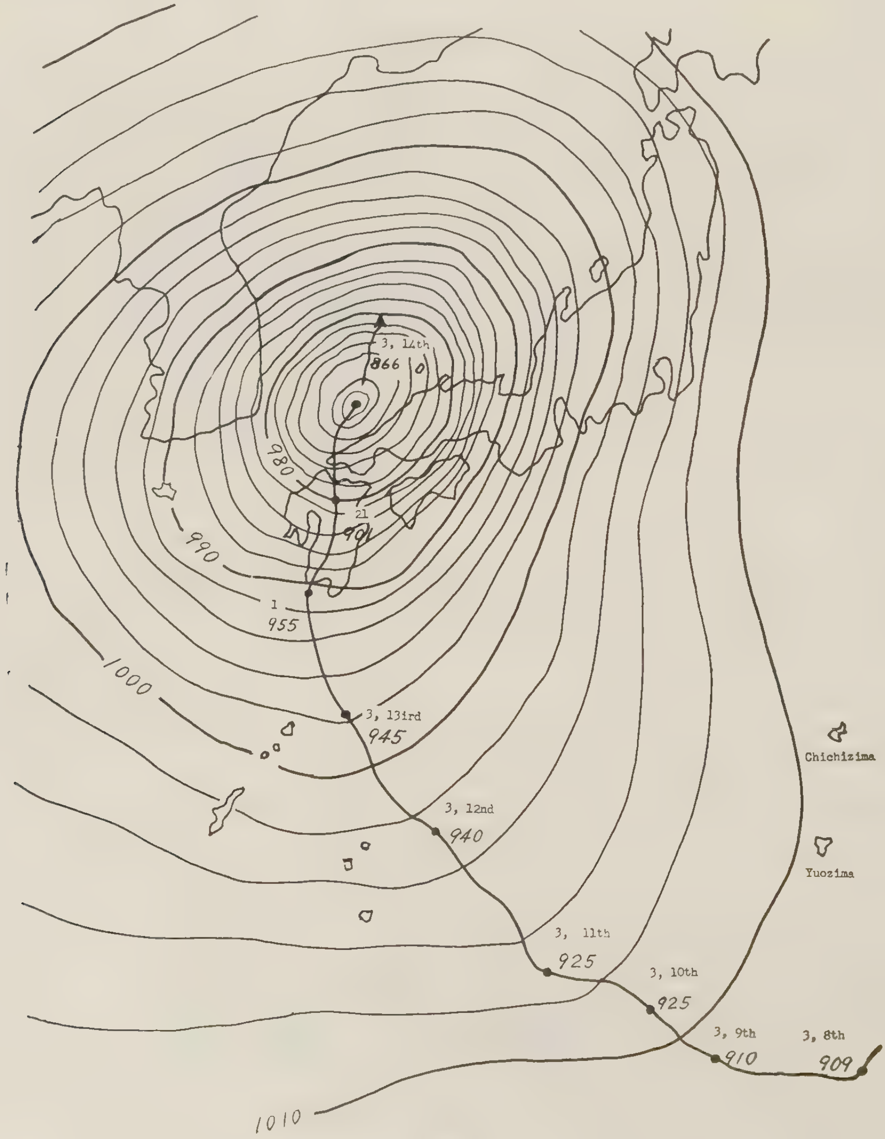

Fig. 8

The Typhoon reached 600 km SW of Yuo-Island on the 9th, and very large swell and high wave attacked around the beach in Tokushima Prefecture. The height of wave was especially large on the 10th, and coastal dikes at Imazu Enoshima and Wadajima were destroyed by the wave action. The max. velocity of wind was 32.7 m/s by common measure, its instant velocity was 44.5 m/s and the direction of wind was SE at 1 : 50 p.m. at Imazu-Sakano Beach.

The wind velocity was larger than that of Jane Typhoon in 1950, but it was still smaller than that of Typhoon on 15th of August, 1941.

The characteristics of No. 12–Typhoon in September of 1954 are as follows:

(a) The circumference of the typhoon was very large ever before.

(b) The advancing velocity of typhoon was rather small and the duration time of strong gale was long, compared with the most typhoon in September.

(c) The core of this typhoon was very large, and the diameter of the zone of storm was 100–200 km.

(d) High swell came to the coast before the arrival of storm and it continued very long. Violent wind more than 13 m/s blew for 28 hours.

Disaster of Coastal Dikes

It is needless to say that heavy storm caused the disasters. Besides that, the dikes damaged by the past typhoons had not been completely reinforced and these dikes became origins of larger destruction.

The damages of dikes and groins by No. 12–Typhoon are summerized in Table 1.

Table 1. Disaster by the Typhoon No. 12

Imazu Beach	Crevasse Lost groins	6 places (614 m) 5 sets
Sakano Beach	Crevasse Lost groins	4 places (583 m) 5 sets
Total	Crevasse Lost groins	10 places 10 sets

2. Causes of Destruction of Coastal Dikes

Causes of destruction of dikes by Typhoon No. 12 in 1954 are considered as follows:

(a) Sand in dike body was sucked out by wave from construction gaps, expansion joints of the concrete revetment and gaps of mortal bond of rubble revetments.

(b) At the sunk well foundation joint of wells opened and sand was drawn out.

(c) The surface of the concrete revetment was very smooth and the wave ran up freely to the top of it. Reflected wave made clapotis with incident wave and increased the scouring in foundation.

(d) Groins had been lost in most part by the wave in the past typhoon and the function of groins could not been expected.

(e) In same pleaces the foundation had sunk by the past Nankai Earthquake.

(f) In same places the height of dike was insufficient and the inner slope was scoured by the overtopping wave.

3. Design section of Coastal Dike

Standard Cross Sections of the Coastal Dikes

The authors determined three typical cross-sections of dikes shown in Figs. 9, 10 and 11 by cooperation of the Section of Disaster Prevention and the Public Works Reaearch Institute of the Ministry of Construction.

These cross sections are described as follows.

(i) Revetment by slab and buttress type (Fig. 11): Sand outflow is checked by 3.5 m long sheet piles or mixed-in-placed piles with 45 cm diameter.

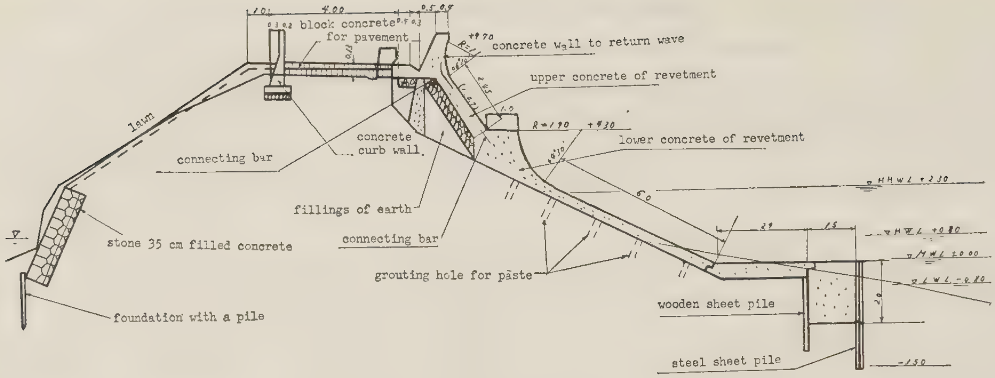

Fig. 9

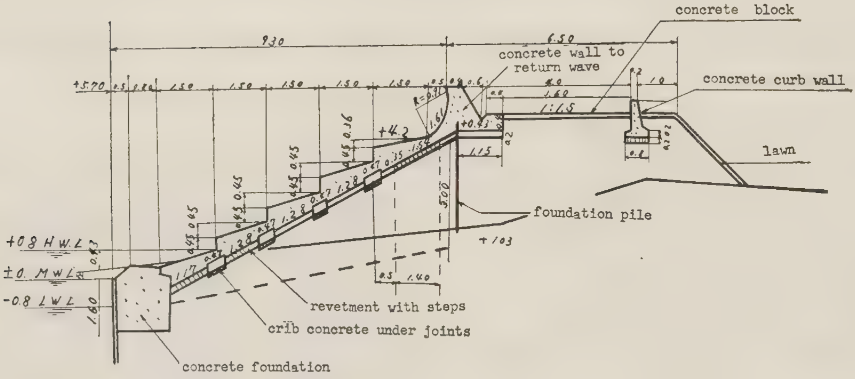

Fig. 10

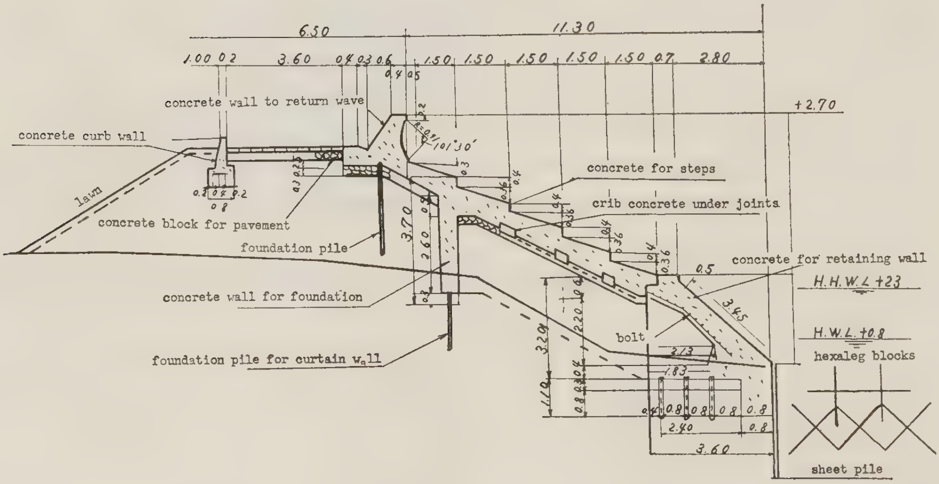

Fig. 11

The revetment consists of three parts: those are the part of lower slab and buttress, that of the stepped slab and the crest. The lower part has reinforced-concrete wall of the outer slope 1 : 0.1 and the buttress apart 5 m c.t.c. The buttress can support the upper part of revetment. Five steps 1.5–0.4 m above the +2.5 m level are designed for the purpose of the dissipation of wave energy and the checking of wave run-up.

The longitudinal curtain wall of 50 cm thickness under the step is designed as a cut-wall from the crest to the bed. For the purpose of the prevention of sand out-flow from the gap of wall-joint and the sliding of the step work, the concrete crib work is laid in 40 cm thickness under each joint. The breadth of the crown is 4.0 m. The dike has cross-sectional partition walls apart 15 m each other. They will check the transmission of damage in longitudinal direction.

(ii) Revetment with middle step (Fig. 9): This section is adopted for the purpose of increase of height and reinforcement of the old concrete revetment. The middle step of 1.0 m wide at the height of 4.3 m may check the occurrence of clapotis on the foundation of the revetment.

(iii) Revetment with steps (Fig. 10): This section is designed for the place where the height of wave is small and scouring force is small. Wooden sheet-piles are driven in its foundation.

Groin (Coastal Jetty)

The present groin which is about 35 m in length, is 1.0~1.5 m above H.W.L. in height and was constructed as a non permeable groin had displayed no sufficient function for the sand nourishment and sometimes caused even beach erosin. The new groin is designed to have the crest nearly at H.W.L. and to be the perveous construction with concrete hexa-leg-blocks. The head of groin is located at about the third breaking point of wave which was estimated by the wave refraction theory. The depth at the head of groin is 2.6-3.0 m, and the direction of groin is perpendicular to the shoreline. The distance of two adjacent groins is 100 m. They have parallel works of 60 m long at their heads, forming T-shape as shown in Fig. 12, for the checking of rip current.

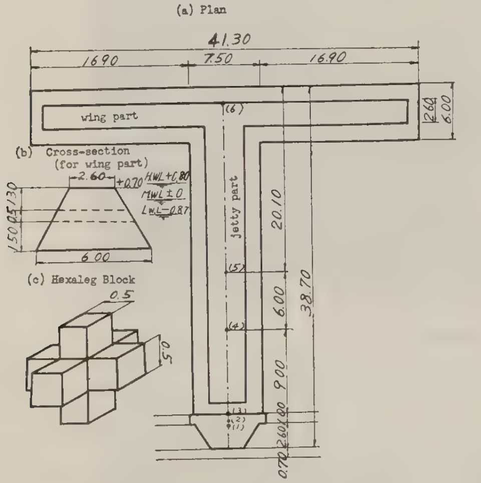

Fig. 12

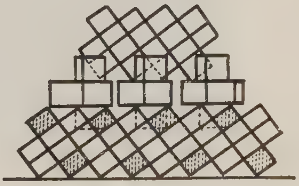

Fig. 13

4. General Schedule.

The total length of coastal dike is 7682.2 m and the number of groins is 48 on this beach, total cost being ¥ 960,000,000.

The length of the revetment of the retaining wall type	2,760 m
The length of the revetment with the middle step type	2,280 m
The length of the revetment with steps type	1,308 m
The length of the grouting	1,336 m

The total length of work	7,678 m
The number of groins of the T-shape	48 sets (60 m)

5. Execution

In March of 1958, the work of 6700 m revetment has completed as shown in Photos 1 and 2, and 19 groins were executed. Concrete hexaleg-blocks were used to construct the groin and the foundation work of dike. This block has the width 0.5 m, and the length of leg is 0.50 or 0.65 m. One set of the groin of the T-shape which the perpendicular length to the shoreline is 32.5 m and the parallel length to that is 41.3 m, was constructed by 523 sets of hexaleg-blocks. In these works, the void of groin is shown as following.

Photo. 1

Photo. 2

In the lowest part	67.9%
In the middle part	56.0%
In the top	59.7%

The crown of groin has settled down about 0.5 or 0.8 m immediately at the head place after the work by the wave action but the assembleness of blocks has not been loosened.

The movement of the littoral drift on the coast has been checked by these pervious groins, and the beach has not been scoured but sediment settled in the shoreline. The beach has already been nourished about 15 m in width. Photos 3 and 4 show the completed groins.

(a)
Sedimentation by old groins

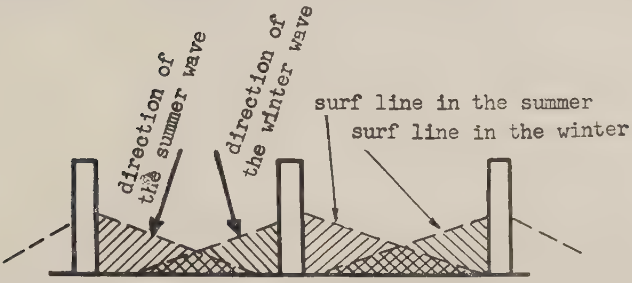

(b)
Sedimentation by present groins
made of hexaleg blocks

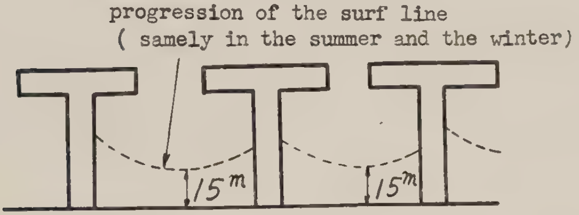
progression of the surf line
(samely in the summer and the winter)
15m
15m

Fig. 14

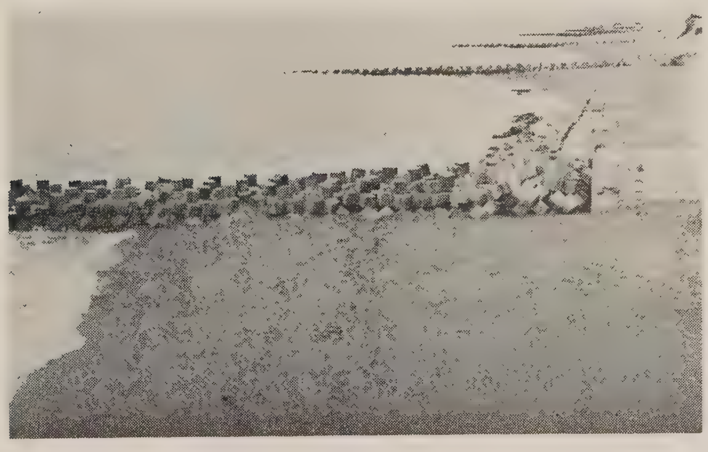

Photo. 3

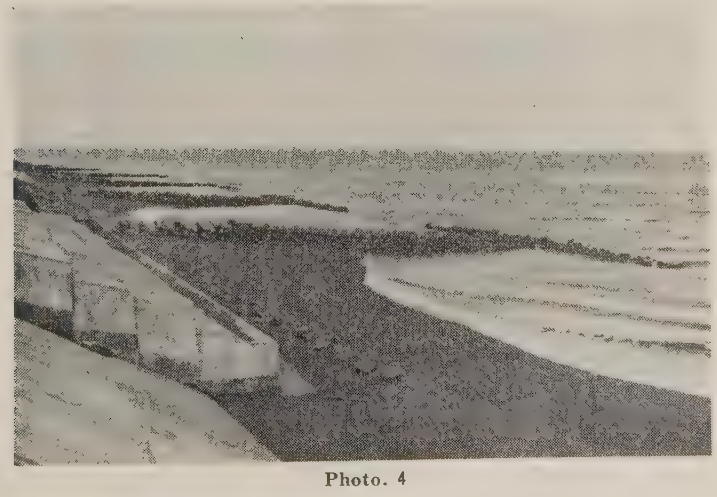

Photo. 4

Coastal Engineering in Japan, Vol. 4

IMPROVEMENT OF THE MOUTH OF THE MUSA RIVER

*Tsutomu Kishi**

*Masahiro Taniguchi***

I. INTRODUCTION

The Musa River drainages the Shibetsu District of Hokkaido Pref. and flows into the Sea of Okhotsk. Its drainage area and design flood discharge are 701 km^2 and 910 m^3/sec, respectively. Though it is only a small river, Shibetsu City and its neighbouring farms situated in the lower reach of the river have been frequently innundated.

As is shown in Fig. 1 the river sharply bends to the south near the shore and flows along the coast line for about 1,300 m. The river, mouth have sometimes been in the states of half-blocking. To prevent floods and faciliate the drainage in the lower reach a plan of cutting a new mouth straightly through the shore has been studied since 1958.

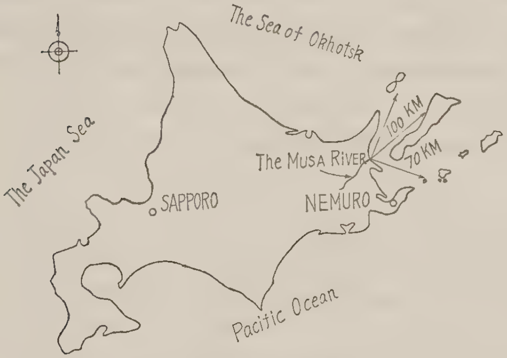

Fig. 1a General view of Hokkaido Prefecture.

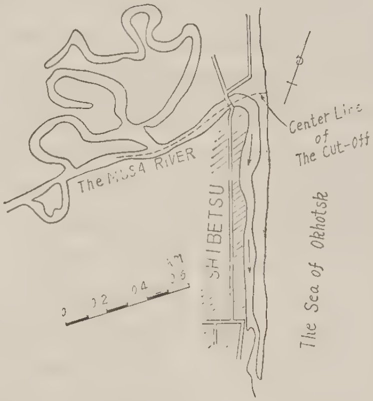

Fig. 1b Mouth of the Musa River

In this paper, the authors reported the progress of cut-off plan. Effects of cut-off of shore on W.L. in the river and the stability of river bed were first calculated before a plan was carried out. Then, characters of sand drift along the bay were investigated. They gave the authors some basic data for the design of sand protection works. Cut-off of shore and a test jetty were carried out in February, 1959. Since then field observations have been continued to confirm the design of sand protection works.

II. EFFECTS OF CUTTING OFF THE SHORE

1. Lowering of W.L. by Cut-off.

Position of designed cut-off is shown in Fig. 1 by dotted line. To evaluate a lowering of W.L. by cut-off, it was necessary to know the value of Manning's roughness coefficient n along the river course.

The authors calculated the value of n, as a first way, by using the data of size distribution of bed materials. When the logarithmic velocity distribution is assumed for a natural river flow, mean velocity U_m is expressed by equation (1).

---

* Dr. of Engr., Professor of Hydraulics, Hokkaido University, Sapporo.

** Engineer, Construction Bureau of Shikoku District, Ministry of Construction.

$$(U_m/U_*) = A_r - \frac{1}{K} + \frac{1}{K}\ln(R/K_s) \qquad (1)$$

where U_m = mean velocity

$U_* = \sqrt{gRI}$ = friction velocity

R = hydraulic mean depth

I = energy gradient

K = Karman's universal constant

$A_r = 8.5$

K_s = equivalent sand roughness of river bed.

According to equation (1), Manning's roughness coefficient n is expressed by equation (2).

$$n = \frac{R^{1/6}}{\sqrt{g}\cdot(U_m/U_*)} \qquad (2)$$

As is seen in eqs. (1) and (2), Manning's n depends upon K and K_s in addition to R. According to Vito A, Vanoni's experiments$^{(1)}$, the value of K decreases as the sediment concentration of flow increases.

However, in the Musa River sediment concentration of flow is not so high that the value of K may be assumed to be a constant value of 0.4. The value of equivalent sand roughness K_s is vary with conditions of bed,——bed is moving or fixed. Roughly speaking, the order of magnitude of K_s is equal to the mean diameter, d_m, of bed materials for a fixed bed. While, the magnitude of K_s is greater than d_m for a moving bed, because the sand dunes and ripples develope.

According to K. Ashida$^{2)}$, the relation between (U_m/U_*) and (d_m/RI) in the case of moving bed is given as Figure 2.

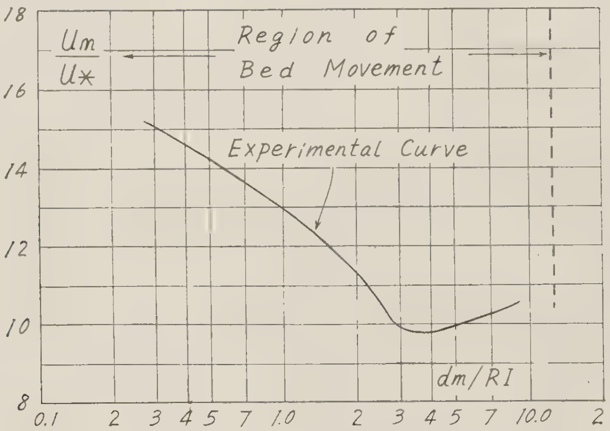

Fig. 2 Relation between (U_m/U_*) and (d_m/RI) (by K. Ashida & others)

Typical example of the size-distribution of bed material is shown in Fig. 3 by full line. The sample shown in the figure was taken at a station 2 km upstream from the mouth. Mean diameter of 0.74 mm is considered as a representative size of bed materials in the related reach.

Introducing the above value of $d_m = 0.74$ mm into the ralation given in Fig. 2, a value of Manning's n corresponding to a value of R is obtained through equation (2). The range of R observed at the station 2 km was about 1 m–2.5 m. The mean value of Manning's n corresponding to the above range of R is 0.0275.

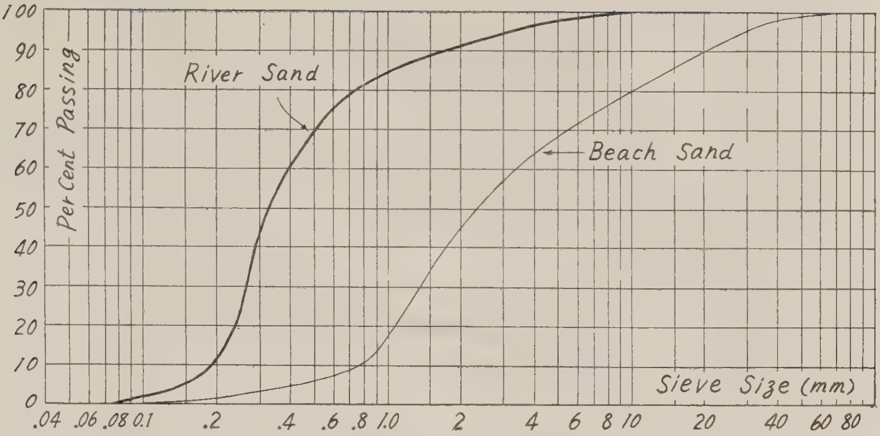

Fig. 3 Typical size distributions of river sand and beach sand.

In addition to the above calculation, the authors calculated the value of Manning's n from the stage-discharge curve prepared at the station 9 km upstream from the mouth.

At this station the effect of back water due to tide at the mouth is thought to be negligibly small. Therefore, the state of uniform flow may be assumed. The value of Manning's n calculated from the above assumption was 0.025. Two values of n; the one calculated from the mean diameter of bed materials at the station 2 km, $n=0.0275$ and the other calculated from the stage-discharge curve at the station 9 km, $n=0.025$ are well agreed.

The authors used a constant value of $n=0.025$ at any section of the river, to calculate the W.L. when the shore being cut off.

In the calculation of back water curve, three kinds of W.L. were given at the mouth. First is $H=1.85$ m, it is the highest sea water level recorded in the past. Second is $H=0.85$ m, it is the mean high water level of spring tide. Third is $H=0.20$ m, it is the mean water level. Calculations of the surface profiles along the river course were carried out under the combinations of the above three values of W.L. and two values of river discharge, 100 m^3/sec and 50 m^3/sec. Two values of river discharge were selected in accordance with the frequency analysis of river discharge. Calculated water profiles are shown in Fig. 4.

Lowering of water level is noticiable as far as about 7 km upstream from the mouth. Especially, at the neighbourhood of Shibetsu City, it is near the mouth, lowering of water level of about 70 cm is expected. This shows that a plan of cutting off the shore is effective for flood prevention and drainage of inland water in the lower reach of the river.

2. Effects of Cut-off on a Stability of River Bed.

There is some fear if the river beds were scoured after cutting off the shore. Suspended load seems to have little importance because the bed materials do not contain so much silts or fine sands, as are seen in Fig. 2. The authors calculated the scour of river bed considering the bed load transportation.

According to the experiments carried by S. Sato, H. Kikkawa and K. Ashida[3] rate of bed load transportation q_B is expressed by the relation (3), when a value of Manning's roughness coefficient n is equal to or larger than 0.025.

$$q_B=0.62\cdot\left(\frac{r_s}{r_s-r_f}\right)\cdot F\left(\frac{\tau_c}{\tau_0}\right)\cdot\tau_0 U_*=0.62\left(\frac{r_s}{r_s-r_f}\right)F\left(\frac{\tau_c}{\tau_0}\right)\cdot w\sqrt{g}\,(HI)^{3/2} \qquad (3)$$

where q_B = weight of bed load passing a section per unit width and time.

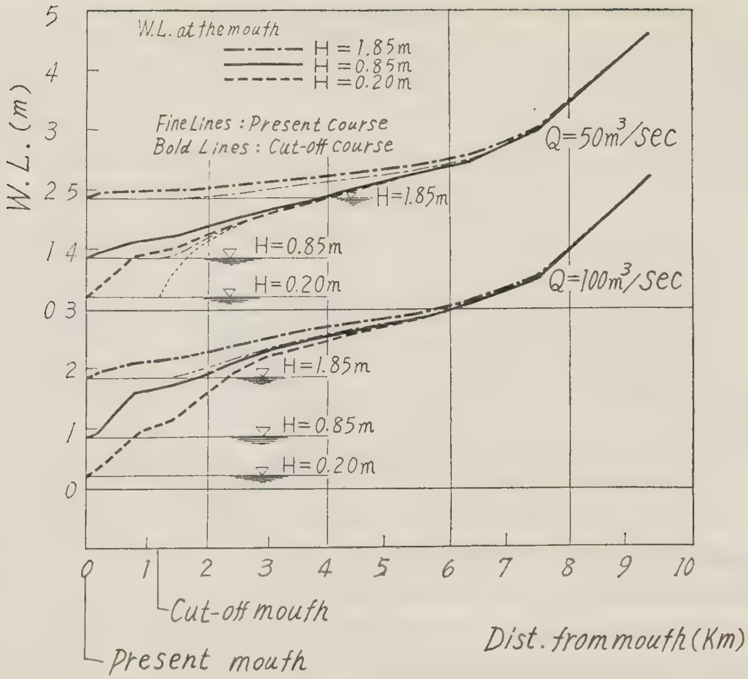

Fig. 4. **Lowering of W.L. by cut-off**

w = weight of river water of unit volume
g = accerelation of gravity
H = water depth
I = slope of water surface
r_s = specific weight of bed material
r_f = specific weight of river water
τ_c = critical tractive force of bed material
τ_0 = tractive force on river bed
F = a function of (τ_c/τ_0)

Critical tractive force of the bed materials in the MUSA River is about 59.2 gr/m, when $r_s=2.6$, $r_f=1.0$, $d_m=0.74$ mm and the critical value of Shields function $\psi=0.05$ are assumed. The value of $F(\tau_c/\tau_0)$ is approximately 1.0 at any place of the river because the value of the ratio, (τ_c/τ_0), is smaller than 0.2. Therefore, the relation (3) is reduced to the relation (4).

$$q_B=w\sqrt{g}\cdot(HI)^{3/2} \tag{4}$$

Rate of bed load transportation, Q_B, at a section having a width of B is expressed by the relation (5), when the Manning's formula for mean velocity is introduced into the relation (4).

$$Q_B=\frac{w\sqrt{g}\cdot n^3Q^3}{B^2H^{7/2}} \tag{5}$$

where Q = river discharge

Rates of bed load transportation were calculated by the relation (5). Results of calculation by combining the above three values of W.L. and the two values of river discharge are shown in Fig. 5.

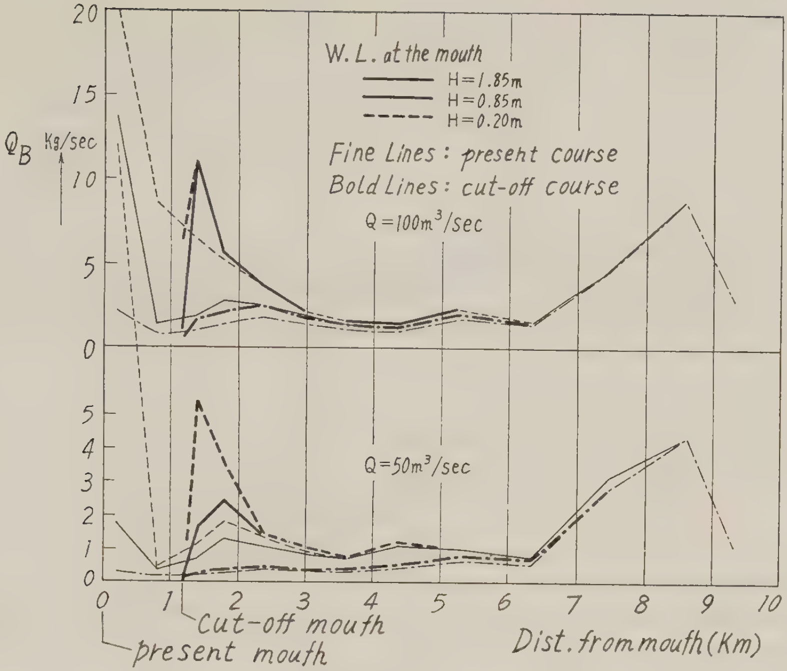

Fig. 5 Bed load transportation in the Musa River

Variation in the rate of bed load transportation due to cutting off the shore is noticed only in the part as far as about 600 m upstream from the new mouth. According to Fig. 5, it is expected that score of river bed may be limited only in the nearer part of the mouth, because a score of river bed which extends upstream would be faded out in relatively a short distance.

III. CAUSE OF RIVER BENT AT THE MOUTH

As is shown in Fig. 3 size distribution of beach sand is obviously different from that of the river sand. Beach sand contains relatively larger particles; gravels and cobbles which are not found in the river sand. Therefore, the sand which are fed by the river would not play an important role in the process of river bent. The river bent would be caused by the drifting sand from the north. Investigation of the source of littoral drift was carried out.

1. Variation of the Size of Shore Material along the Bay.

To find the direction of littoral drift variation of the size of shore material along the bay was investigated. There exist the Churui River about 6 km north of the Musa River. This is a torrent stream which feeds the shore a lot of sediment. As the Churui River was considered to be the source of the littoral drift shore materials were sampled every 200 m from the mouth of the Churui towards the south and the mean sizes of samples were compared. Fig. 6 shows the variation of the mean value of a product of major and minor axes of cobbles sampled on fore shore.

According to Fig. 6 a general trend shown by a broken line is noticed with respect to the size variation of shore cobbles. The broken line showing the gradual decrease of cobble size from the Churui toward the south would indicate a sorting of cobbles size during their drifting, so that it would be found that a privailing sand drift moves from the Churui towards the south. And size variation shown in Fig. 6 tells us that cobbles of about 7~8 cm

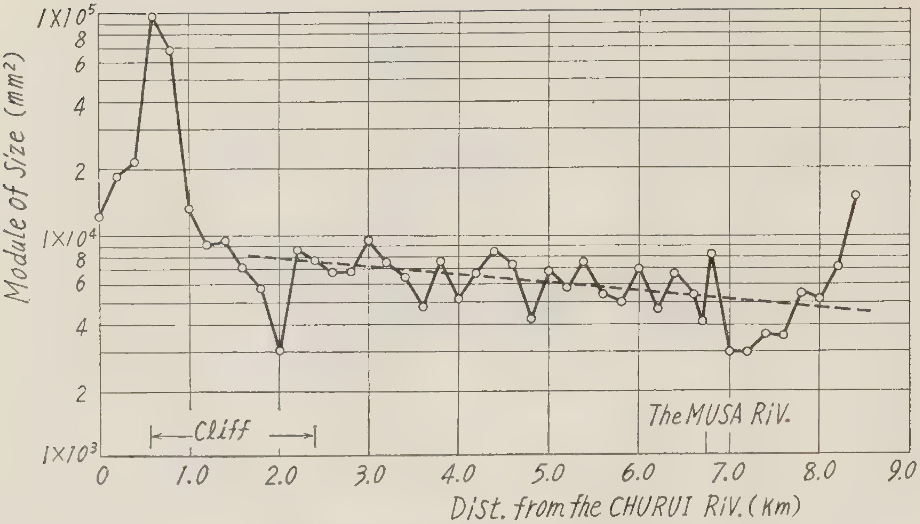

Fig. 6 Variation of cobbles size along the bay coast.

dia. would have been vigorously moved by storm waves but cobbles larger than about 10 cm dia. would have been hardly moved.

2. Monthly Variation of the Direction of Sand Drift.

By the above stated investigation, privailing direction of sand drift throughout a year was found. To carry out a design of sand protection works at the river mouth it is, then, necessary to investigate the monthly variation of the direction of sand drift. Following method of wind data analysis was adopted to this end.

1) Suppose that a sand drift is negligible when the wind velocity is less than 5 m/sec.
2) Suppose that amount of sand drift caused by a strong wind having a velocity greater than 10 m/sec is double of that caused by a wind less than 10 m/sec.
3) Suppose that direction of sand movement follows the direction of wind component with respect to the shore line.
4) Wave height and period are governed by the fetch length, when the wind velocity and duration are equal. Therefore, the effect of an inequality in fetch length for various wind directions has to be considered in the analysis of wind data. In this analysis, southern wind was weighted by one-third comparing with the northern wind in accord with the fetch length.

Wind data observed at the Nemuro meteorological station during January, 1953 and December, 1957 were analysed. The number of times of wind calculated under the above assumptions are algebraically summed up and the results are shown in Fig. 7.

Fig. 7 is considered to show the scheme of monthly variation of the direction of sand drift.

Results of wind data analysis shown in Fig. 7, as well, support the privailing direction of sand drift found from the shore materials. And according to Fig. 7 there are some months that the shore sand drifts from south to north. However, the number of times of winds in such months is relatively small. Therefore, sand protection work on the south side would be omitted.

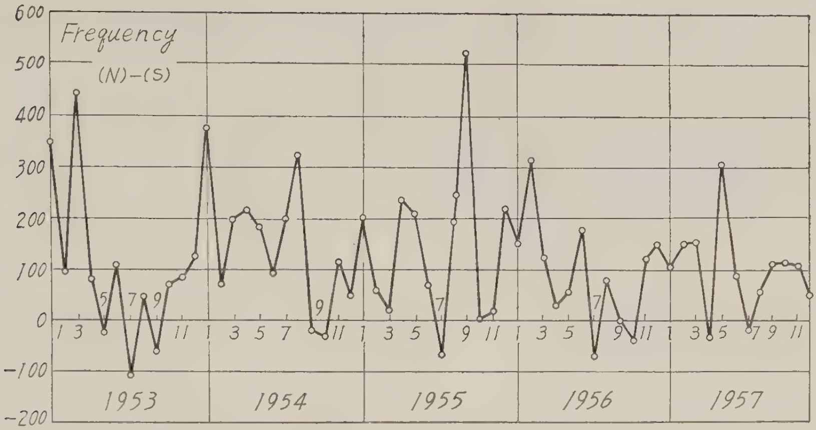

Fig. 7 Number of times of strong wind (Nemuro Met, st,)

IV. DESIGN OF JETTY AT THE RIVER MOUTH AND ITS EFFECTS AFTER THE CONSTRUCTION

To protect the cut-off channel from being buried a test jetty was constructed along the north side of the channel. Only a jetty on the north side seemed sufficient to prevent sand drift when the characters of sand drift studied in the preceding chapter are considered.

Ground height at the tail of the jetty was determined by the run-up height of a design storm wave. Design storm wave has the height of 2.2 m and the length of 75 m in deep water and this is expected to occur once a year, in the mean, according to the frequency analysis of storm waves. Run-up height of a wave depends upon the shore slope as well as the wave character. Slope of the shore, in this case, is about 1/7∼1/10. According to the experiments by S. Sato and T. Kishi4), run-up height of the above design wave on the shore is estimated about 1.1 m above the water level. As the height of M.H.W. is 0.85 m above D.L., ground height at the tail of the jetty was determined to be 1.95 m above D.L..

On the foreshore the jetty height was designed to be higher than the incident wave height.

According to the experiments by S. Sato and T. Kishi5), the height of the crest at the shore line of the above design wave at the shore line is estimated to be 0.88 m above S.W.L.. And the jetty height at the shore line was designed to be 1.7 m above D.L.. The jetty length was designed to reach a point of 2 m deep at the tip.

The cut-off channel and test jetty were carried out in February, 1959. In one or two months after the completion of the jetty sands deposited on the north side of the jetty and shore line advanced to the tip of the jetty. After that, a slender sand spit about 60 m long was formed on the south side of the jetty in July, 1959. However the sand spit did not grow farther but sonetimes flushed away by floods, and the cut-off mouth has been maintained in relatively stable state. The above progress of the mouth after the jetty construction would show that the sand protection effect of the jetty is almost satisfactory.

Topographical surveys and soundings have been scheduled hereafter to observe the conditions near the mouth and confirm the design of the jetty.

REFERENCES

1) Vanoni, V.A. : Some effects of suspended sediment on flow characteristics. Proc. of the Fifth Hyd. Conv., 1952.

2) Ashida, K. : Roughness in a erodible channel. Technical Memorandum, Public Works Res. Inst., Ministry of Construction, Vol. 1, No. 7, 1959. (in Japanese)

3) Sato, S., H. Kikkawa, and K. Ashida : Study on the bed load transportation (1). Report No. 98, Public Works Res. Inst., Ministry of Construction, Oct., 1956. (in Japanese)

4), 5) Sato, S., and T. Kishi : Experimental study of wave run-up on sea wall and shore slope. Coastal Engineering in Japan, Vol. 1, 1958.

ANNOUCEMENT

COASTAL ENGINEERING IN JAPAN, VOL. 1, 1958 (pp. 147)

…… US $ 1.50

TABLE OF CONTENTS

1. Y. Mashima :
   Study on the Typhoon Characteristics in respect of Wave Development and the Distribution of Longshore Current.
2. S. Hayami :
   Type of Breakers, Wave Steepness and Beach Slope.
3. T. Hayashi and S. Hattori :
   Pressure of the Breaker against a Vertical Wall.
4. S. Sato and T. Kishi :
   Experimental Study of Wave Run-up on Sea Wall and Shore Slope.
5. T. Shimano, M. Hom-ma and K. Horikawa :
   Effect of a Jetty on Nearshore Current.
6. K. Horikawa and C. Sonu :
   An Experimental Study on the Effect of Coastal Groins.
7. Y. Iwagaki and T. Sawaragi :
   Experimental Study on the Equilibrium Slopes of Beaches and Sand Movement by Breaker.
8. Y. Mashima :
   Study on Littoral Drift and Longshore Current.
9. T. Ishihara, Y. Iwagaki and M. Murakami :
   On the Investigation of Beach Erosion along the North Coast of Akashi Strait.
10. K. Shinohara, T. Tsubaki, M. Yoshitaka, and Ch. Agemori :
    Sand Transport along a Model Sandy Beach by Wave Action.
11. H. Fukushima and Y. Mizoguchi :
    Field Investigation of Suspended Littoral Drift.
12. T. Kubo :
    Considerations by Fundamental Test of Jetty in River Mouth.

COASTAL ENGINEERING IN JAPAN, VOL. 2, 1959 (pp. 122)

…… US $ 1.50

TABLE OF CONTENTS

1. S. Unoki :
   On the Ocean Waves due to Tropical Cyclones.
2. T. Kishi :
   The Possible Highest Gravity waves in Shallow Water.
3. T. Kuribayashi :
   Field Investigation of Wave Forces on Breakwater.
4. K. Shinohara and T. Tsubaki :
   Laboratory Study on Sand Movement and Equilibrium Profiles of Beaches.

5. T. Ishihara, T. Sawaragi and T. Amano :
   Fundamental Studies on the Dynamics of Sand Drifts (Reports 1 and 2)
6. H. Fukushima and M. Kashiwamura :
   Field Investigation on Suspended Sediment by the Use of Bamboo Samplers.
7. N. Shiraishi :
   The Measurement of Littoral Drift at Shoreline Harbors.
8. J. Kato :
   Shapes of Shore Structures (Dikes) and its Damping Effect for Wave Forces.
9. S. Adachi, T. Sawaragi and A. Ogo :
   The Effects of Coastal Structures on the Littoral Sand Drifts.
10. S. Nagai and H. Kubo :
    Arrangement of Groins on a Sandy Beach.
    Motion of Sand Particles Between Groins.
    The Shock Pressures Exerted by Breaking Waves on Breakwaters.
11. M. Hom-ma and T. Sakou :
    An Experimental Study on the Submerged Breakwater.
12. Y. Fujino :
    The Construction of a Lighted Beacon on a Reef in the Open Sea.

COASTAL ENGINEERING IN JAPAN, VOL. 3, 1960 (pp. 125)
…… US $ 2.50

TABLE OF CONTENTS

1. T. Kishi, M. Tominaga, and I. Oeda :
   Studies on Meteorological Tides at the mouth of the Tone River.
2. S. Hayami, H. Higuchi, and K.H. Yoshida :
   On the Similitude of Hydraulic Models Involving Tidal Motion.
3. T. Ito, S. Sato, T. Kishi and M. Tominaga :
   On the Density Currents in the Estuary.
4. T. Iwasaki and K. Horikawa :
   Tsunami caused by Chile Earthquake in May, 1960 and Outline of Disasters in North-eastern Coasts of Japan.
5. K. Horikawa :
   Some Additional Remarks on the Chilean-Earthquake Tsunami.
6. T. Ishihara, I. Iwagaki, and H. Mitsui :
   Wave Overtopping on Sea Walls.
7. Y. Mashima :
   A Study on the Volume of Littoral Drift.
8. N. Shiraishi, A. Numata and N. Hase :
   The Effect and Damages of Submerged Breakwater in Niigata Coast.
9. M. Hom-ma, K. Horikawa and C. Sonu :
   A Study on Beach Erosion at the Sheltered Beaches of Katase and Kamakura, Japan.